Theresa Voit, BSc

3D - FEM Modelling of a Deep Excavation

MASTER'S THESIS

to achieve the university degree of

Diplom-Ingenieurin

Master's degree programme: Civil Engineering, Geotechnics and Hydraulics

submitted to

Graz University of Technology

Supervisor

Ao.Univ.-Prof. Dipl.-Ing. Dr.techn. M.Sc. tit.Univ.-Prof.
Helmut Schweiger

Institute for Soil Mechanics and Foundation Engineering

Second Supervisor
Dipl.-Ing. Patrick Pichler, BSc

Graz, September 2016

AFFIDAVIT

I declare that I have authored this thesis independently, that I have not used other than the declared sources/resources, and that I have explicitly indicated all material which has been quoted either literally or by content from the sources used. The text document uploaded to TUGRAZonline is identical to the present master's thesis.

Graz, am 02.09.2016
Date

Theresa Veit
Signature

Danksagung

Meine Begeisterung für das Masterstudium in Geotechnik und Wasserbau hat mir gezeigt und bestätigt, dass es die richtige Entscheidung war, dieses Studium zu wählen. Insbesondere die Ausbildung im numerischen Bereich der Geotechnik hat meinen favorisierten Interessensbereich maßgeblich beeinflusst, weshalb auch mein Wunsch, eine Masterarbeit in diesem Bereich zu schreiben, sehr groß war. Dazu möchte ich mich bei Dipl.-Ing. P. Pichler bedanken, der im Grunde die ersten Bausteine in diese Richtung für mich gelegt hat.

Aufgrund des großen Interesses für diese Arbeit war meine Motivation bis zum Schluss sehr hoch. Das habe ich vor allem meinem Betreuer, Univ.-Prof. Dr. techn. H. F. Schweiger, zu verdanken, der mir die Möglichkeit geboten hat, diese Arbeit zu verfassen. Ein aufrichtiges Danke dafür! Seine hervorragende und gut organisierte Betreuung hat mich auch davor bewahrt, „to go bananas“, wie er selbst in seinen Vorlesungen oft zu sagen pflegte, um auf kritische Aspekte hinzuweisen.

Ein herzliches Dankeschön gilt auch meiner Familie, die mich während des Studiums durch alle Höhen und Tiefen begleitet und immer bestärkt hat. Ganz besonders möchte ich mich bei meinen Eltern bedanken, die mir den Weg, meine Ziele zu erreichen, ermöglicht haben. Ein weiterer Dank ergeht an all meine Freunde und Wegbegleiter, die mich auf ganz unterschiedliche Art und Weise unterstützt haben.

Kurzfassung

In dieser Arbeit werden 3D FE – Modellierungen einer tiefen Baugrube im Salzburger Seeton mit dem FE – Programm Plaxis 3D durchgeführt. Eine 80 cm starke Schlitzwand und vier Steifenhorizonte bilden die Baugrubensicherung. Die Arbeit befasst sich mit unterschiedlichen Modellierungsmöglichkeiten der Schlitzwand, um das Verhalten dieser möglichst realitätsnah zu simulieren. Der Schwerpunkt bezieht sich auf den Unterschied zwischen isotropen und anisotropen Materialverhalten der Schlitzwand, da dieses maßgebend durch die Herstellungsfugen beeinflusst wird. Aus diesem Grund ist es von großem Interesse, passende anisotrope Materialmodelle und Modellierungsansätze zu finden, damit Schlitzwandverformungen und -kräfte sowie Oberflächensetzungen im Nahbereich der Baugrube plausibel abgeschätzt bzw. prognostiziert werden können. Zudem wird zwischen der Modellierung mit „Kontinuums- und Plattenelementen“ unterschieden. Beide Modellierungsansätze ermöglichen die Berücksichtigung von anisotropen Materialverhalten. Plattenelemente sind in Plaxis 3D als linear elastische Biegeelemente definiert. Die Berücksichtigung anisotroper Materialeigenschaften ist optional. Für die anisotrope Modellierung der Wand mit Kontinuumselementen wurde das „Jointed Rock Model“ verwendet, welches in zwei normal zueinander stehenden Richtungen verschiede elastische Materialeigenschaften berücksichtigen kann. Durch die Modellierung in 3D kann auch das unterschiedliche Verhalten zwischen "Schlitzwandmitte" und -"ecke", welches sich aufgrund des großen Steifigkeitsunterschieds zeigt, analysiert werden. Des Weiteren wird auch der Einfluss verschiedener Drainagebedingungen (drainiert, undrainiert, teilkonsolidiert) auf das Verformungsverhalten der Schlitzwand untersucht. Da sich im Zuge des Baugrubenaushubs, vor allem unter Baugrubenniveau, negative Porenwasserüberdrücke bilden, die den Scherwiderstand des Bodens erhöhen, zeigen die verschieden Varianten unter undrainierten Bedingungen nahezu keine Unterschiede. Im Vergleich dazu nehmen die Unterschiede stark mit steigenden Konsolidierungsgrad zu. Um das Verhalten der Schlitzwand möglichst realistisch abschätzen zu können, ist es notwendig anisotrope Materialeigenschaften zu berücksichtigen, da diese das Verhalten der Wand wesentlich beeinflussen.

Abstract

This thesis is about 3D-FE modelling of a deep excavation in Salzburger Seeton in Plaxis 3D, supported by a surrounding diaphragm wall and four levels of struts. It deals with different modelling approaches in order to consider appropriate mechanical behaviour of the diaphragm wall. Therefore, the main focus lies on the different options available to model the material behaviour as realistically as possible. Due to the construction joints diaphragm walls are expected to behave anisotropic rather than isotropic. A further distinction is made by modelling the wall either as continuum (volume elements) or as plate (defined as a structural element in Plaxis 3D). Both options allow for anisotropy, whereas plate elements can either be defined as isotropic or anisotropic, the continuum model requires a material model, able to account at least for cross anisotropy. This is only provided by the Jointed Rock Model implemented in Plaxis 3D. Since anisotropy of diaphragm walls is only induced by the vertical joints, cross anisotropy is considered to be sufficient. In addition, 3D modelling automatically accounts for 3D effects, resulting in corners acting stiffer than centre parts of the wall. Furthermore the influence of different drainage conditions like drained, undrained, partly consolidated is investigated as well. Concerning the results of all variations, the main emphasis lies on the differences between wall deformations and bending moments as well as surface settlements in the area adjacent to the excavation. Since excavations involve unloading mechanisms, the soil experiences at least in some parts, negative excess pore pressures, which increase the shear strength of the soil. Consequently, undrained conditions are almost not affected by the differing modelling options when compared to other drainage conditions where the difference increases with increasing degree of consolidation. In order to make appropriate predictions, especially concerning wall deformations and surface settlements, consideration of anisotropic behaviour is of significance and is recommended.

Table of contents

List of figures

List of tables

List of symbols and abbreviations

Capital letters

A	[m²]	Cross section area
E	[kN/m²]	Young´s modulus
E_{oed}	[kN/m²]	Oedometer modulus
G	[kN/m²]	Shear modulus
I	[m⁴]	Moment of inertia
K_0	[-]	Coefficient of lateral earth pressure
M	[kNm]	Bending moment
N	[kN]	Axial force
Q	[kN]	Shear force
R_f	[-]	Failure ratio
R_{inter}	[-]	Interface reduction factor

Small letters

b	[m]	Width
c	[kN/m²]	Cohesion
d	[m]	Thickness
h	[m]	Height
k	[m/d]	Permeability of the soil
l	[m]	Length
m	[-]	Power for stress dependency of stiffness
p^{ref}	[kN/m²]	Reference stress
q	[kN/m²]	Uniformly distributed load

Greek letters

α_1	[°]	Dip angle
α_2	[°]	Dip direction
γ	[kN/m³]	Unit weight
γ_{sat}	[kN/m³]	Saturated unit soil weight
ε	[-]	Strain
ν	[°]	Poisson´s ration
σ	[kN/m²]	Normal stress
σ_t	[kN/m²]	Tensile strength
τ	[kN/m²]	Shear stress

φ	[º]	Friction angle
ψ	[°]	Dilatancy angle

Abbreviations

FEM	Finite Element Method
HS	Hardening Soil
JRM	Jointed Rock Model
MC	Mohr Coulomb
OCR	Over-consolidation ratio
POP	Pre-overburden pressure

1 Introduction

This thesis is about a deep excavation in Salzburger Seeton, modelled with the FE program Plaxis 3D. Besides the ultimate limit state, serviceability is of high interest for designing supporting systems of deep excavations in urban zones. The magnitude of surface settlements is of crucial importance for adjacent buildings, especially for listed buildings, which are often present in inner-city areas. FE-tools are ideally suited to predict deformations, including surface settlements. In order to prevent damage to adjacent buildings due to settlements, an appropriate FE-model, with all its assumptions, is required to simulate the overall behaviour realistically. This approach leads to the primary purpose of this thesis, which deals with possible modelling variations of diaphragm walls and focuses on the differences between the individual options. The influence of different drainage conditions (drained, undrained, partly consolidated) is investigated as well.

Due to the construction sequence of a diaphragm wall, joints are created between individual wall sections. This implies that the wall does not behave like an isotropic continuum. When modelling an isotropic wall, as usually done in practice, the influence of the construction joints on the wall´s behaviour is neglected. Therefore, a more realistic approach is allowing for an anisotropic material behaviour of the wall. In order to consider different elastic properties in the horizontal direction of the wall, Plaxis 3D provides 2 options, both of which are able to account for anisotropy. The wall can be modelled as a structural element, more precisely as plate or as continuum (volume elements). For plate elements anisotropy is optional, whereas the continuum requires an appropriate material model.

Anisotropy normal to the construction joints cannot be considered in a 2D analysis, which is why all calculations are performed in 3D. In addition, 3D modelling also has the advantage of taking 3D effects automatically into account. Hence, the differences between the “centre” and the “corner” parts of the wall are also observed. This is of interest because the wall near the corner acts stiffer than the “centre” part of the wall.

1.1 Aim of the Thesis

The main objective of this thesis is to highlight the differences between isotropic and anisotropic diaphragm wall modelling. The emphasis lies on the difference in wall displacements and bending moments as well as surface settlements in the adjacent excavation area.

2 Literature Research

Zdravkovic et al. (2005) led to useful knowledge in order to create an appropriate anisotropic diaphragm wall model. This paper also served as the necessary reference to validate obtained results between isotropic and anisotropic as well as continuum and plate modelling qualitatively. Similarly, an investigation on anisotropic as well as continuum and plate wall modelling is presented in Dong, et al. (2016).

The effect induced by 3D modelling is decisively determining the behaviour obtained near the corners of the wall and is therefore of interest. Moormann & Klein (2014) and Zdravkovic et al. (2005) give information about 3D effects, which is why they partly served as guidance for result interpretations.

In order to start directly with the investigation on diaphragm walls, an existing and appropriate excavation was required. This provided the general input parameters to create a suitable model. The complete excavation model (dimensions, support, etc.) and additional input (soil profile, adjacent buildings, etc.) were obtained from the Masters thesis of Lüftenegger (2006). However, the present excavation model is not entirely identical to the one in Lüftenegegger (2006), due to a few necessary adjustments, mentioned and explained in following chapters.

3 Project Description

The excavation model including geometry, dimensions and supporting system as well as the soil profile and adjacent surface loads, are taken, with a few simplifications, from the Masters thesis of Lüftenegger (2006). This thesis deals with modelling an existing excavation in Plaxis 2D and 3D Foundation in order to compare the diaphragm wall displacements from FE-modelling with the measured ones. Due to the excavation dimensions (symmetric along the X- and Y-axis) and the final excavation level at 17 m below surface, this excavation seemed to be quite appropriate for investigations on different ways of diaphragm wall modelling, as well as for examining different drainage conditions. The excavation is supported by a diaphragm wall (d = 80 cm), 3 strut levels and a jet grout slab. The main simplification that have been made for this thesis neglects the jet grout slab. Instead, an additional 4th strut level is considered as indicated in red in Fig. 3.

3.1 Excavation Model

In order to increase the feasible mesh fineness to obtain a satisfying mesh quality, the advantage of symmetry is used. Hence, only ¼ of the excavation is modelled. The horizontal dimensions of the excavation are l/b = 20/18 m and the diaphragm wall has a thickness of 80 cm. As shown in Fig. 1, the excavation pit is surrounded by adjacent surface loads as they are considered in the FE-model, whereas the middle strip foundation transfers the highest concentrated load (q = 250 kN/m²) into the soil compared to the outer ones (q = 200 kN/m²) and the plate foundation (q = 80kN/m²). The symmetrical characteristics and the modelled part of the excavation are indicated as well.

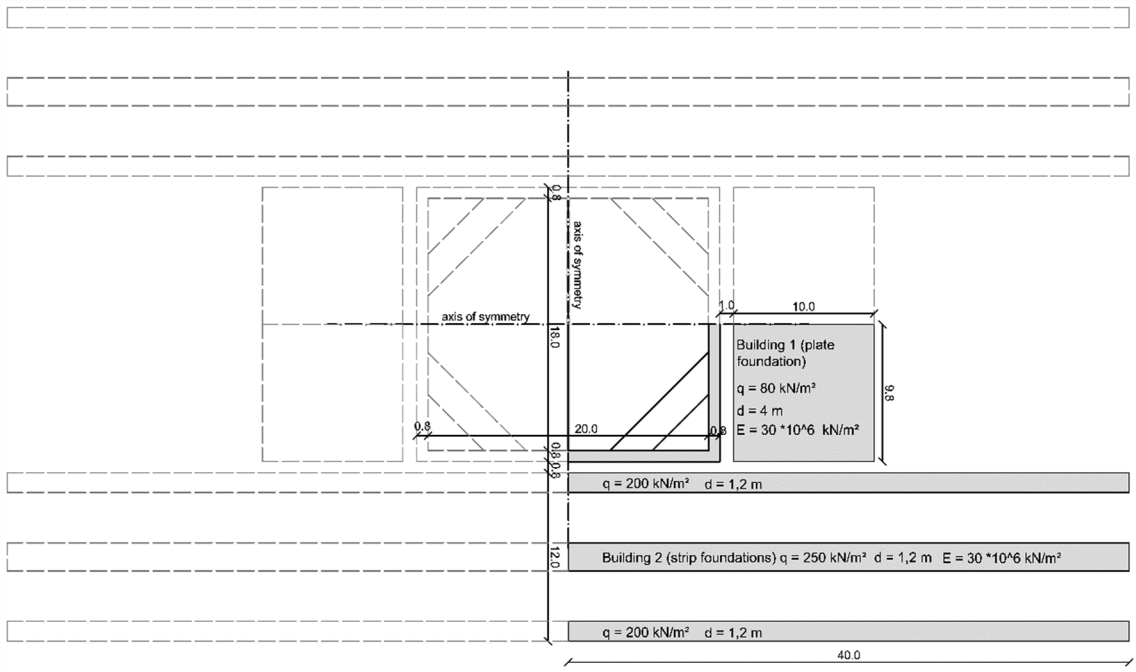

Fig. 1: Plan view of excavation

The main supporting direction is parallel to the short side (b = 18 m). All calculations are performed by positioning the struts and waling as indicated in green in Fig. 2.

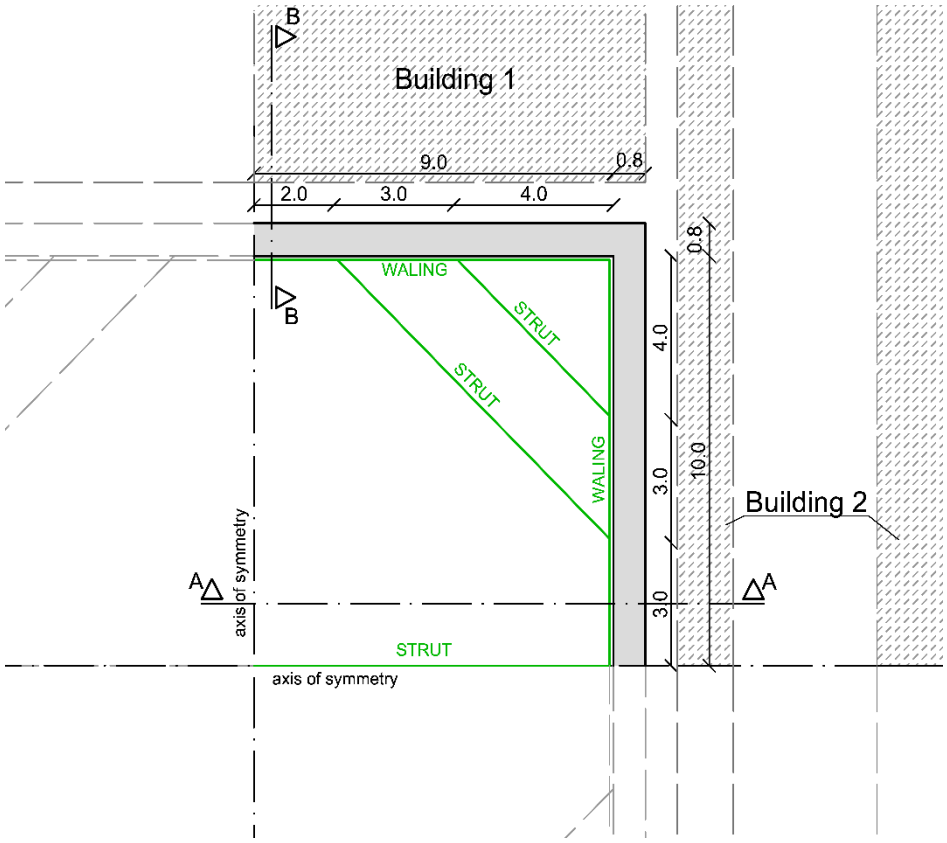

Fig. 2: Modelled excavation section

The diaphragm wall is constructed down to z = -28 m and the final excavation level corresponds to z = -17 m. Ground water is present from -3.4 m below surface. The excavation sequence consists of 5 excavation steps and the intermediate excavation levels as well as the 4 strut levels are considered as shown in Fig. 3. The soil profile consists of three major layers:

- z = 0 – -4 m: Fine Sand
- z = -4 – -20 m: Seeton 1
- z > -20 m: Seeton 2

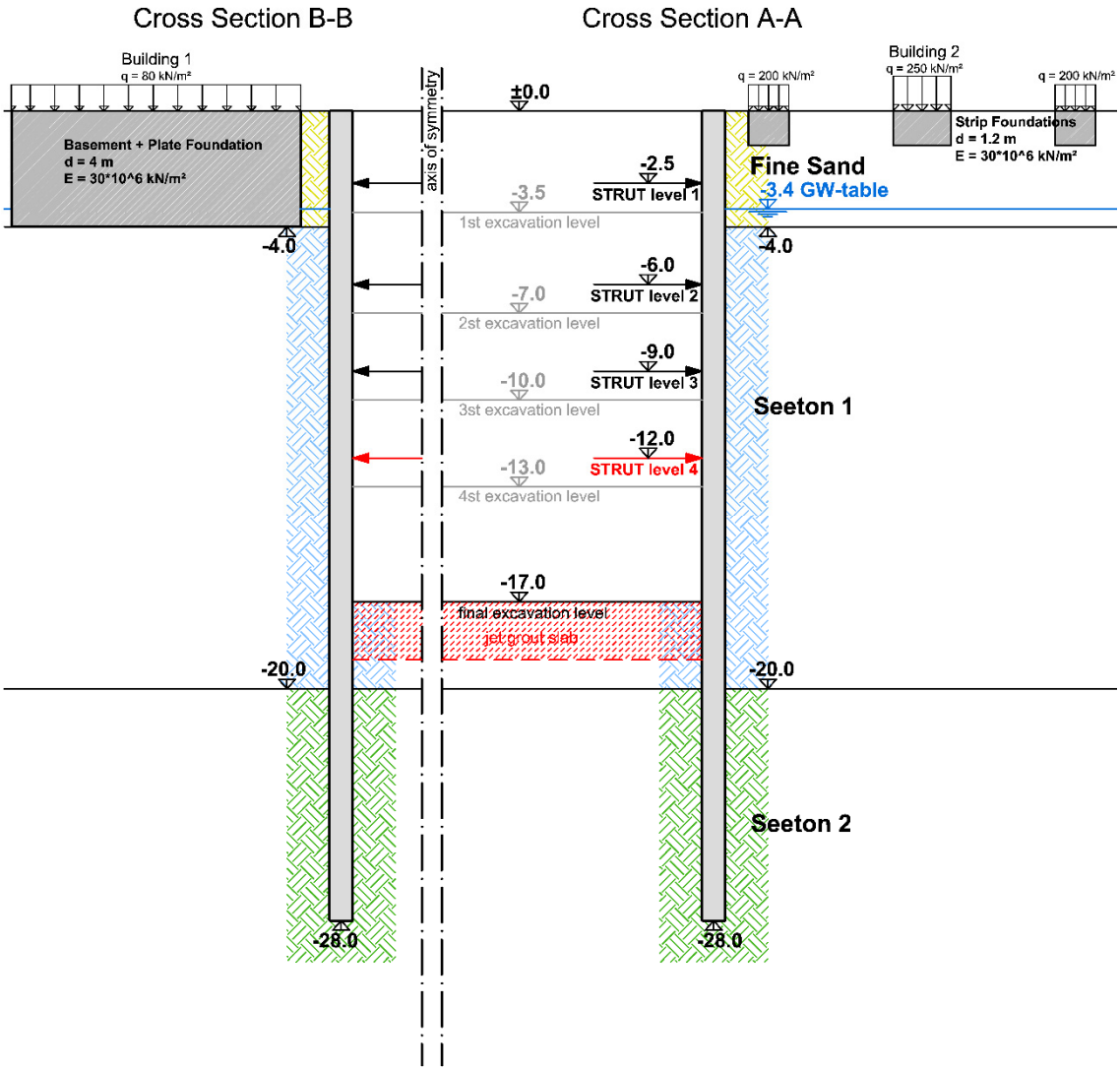

Fig. 3: Cross sections A and B according to Fig. 2

4 Modelling Approach – Plaxis 3D

The overall dimensions of the 3D - model are x/y/z = 50/60/60 m. These dimensions are required to ensure a negligible influence of the boundary conditions.

Continuum as well as structural elements are used in the finite element model. The continuum elements consist of 10 - noded tetrahedral elements, which correspond to a second-order interpolation of displacements. In addition, plates and node-to-node anchors, defined as structural elements, are used as well. Plate elements are 2 - dimensional and composed of 6 - noded triangles. Node-to-node anchors are 1 - dimensional, 2 - noded line elements.

4.1 Constitutive Models

All material models applied for modelling the excavation in Plaxis 3D are briefly explained below. All expressions, formulas and input parameters, which are required to fully describe the considered material models are according to Brinkgreve et al. (2015).

4.1.1 Linear Elastic Model

The linear elastic material model corresponds to Hooke´s law, which considers for isotropic linear elasticity. Therefore, the stress-strain relation is linear and the material behaviour can be defined either by E and ν or G and E_{oed}. The parameters of the two options are dependent on each other, which is why G and E_{oed} can be derived from following formulations:

$$G = \frac{E}{2(1+\nu)} \quad (1)$$

$$Eoed = \frac{(1-\nu)E}{(1-2\nu)(1+\nu)} \quad (2)$$

E	[kN/m²]	Young´s modulus
ν	[-]	Poisson´s ratio
G	[kN/m²]	Shear modulus
E_{oed}	[kN/m²]	Oedometer modulus

The model accounts for linear elasticity only. Consequently, failure mechanisms cannot be developed.

Structural plate elements in Plaxis 3D

Plate elements are also linear elastic in Plaxis 3D, whereas isotropic or anisotropic modelling is optional.

4.1.2 Jointed Rock Model

The JRM is an anisotropic elastic perfectly-plastic material model, as indicated in Fig. 4. The horizontal line in Fig. 4 corresponds to both the yield and the failure stress line. In general this model is used for modelling rock materials, as the behaviour of rock is often characterized by the orientation of joints and/or stratification. The JRM is limited by the condition that plastic shear stresses (Mohr-Coulomb failure criterion) can only occur along the defined stratification/joint directions. It allows for modelling a maximum of 3 different joint directions, whereas the first direction corresponds to the stratification direction.

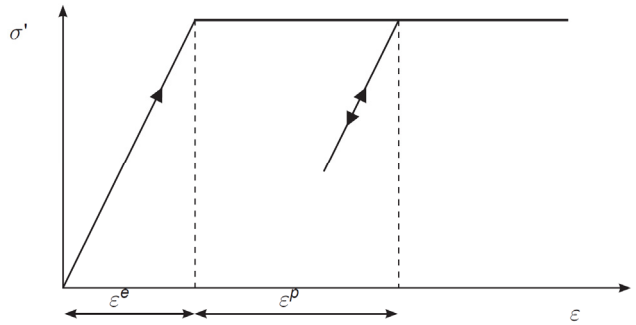

Fig. 4: Stress strain relation of an elastic perfectly-plastic model (Brinkgreve et al. 2015)

Usually the main stratification has a particular orientation, as a result rock material shows different stiffness behaviour, especially perpendicular to this direction compared to others. Therefore, the JRM provides for the input of elastic cross anisotropic parameters. This allows for a different stiffness normal to the desired stratification direction to be taken into account. Cross anisotropy is defined by the following 5 parameters:

E_1	[kN/m²]	Young´s modulus (parallel to plane of stratification)
E_2	[kN/m²]	Young´s modulus (normal to plane of stratification)
ν_1	[-]	Poisson´s ratio
ν_2	[-]	Poisson´s ratio
G	[kN/m²]	Shear modulus (parallel to plane of stratification)

In addition, 2 more major joint directions can be defined. Anisotropy can only be considered normal to the first plane direction, whereas the Mohr-Coulomb failure criterion and the consideration of a tensile strength are possible for all 3 plane directions. This

requires the input of strength parameters according to the strength properties in stratification/joint direction (i = 1, 2, 3). However, in this work the model is “misused” to model anisotropic behaviour of diaphragm walls and therefore only the feature of considering anisotropic elasticity is utilized in this thesis.

The exact orientations of the 3 plane directions (i = 1, 2, 3) are defined by:

$\alpha_{1,i}$	[°]	Dip angle
$\alpha_{2,i}$	[°]	Dip direction

4.1.3 Hardening Soil Model

Soil is generally known to behave highly nonlinear, especially when initially loaded. This implies that elastic material models are inappropriate. The HS-model is able to account for nonlinearity, as well as for other features soil usually exhibit.

The HS-model distinguishes between two yield surfaces. One accounts for deviatoric hardening due to shear loading and the second for volumetric hardening due to compression loading. Compared to linear elastic – perfectly plastic models, the shear yield stress surface is not fixed in space and can vary from the initial yield stress to the failure stress surface as defined by the MC failure criterion. Within the area limited by the two yield stress surfaces, soil is considered elastic (Fig. 5). Therefore, stress states above the yield surfaces cause plastic deviatoric and/or volumetric strains.

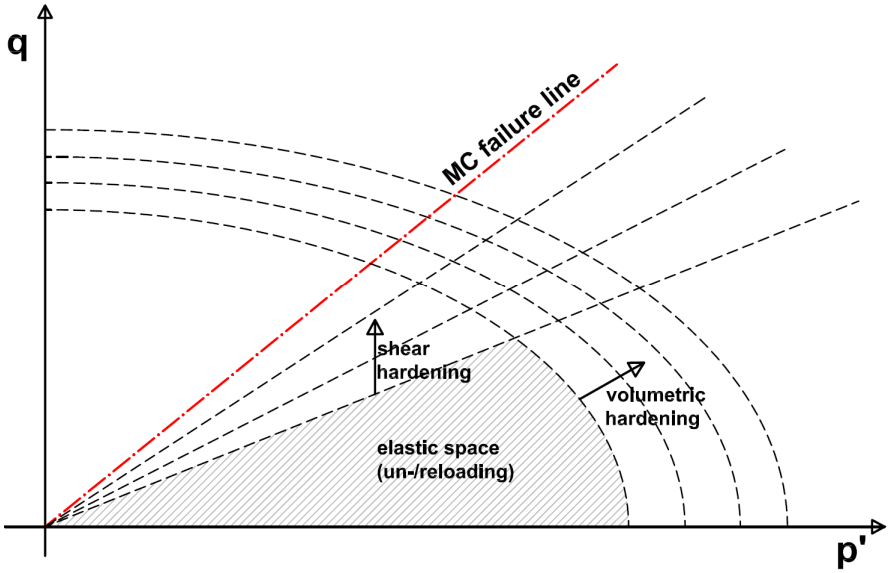

Fig. 5: Principle idea of HS-model (adapted from Brinkgreve et al. 2015)

Deviatoric Hardening

Fig. 6 shows the nonlinear stress strain relation for primary loading, described by a hyperbolic function. When the soil is subjected to un-/reloading, the soil response is much stiffer and it behaves elastic. As long as the stress state remains below the yield surfaces, a different modulus and elastic behaviour are applied to account for conditions within the elastic region. The failure line corresponds to the MC failure criterion.

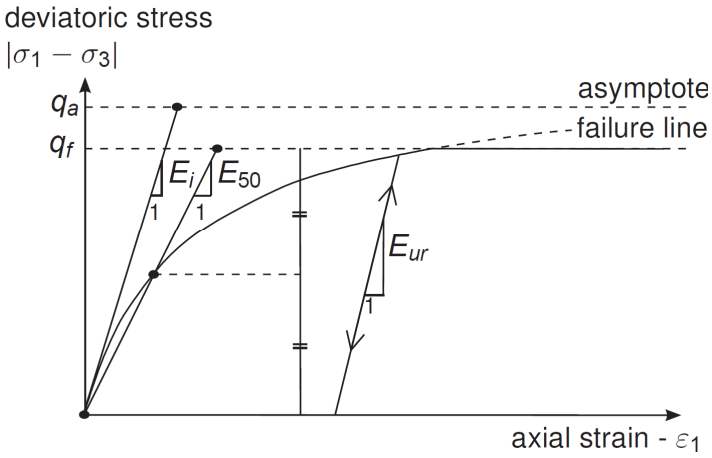

Fig. 6: Deviatoric stress-strain relation (Brinkgreve et al. 2015)

E_{50}	[kN/m²]	Modulus at 50% of strength for primary loading – derived from (3)
E_{ur}	[kN/m²]	Modulus for unloading/reloading – derived from (4)
R_f	[-]	$R_f = q_f/q_a$ – by default 0.9

In order to obtain the desired hyperbolic function, E_{50} is necessary. E_{ur} considers the stiffer behaviour during un-/reloading. Due to the stress dependency of soil stiffness, Plaxis requires the input of reference parameters E_{50}^{ref} and E_{ur}^{ref}. R_f limits the strain at failure, since the hyperbolic function would reach the asymptote q_a at infinite strain.

Stress dependency is considered by the following formulas:

$$E_{50} = E_{50}^{ref} \left(\frac{c' cos\varphi' - \sigma_3' \, sin\varphi'}{c' cos\varphi' + \sigma_3'^{ref} \, sin\varphi'} \right)^m \quad (3)$$

$$E_{ur} = E_{ur}^{ref} \left(\frac{c' cos\varphi' - \sigma_3' \, sin\varphi'}{c' cos\varphi' + p^{ref} \, sin\varphi'} \right)^m \quad (4)$$

E_{50}^{ref}	[kN/m²]	Secant modulus from triaxial testing
E_{ur}^{ref}	[kN/m²]	Modulus for unloading/reloading
p^{ref}	[kN/m²]	Reference stress (corresponds to $\sigma_3'^{ref}$)

m	[-]	Power for stress dependency of stiffness (depends on the soil)

In order to completely describe linear elasticity within the elastic space, Plaxis demands the input of $\nu_{ur.}$

ν_{ur}	[-]	Poisson´s ratio for unloading/reloading (by default 0.2)

Volumetric Hardening

The two yield surfaces implied in the HS-model are independent from each other. In order to fully describe the second yield surface (Fig. 5), the modulus E_{oed}, derived from Oedometer tests and the K_0^{nc} value are needed. Together they control volumetric hardening.

$$E_{oed} = E_{oed}^{ref} \left(\frac{c' cos\varphi' - \sigma_1' \, sin\varphi'}{c' cos\varphi' + p^{ref} \, sin\varphi'} \right)^m \qquad (5)$$

E_{oed}^{ref}	[kN/m²]	Tangential modulus from Oedometer testing
p^{ref}	[kN/m²]	Reference stress (corresponds to $\sigma_1'^{ref}$)
m	[-]	Power for stress dependency of stiffness (depends on the soil)
K_0^{nc}	[-]	K_0 for normal consolidation

The volumetric yield surfaces below the MC failure line correspond to surfaces with equal volumetric strains (Fig. 5). Fig. 7 represents the yield contours of shear and volumetric hardening, defining the 3 dimensional elastic stress space.

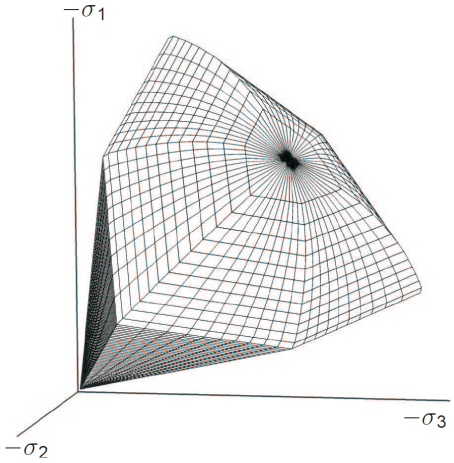

Fig. 7: Yield contours of the HS-model in principle stress space (Brinkgreve et al. 2015)

Failure Criterion

The failure criterion is given by the MC criterion, requiring the input of the strength parameters φ' and c'. Additionally, tensile strength $\sigma_{t,}$ as well as dilatancy ψ are necessary.

φ'	[°]	Effective friction angle
c'	[kN/m²]	Effective cohesion
$\sigma_{t,}$	[kN/m²]	Tensile strength
ψ	[°]	Dilatancy angle

Overconsolidation

When soil is over-consolidated, Plaxis 3D provides the input of an over-consolidation ratio OCR or a pre-overburden pressure POP, in order to define the initial stress state as well as the initial yield surfaces correctly.

4.1.4 Hardening Soil Model with Small Strain Stiffness

The HS-small model is based on the HS-model, but with the enhancement of taking small strain stiffness into account. At very low strain rates, including initial loading as well as strain reversal (e.g. un- /reloading), soil shows a linear elastic behaviour and responds with a very high stiffness compared to higher strain regions. Therefore, two additional parameters are required to describe the soil´s behaviour:

G_0^{ref}	[kN/m²]	Initial shear modulus at very small strains
$\gamma_{0.7}$	[-]	Shear strain level where G_0 is reduced to 70%

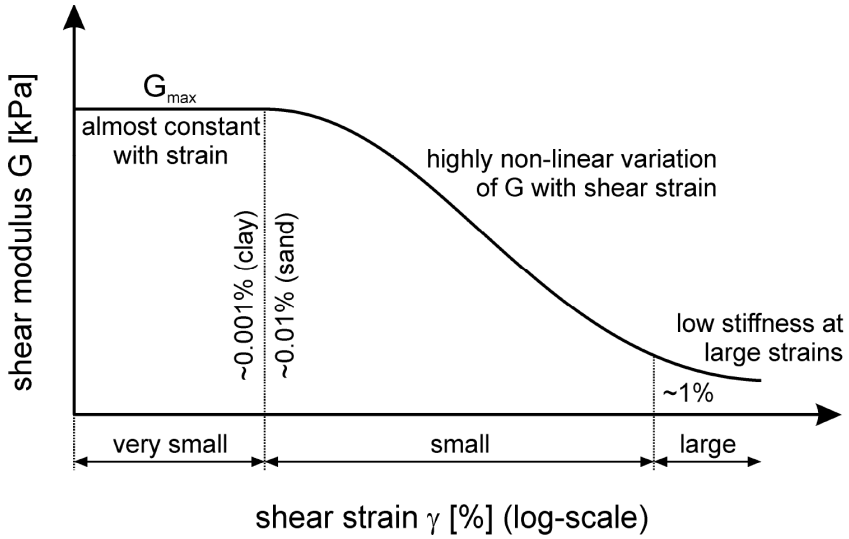

Fig. 8: Development of shear modulus G with increasing shear strains γ (Schweiger, 2015)

G_{max} acts at very small strains – this corresponds to the true linear elastic region soil has. This characteristic can be explained by the fact that no rearrangement of soil particles occurs within the range of very small strains.

4.2 Soil Parameters

The parameters of the top layer – Fine Sand – have been chosen according to Lüftenegger (2006) (see Tab. 1). There were no small strain values available, which is why the HS-Model has been used. Since it only concerns the surface layer, which has a thickness of 4 m, the difference between the two models will not be significant. Due to the comparatively high permeability, the drainage type of this layer is always considered as drained, independent of the desired drainage condition for the investigation of the influence between different modelling variations.

The parameters of the two Seeton layers (1 and 2) in Tab. 1 match with the latest available parameters from Schweiger (2015), which is why they differ from Lüftenegger (2006). These layers are modelled with the HS-small model. Dependent on the current drainage condition being considered, the drainage type changes.

Tab. 1: Soil parameters according to Lüftenegger (2006) and Schweiger (2015)

	Soil Layers			
	Fine Sand	**Seeton 1**	**Seeton 2**	**Unit**
h	0 - 4	4 - 20	> 20	m
Model	HS-Model	HSS-Model	HSS-Model	
Type	D	D/UD	D/UD	
γ	20	20	20	kN/m³
γ_{sat}	20	20	20	kN/m³
$E_{50\ ref}$	3000	35 000	25 000	kN/m²
$E_{ur\ ref}$	12 000	140 000	100 000	kN/m²
$E_{oed\ ref}$	3000	35 000	20 000	kN/m²
φ'	28	30	28	°
ψ	0	0	0	°
c´	5	2	10	kN/m²
ν_{ur}	0.2	0.2	0.2	-
p_{ref}	40	100	100	kN/m²
m	0	0.7	0.7	-
K_{0nc}	0.531	0.5	0.531	-
$K_{0,\ manual}$	0.55	0.55	0.55	-
R_f	0.9	0.9	0.9	-
R_{inter}	0.7	0.67	0.67	-
k_x/k_y	8.64*E-01	4.32E-03	8.64E-04	m/d
k_z	8.64*E-03	4.32E-04	8.64E-05	m/d
$\gamma_{0,7}$	-	2.00E-04	2.00E-04	kN/m²
G_0	-	175000	125000	kN/m²

4.3 Adjacent Surface Loads

Surface loads resulting from adjacent buildings near the excavation are listed in Tab. 2. The structures are considered by modelling the foundations of the buildings as a continuum (strip foundations, basement plus plate foundation) and subjecting these with the corresponding loads from above. The concrete structures are modelled as linear elastic material and the Young´s modulus was chosen to E = 29 MPa. The weight of the foundations is already included in the surface loads. Hence, the weight γ of the modelled continuum structures is set to zero.

Tab. 2: Material parameters of adjacent structures considered in the model

	Adjacent Buildings/Foundations		
	Strip foundation	**Basement + plate foundation**	**Unit**
Model	Linear elastic	Linear elastic	
Type	Non-porous	Non-porous	
d	1.2	4	m
q	200/250	80	kN/m²
γ	0	0	kN/m²
E_1	29 000 000	29 000 000	kN/m²
ν_1	0.2	0.2	-

4.4 Diaphragm Wall Modelling

Within this thesis, the major distinction is made between modelling the wall either as continuum or as structural 2D element, defined as “plate” in Plaxis 3D. Whereas continuum elements account for a real wall thickness, plate elements have only a virtual thickness. This causes differences in wall behaviour as explained in 5.3 Continuum vs. Plate Modelling.

In order to account for the influence of construction joints, isotropic material behaviour is insufficient. Especially the bending stiffness of the wall in the horizontal direction is affected by the joints. Therefore, a more realistic approach results when the wall is modelled as anisotropic material. Anisotropy is induced by reducing the normal stiffness *EA* as well as the bending stiffness *EI* in horizontal direction. The assumption of lowering the normal stiffness is based on the idea that the joints are closing with an increasing normal force in horizontal direction. Thus, the lowered normal stiffness represents an equivalent stiffness to consider the total deformations, which result from the contractions of the wall material itself as well as the joint closure. Since the diaphragm wall practically consists of separate concrete sections, it seems reasonable that the wall has only a low resistance against bending in horizontal direction. Therefore, the horizontal stiffnesses are assumed to be 25 % of the vertical ones.

Nevertheless, the wall is also modelled as isotropic material in an additional analysis, which is used as a reference model.

Plate elements are limited in terms of material behaviour, i.e. linear elastic modelling is only possible. However, isotropic and anisotropic modelling is optional. For most geotechnical applications, concrete structures can be assumed to behave linear elastic, thus this restriction is not a problem.

For modelling the wall as a continuum, isotropic behaviour is automatically considered when choosing the linear elastic material model (see also 4.1.1). The only option to account for anisotropy of volume elements is provided by the Jointed Rock Model. As briefly explained in chapter 4.1.2, anisotropy is limited to cross anisotropy. This is sufficient when investigating on the behaviour of diaphragm walls. Since anisotropy is only induced by the construction joints, the joint direction can be considered as the present stratification direction – defined as the plane of anisotropy in the JRM. The two additional plane directions (joint directions) available are therefore not activated.

4.4.1 Continuum Elements

Modelling approach

The downside of modelling the wall as a continuum is the lack of output options concerning structural forces. By comparison, structural forces can be easily obtained for plate elements, since they are defined as structural elements. Therefore, a trick can be used, by positioning a flexible plate along the centre line of the wall, deforming as the continuum without developing any resistance against occurring deformations. To ensure there is no influence on the behaviour of the wall, the assigned elastic properties are 1/1000 of the ones the actual diaphragm wall has. The representing structural forces of the continuum wall are obtained by multiplying the plate output data by 1000. The only limitation the plate implicates is that it can only be considered linear elastic.

Isotropy

In general, isotropic wall behaviour is modelled with the linear elastic material model. For checking reasons concerning the JRM approach, the JRM was also used for isotropic modelling by choosing the parameters as shown in Tab. 3.

Anisotropy

As already mentioned, cross anisotropy can be modelled by the JRM, this requires the input of the 5 independent parameters listed below. The ratio between vertical and horizontal elastic properties is assumed to be ¼, which leads to the following relations:

$$E_2 = \frac{1}{4} E_1 \quad (6)$$

$$G_2 = \frac{E_2}{2(1+\nu)} \quad (7)$$

$$\nu_1 = \nu_2 = 0.2 \quad (8)$$

Isotropic linear elastic parameters considered for the concrete as continuum:

E_1	[kN/m²]	Young´s modulus 1
ν_1	[-]	Poisson´s ratio

Anisotropic linear elastic parameters, which account for the joints:

E_2	[kN/m²]	Young´s modulus 2
G_2	[kN/m²]	Related shear modulus of E_2
ν_2	[-]	Poisson´s ratio

The related directions of action to the input parameters are indicated in Fig. 9.

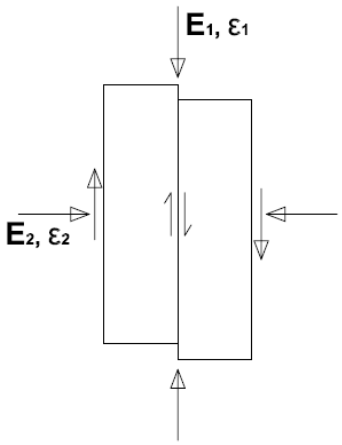

Fig. 9: Parameters required for cross anisotropy (JRM)

In addition, the JRM model requires the input of failure parameters, acting along the defined plane of anisotropy. As explained above, failure development is not desired, which is why the parameters are chosen in such a way that failure cannot occur. As shown in Tab. 4, the cohesion and tensile strength are set to high values to prevent development of shear or tension failure.

Interface elements

Interface elements are present between the wall and the soil continuum. The interface properties correspond to those defined in the soil material data sheet (Tab. 1).

4.4.2 Plate Elements

Isotropy

The necessary parameters are the same as for continuum wall modelling and are given in Tab. 3.

Anisotropy

When the structure shows geometric anisotropy and is mainly subjected to bending, Brinkgreve et al. (2015) recommends the use of the equations given below (Eqn. 12 – 17). In order to apply these relations and derive the same anisotropic properties as for continuum wall elements, the following assumptions (Eqn. 9 – 11) must be made:

$$EI_2 = \frac{1}{4} EI_1 \quad (9)$$

$$EI_{12} = \frac{1}{4} EI_1 \quad (10)$$

$$EA_{23} = \frac{1}{4} EA_{13} \quad (11)$$

The different indices used in Eqn. 10 – 18, correspond to the definitions in Fig. 10. Additionally the input of the actual Young´s modulus *E* and Poisson´s ratio ν of the concrete itself (E = 29 MPa; ν = 0.2) is required as well.

$$E_1 = \frac{12EI_1}{d^3} \quad (12)$$

$$E_2 = \frac{12EI_2}{d^3} \quad (13)$$

$$G_{12} = \frac{6EI_{12}}{(1+\nu)d^3} \quad (14)$$

$$G_{13} = \frac{EA_{13}}{2(1+\nu)d} \quad (15)$$

$$G_{23} = \frac{EA_{23}}{2(1+\nu)d} \quad (16)$$

$$\nu_{12} = \nu \quad (17)$$

E	[kN/m²]	Actual Young´s modulus
E_1	[kN/m²]	Young´s modulus 1
E_2	[kN/m²]	Young´s modulus 2
I_1	[m⁴]	First moment of inertia
I_2	[m⁴]	Second moment of inertia
G_{12}	[kN/m²]	Shear modulus in plane
G_{13}	[kN/m²]	Shear modulus out of plane

G_{23}	[kN/m²]	Shear modulus out of plane
A_{13}	[m²]	Effective cross section area against shearing
A_{23}	[m²]	Effective cross section area against shearing
ν	[-]	Poisson´s ratio
ν_{12}	[-]	Poisson´s ratio
d	[m]	Wall thickness

The related directions of action to the input parameters are shown in Fig. 10.

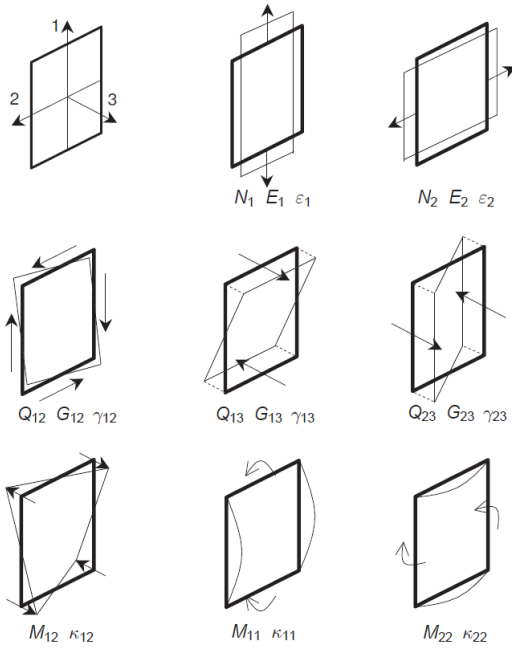

Fig. 10: Geometric anisotropy for 3D plate elements (Brinkgreve et al. 2015)

4.4.3 Parameters

Tab. 3: Isotropic material parameters

ISOTROPIC					
	Plate		**Volume elements**		**Unit**
Model	Linear elastic	Model	Linear elastic	Jointed Rock Model	
Type	Non-porous	Type	Non-porous	Non-porous	
d	0.8	d	0.8	0.8	m
γ	5.0	γ	5.0	5.0	kN/m³
E_1	29.0 *10^6	E_1	29.0 *10^6	29.0 *10^6	kN/m²
E_2	29.0 *10^6	E_2	-	29.0 *10^6	kN/m²
ν_1	0.2	ν_1	0.2	0.2	-
	-	ν_2	-	0.2	-
G_{12}	12.1 *10^6	G_1	12.1 *10^6	12.1 *10^6	kN/m²
G_{13}	-	G_2	-	12.1 *10^6	kN/m²
G_{23}	-		-	-	kN/m²
			MC criterion – 1st plane of anisotropy		
			φ'	45	°
			c´	6000	kN/m²
			σ_t	12 000	kN/m²
			α_1	90/90	°
			α_2	0/90	°

In order to obtain the correct stresses after the wall is constructed, the weight γ corresponds to the additional weight the wall has compared to the weight of the soil volume the wall replaces.

Tab. 4: Anisotropic material parameters

	ANISOTROPIC			
	Plate		**Volume elements**	**Unit**
Model	Linear elastic		Jointed Rock Model	
Type	Non-porous	Type	Non-porous	
d	0.8	d	0.8	m
γ	5.0	γ	5.0	kN/m³
E_1	29.0 *10^6	E_1	29.0 *10^6	kN/m²
E_2	7.3 *10^6	E_2	7.3 *10^6	kN/m²
ν_1	0.2	ν_1	0.2	-
	-	ν_2	0.2	-
G_{12}	3.0 *10^6	G_1	12.1 *10^6	kN/m²
G_{13}	12.1 *10^6	G_2	3.0 *10^6	kN/m²
G_{23}	3.0 *10^6		-	kN/m²
		MC criterion – 1st plane of anisotropy		
		φ'	45	°
		c´	6000	kN/m²
		σ_t	12 000	kN/m²
		α_1	90/90	°
		α_2	0/90	°

4.4.4 Struts and Waling´s

The dimensions of the struts and waling´s are according to Lüftenegger (2006). The excavation considered in Lüftenegger (2006) is supported by three strut levels and a jet grout slab at the bottom, which is replaced by an additional strut level as indicated in red in Fig. 3. The struts are modelled as node-to-node anchors. Since they are defined as one - dimensional structural elements in Plaxis 3D, they require only the normal stiffness *EA* as input parameter.

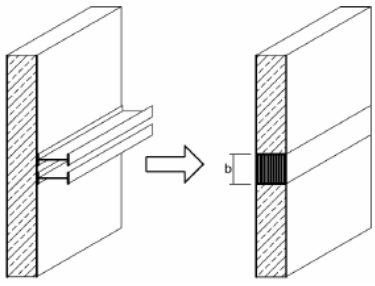

Fig. 11: Model consideration of walling´s (Lüftenegger 2006)

Due to modelling reasons, the waling´s are integrated in the wall, as indicated in Fig. 11. As a result, an equivalent Young´s modulus is calculated by considering the higher modulus of steel. The ratio of the actual beam area to the total area where the beam is

integrated, determines the equivalent Young´s modulus. Since the horizontal Young´s modulus of the wall is assumed to be ¼ of the vertical one, the equivalent modulus is by coincidence approximately as high as the vertical one.

The material behaviour within the area where waling´s are considered is assumed to be isotropic. The influence of a higher Young´s modulus in the vertical direction is small and therefore neglected.

All required input parameters and values are given in Tab. 5.

Tab. 5: Struts and waling´s material parameters

	STRUTS			
	1	**2/3**	**4**	**Unit**
	Ø 500*10	2 Ø 660*12^5	Ø 660*12^5	mm
Model	Elastic	Elastic	Elastic	
Structure	Node-to-Node Anchor	Node-to-Node Anchor	Node-to-Node Anchor	
EA	3.2 *10^6	10.7 *10^6	5.3 *10^6	kN
	WALING'S			
	1	**2/3**	**4**	
	HEB 500	2 HEB 800	2 HEB 800	
Model	Linear elastic/Isotropic	Linear elastic/Isotropic	Linear elastic/Isotropic	
d	0.8	0.8	0.8	m
b	0.3	1.2	0.8	m
γ	5	5	5	kN/m³
E_1	29.0 *10^6	29.0 *10^6	29.0 *10^6	kN/m²
ν_1	0.2	0.2	0.2	-

4.5 Mesh Configuration

Concerning satisfying outputs, stresses are always more critical than displacements. Therefore, the model is meshed with approximately 150,000 elements, this complies with an acceptable calculation time frame and good quality outputs.

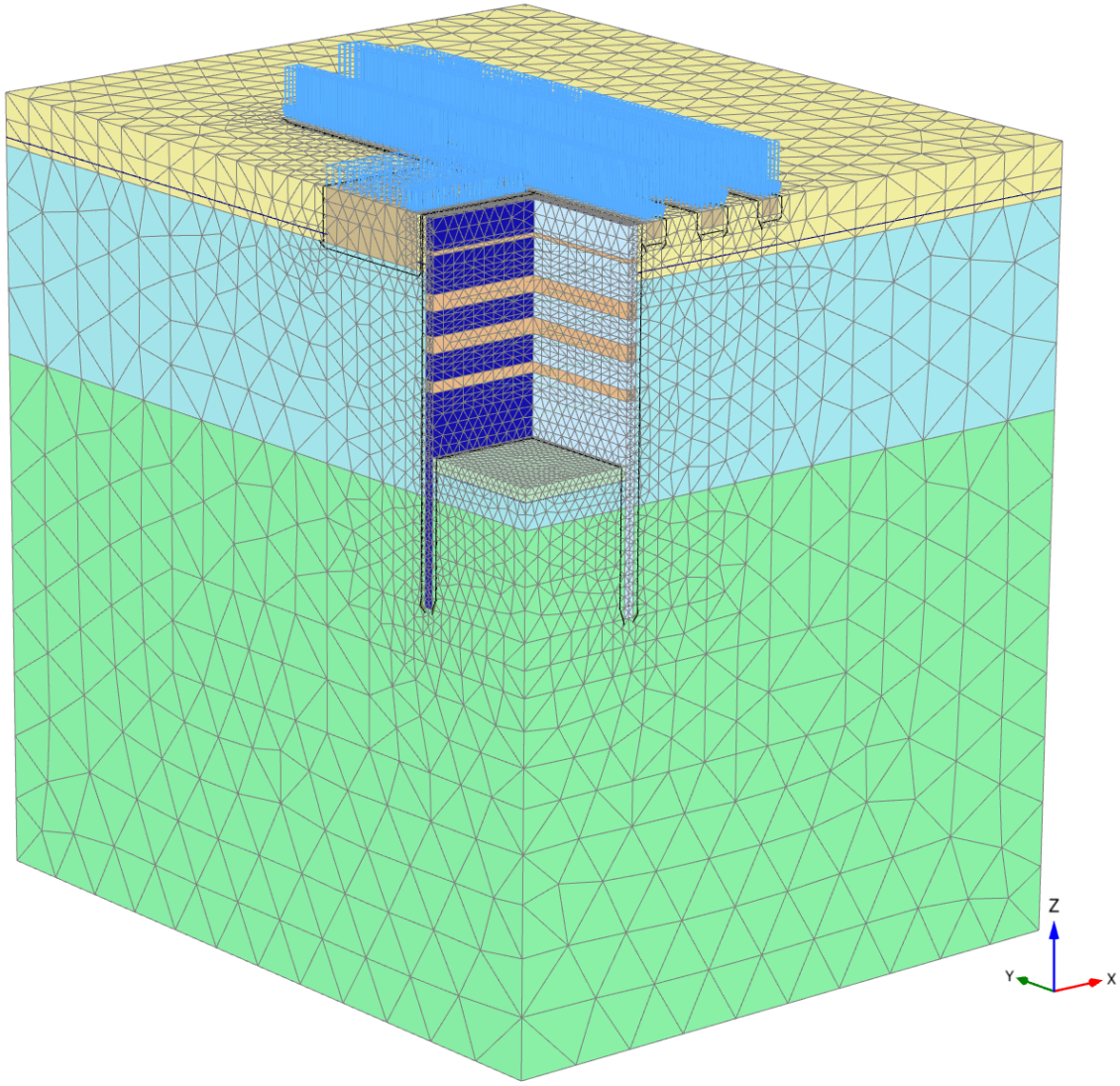

Fig. 12: Complete model in Plaxis 3D

4.6 Flow Conditions

The excavation is constructed under dry conditions. Consequently, groundwater lowering inside the excavation area is required due to groundwater present at 3.4 m below surface. The excavation is divided into 5 intermediate excavation steps (see Fig. 3) and the GW-table is always lowered 1 m below the current excavation level. In terms of modelling, GW lowering is performed, by assigning the GW-table of all clusters above the lowered GW-table to this temporary water table. Since GW lowering induces ground water flow around the diaphragm wall, steady state pore pressures need to be interpolated between the two GW-levels (general GW-level outside the excavation z = -3.4 m; current GW-level, depending on the excavation step) within the affected area from GW-lowering in order to consider for correct pore water pressures below the excavation level. Due to the low permeability of Seeton, the region below -20 m is assumed not to

be affected by the GW-lowering during the construction of the first 3 excavation steps (Fig. 13). In comparison to the last 2 excavation steps, where interpolation is considered down to - 28 m (Fig. 14). Before an excavation step is performed, the cluster (1 m thick) between the current GW level and the resulting excavation level is set to drained, to prevent further development of additional excess pore pressures during the construction of the considered excavation step within this cluster.

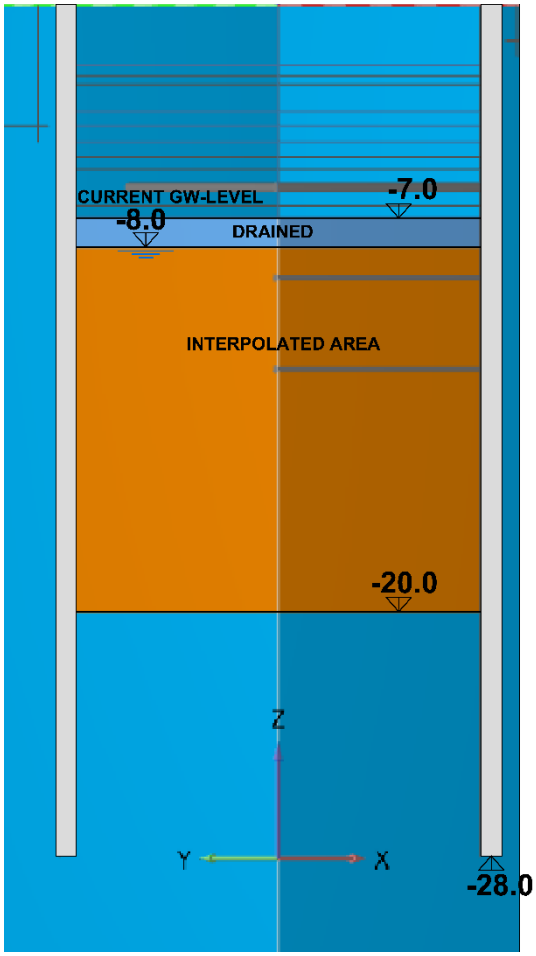

Fig. 13: Flow condition 2nd excavation step

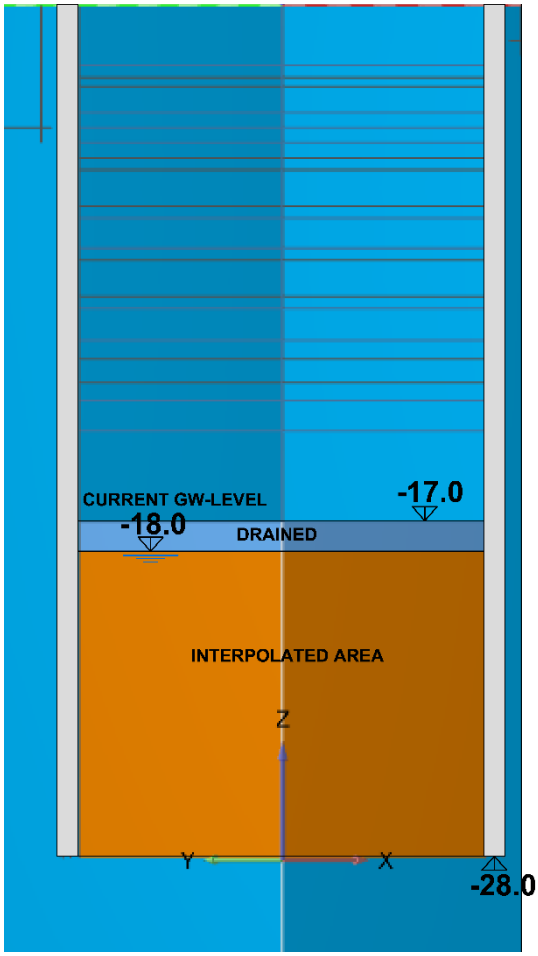

Fig. 14: Flow condition 5th excavation step

Fig. 13 and Fig. 14 represent the considered flow conditions. Besides the interpolated area, they remain basically the same for all 5 excavation steps performed.

4.7 Calculation Phase Sequence

The calculations are performed according to the phase sequence shown in Fig. 15. The displacements resulting from the adjacent loads and weight of the diaphragm wall are assumed to already be finished. Hence, they are set to zero before the construction of the excavation starts. It is noted that the diaphragm wall is modelled as wished – in – place, i.e. possible displacements due to wall construction are neglected.

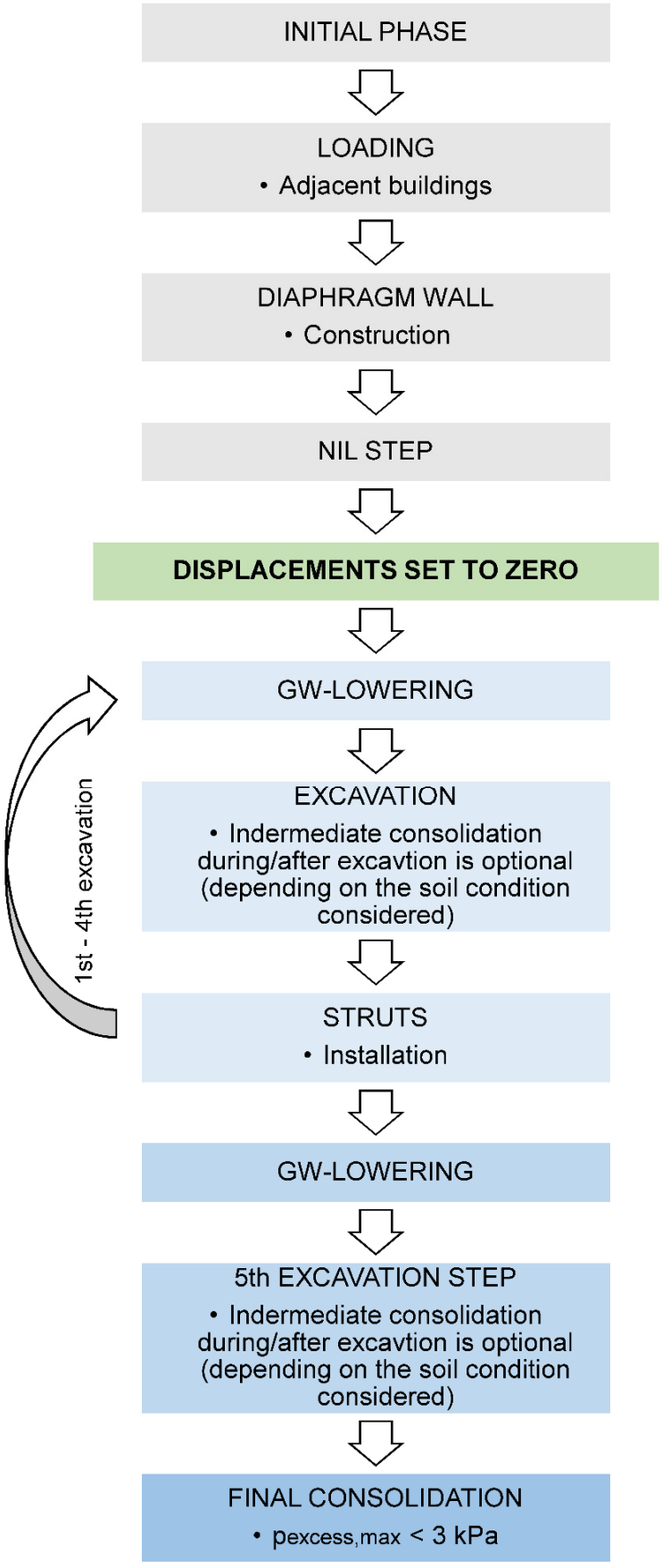

Fig. 15: Calculation phase sequence

In order to check generated results independently, GW-lowering, excavation and struts installation are always performed in separate phases, e.g. steady state pore pressure generation during GW-lowering or wall displacements resulting from one excavation step, without struts already supporting the diaphragm wall. Undrained calculations are completed with a final consolidation phase till the maximum remaining excess pore pressure $p_{excess,max}$ of 3 kPa is reached.

4.8 Performed Calculations

Several calculations, varying between plate and continuum wall modelling as well as between isotropic and anisotropic wall behaviour were performed. The variation of the corner connection between rigid or hinged (connections of plate elements provide for these two options) was completed out of interest, since the investigation on isotropic hinged connections from Zdravkovic et al. (2005) show meaningful outcomes. Furthermore, the influence of different drainage conditions on the wall behaviour and the surrounding area was investigated as well (Tab. 6). The results obtained from drained and undrained calculations can be seen as upper and lower boundaries in order to check reliability and relative differences between individual conditions, since both conditions are not found in reality during construction time for the considered soil profile. The undrained calculations are followed by a final consolidation, where the remaining excess pore pressures $p_{excess,max}$ are almost zero, in order to compare it with drained calculations.

A more realistic approach, concerning an appropriate simulation of the excavation is to consider consolidation during the construction time. Therefore, two possible options, named coupled 1 and coupled 2 are investigated. Both options include consolidation for each excavation step over a chosen time period of 2 weeks, either after or during each excavation step. This corresponds to a total consolidation time of 10 weeks. It is assumed that the construction of planned structures, buildings etc. starts immediately after the completion of the final excavation step and/or the consolidation over the last two weeks. As a result, the loading condition of the soil is reversed (change in stress paths of the soil), which is why no further consolidation of the soil is considered. Therefore, the consolidation time frame of 10 weeks is expected to correspond to a relevant and realistic condition.

Regarding the most realistic possible simulation of the excavation, the second option would represent the more suitable one. However, the coupled 1 option is preferred, because it allows for the consolidation performance to be checked separately. Moreover,

the results of these two options show that the difference between them is quite small (see also 5.2).

Tab. 6: Performed calculations

DIAPHRAGM WALL	DRAINAGE CONDITION

• ISOTROPIC
  • Plate
  • rigid corner
  • hinged corner
  • Continuum
• ANISOTROPIC
  • Plate
  • Continuum
	• UNDRAINED
	• COUPLED 1
	  • Consolidation after each excavation step (2 weeks)
	• COUPLED 2
	  • Consolidation during each excavation step (2 weeks)
	• FINAL CONSOLIDATION
	  • $p_{excess,max} < 3$ kPa
	• DRAINED

5 Results

All results presented in this thesis correspond to the final excavation stage. The behaviour of the diaphragm wall has been mainly analysed at the centre of its long side as indicated in Fig. 16. This is also the side that is subjected to higher surface loads from adjacent buildings (strip foundations in Fig. 1). Therefore, this is the most relevant cross section for further considerations, because maximum wall deflections and structural forces are expected.

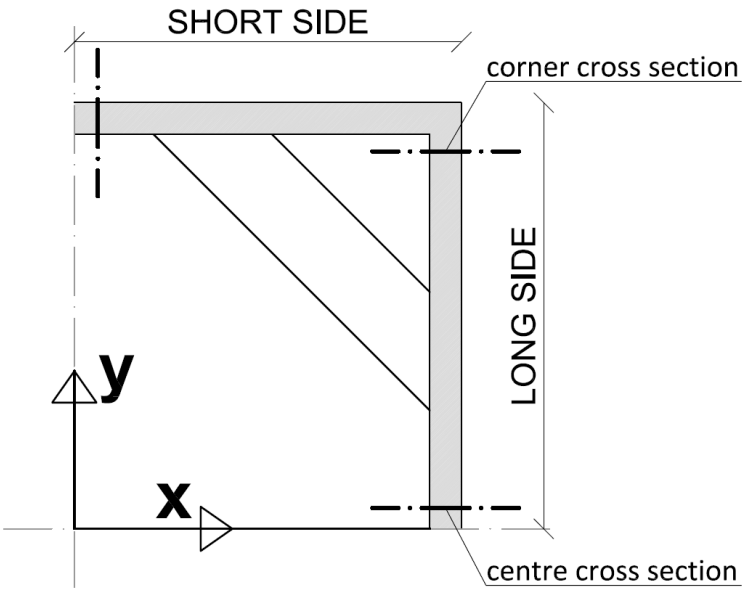

Fig. 16: Schematic overview concerning diaphragm wall outputs

In diagrams presenting the results the cross section is always indicated as shown in Fig. 16.

Possible line cross sections for surface settlement outputs are numbered (Fig. 17). Together with the given number in the head line of the diagram, the section is specified. Each line cross section reaches up to the model boundary.

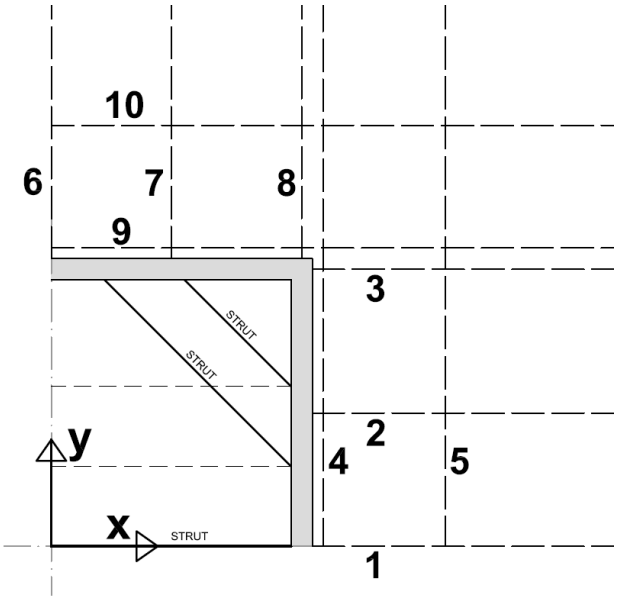

Fig. 17: Schematic overview concerning surface settlement outputs

The basic idea of the abbreviations used in the legends of the diagrams is explained in Fig. 18.

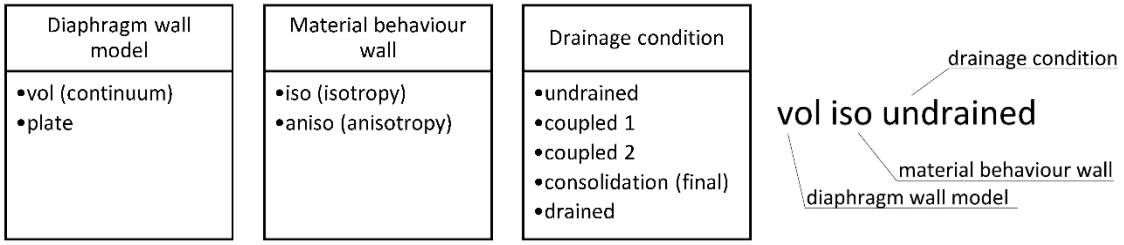

Fig. 18: Abbreviations used in outputs

Bending moments of the wall presented in outputs are named as is Fig. 19.

Fig. 19: Bending moment convention

5.1 Isotropic Continuum Diaphragm Wall

The “isotropic continuum diaphragm wall model” was chosen to serve as reference solution and differences obtained between different modelling options are generally related to the isotropic continuum model.

5.2 Drainage Conditions

During the construction of an excavation the generated excess pore pressures, especially below the excavation level, are negative (suction pore stresses). This leads to an increase in soil strength. The higher the negative excess pore pressures, the lower the resulting wall deformations and stresses as well as surface settlements.

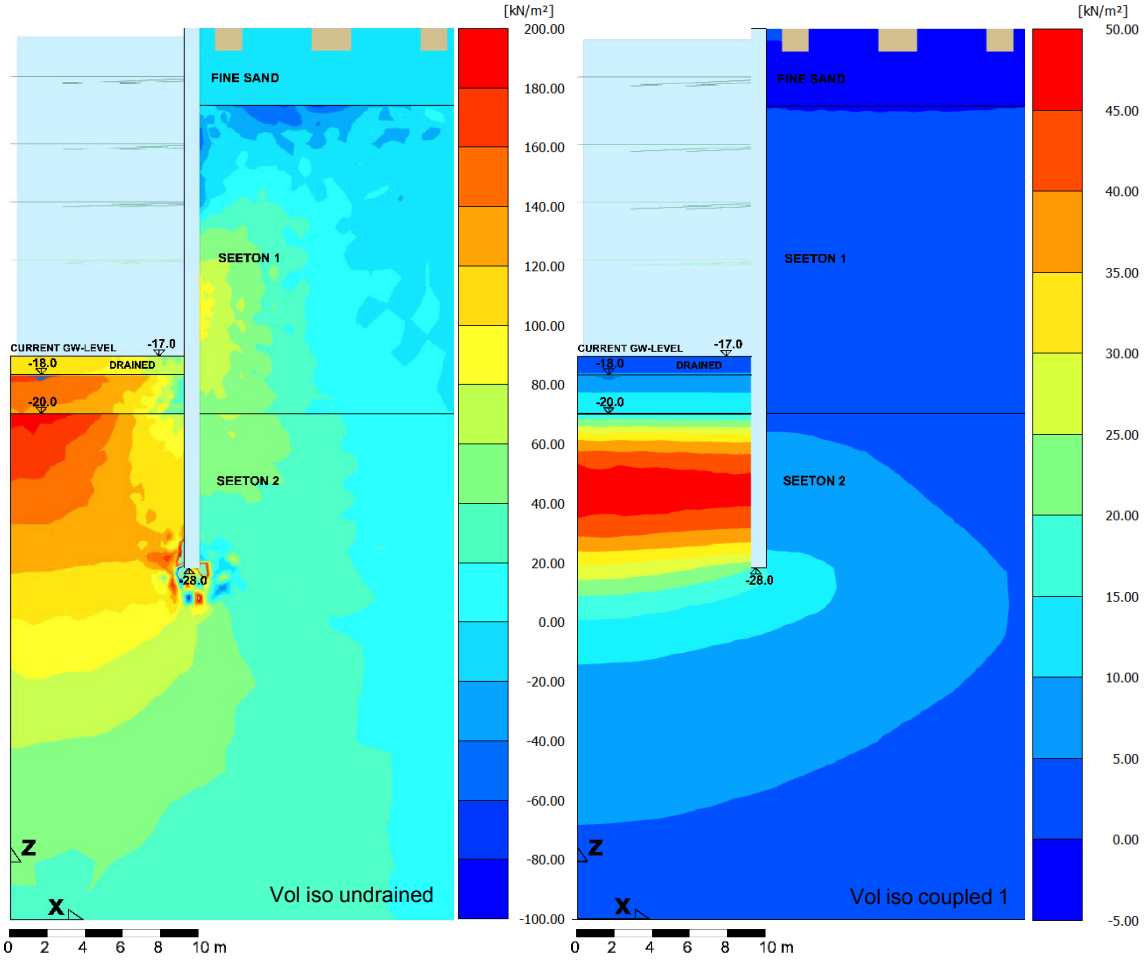

Fig. 20: Excess pore water pressure distribution (negative excess pore pressures are displayed positive)

The left contour plot in Fig. 20 displays the generated excess pore water pressures at the final excavation stage for undrained conditions. The generation of negative excess pore pressures is dependent on the unloading weight, the soil profile (varying soil parameters) and the initial stress state. Due to the change of the soil layer near the final excavation level (z = -20 m), maximum values do not necessarily develop at the drained – undrained condition boundary (current GW-table: z = -18 m) as it is the case for this specific excavation and the soil profile. The maximum negative excess pore pressure $p_{excess,\ max}$ is at about 190 kN/m² and occurs in the centre of the excavation area below the final excavation level at z = -20 m where the 3rd soil layer – Seeton 2 starts. The

decrease of negative excess pore pressures inside the excavation area towards the diaphragm wall can be explained by the increasing influence of wall deformations, as these movements correspond to a horizontal loading condition the soil experiences. In comparison, the soil behind the wall experiences an unloading. This also leads to the generation of negative excess pore pressures behind the wall, especially where largest wall deformations occur.

The maximum remaining negative excess pore pressures for the coupled options (coupled 1 $p_{excess,\ max}$ = 49 kN/m², coupled 2 $p_{excess,\ max}$ = 56 kN/m²) are around 4 times lower as for undrained conditions as shown in Fig. 20, right plot and Fig. 21. Maximum values for both coupled options remain within the Seeton 2 layer, since it has a lower permeability and a larger drainage distance when compared to the Seeton 1 layer.

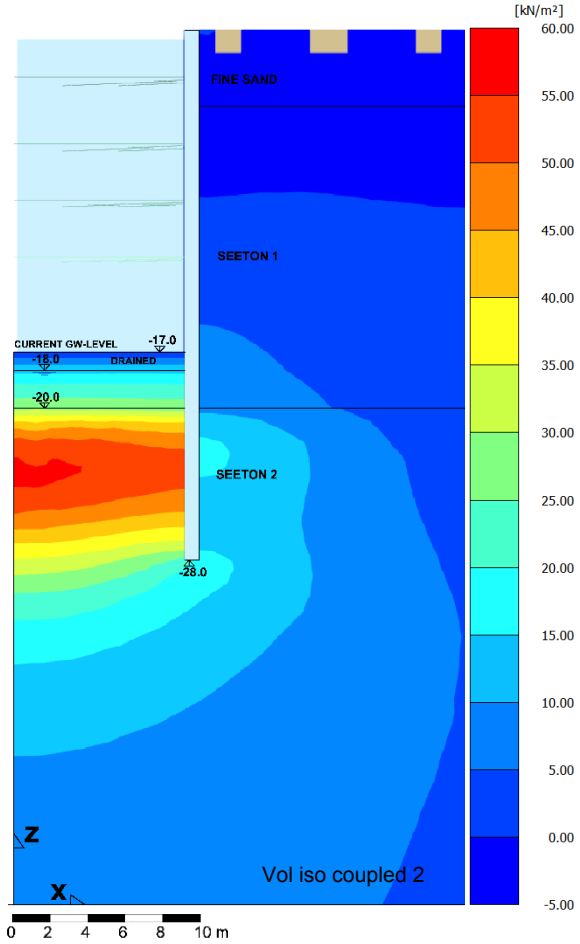

Fig. 21: Excess pore water pressure distribution (negative excess pore pressures are displayed positive)

5.2.1 Diaphragm Wall

Horizontal wall displacements

Fig. 22 shows the difference of the horizontal wall displacements between all drainage conditions considered. As expected, the wall deflections from the coupled calculations (coupled 1, 2) lie between undrained and drained calculations. A striking feature is the difference obtained between the drained and final consolidation results. However, the differences are not very large and can be attributed to the different stress paths followed in the two analyses and different strut forces, see below.

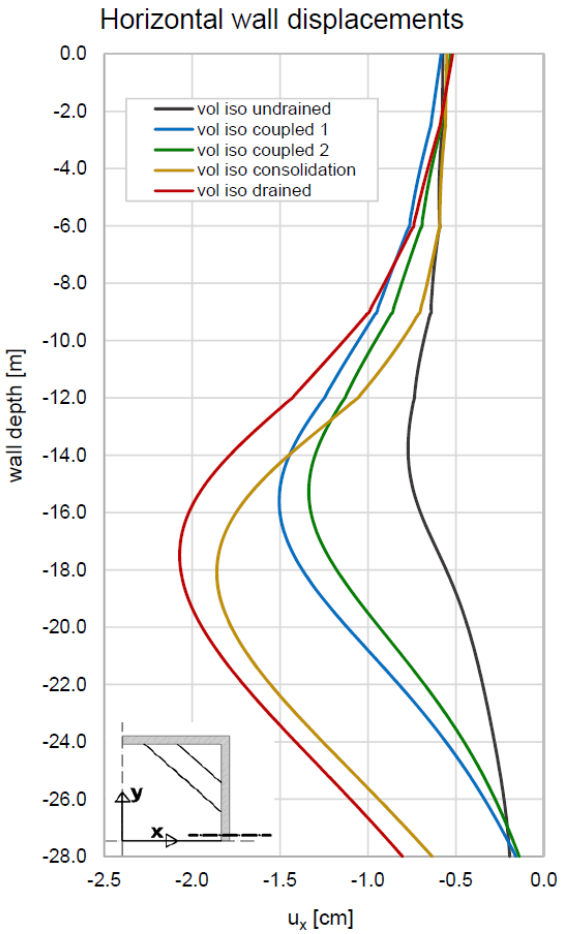

Fig. 22: Horizontal wall displacements

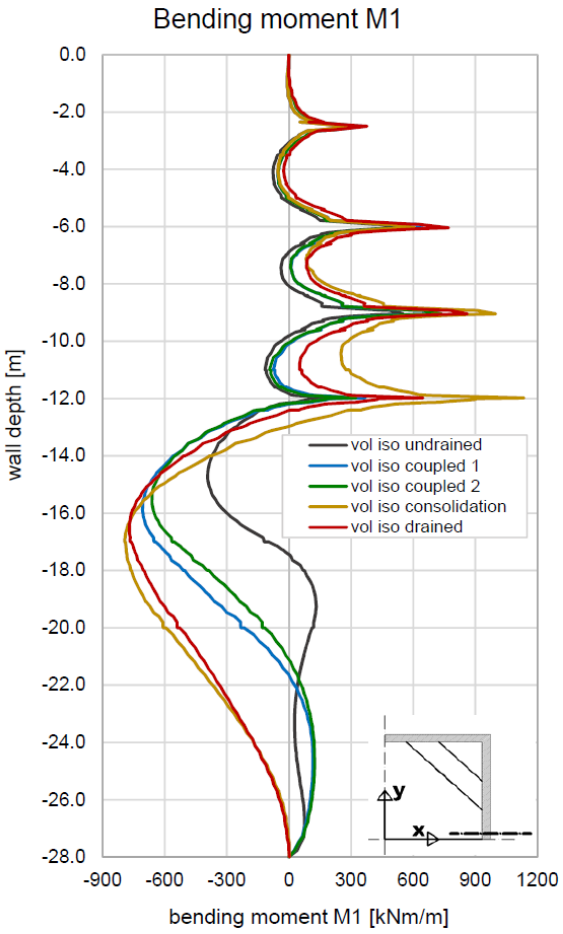

Fig. 23: Bending moments M1

Differences in wall movements

In principal, the characteristic behaviour is governed by the presence of negative excess pore pressures. Moreover, the differences are also affected by the considered phase and consolidation sequences (Fig. 15), since the developed stresses in the struts are influenced by it. The combination of these aspects determines the observed differences between all five options:

- **Difference in maximum wall displacements**
  In general, the increase of soil strength caused by the generation of negative excess pore pressures results in lower wall deformations for undrained conditions than for drained. Thus, the struts are subjected to higher stresses when drained conditions are present compared to undrained ones as seen in Tab. 7.

  The final consolidation step, performed after a complete undrained calculation, leads to the development of additional wall movements induced by the decrease of negative excess pore pressures. Hence, the stresses in the struts increase. Although only the 3rd and 4th strut levels are affected, since additional deformations mainly develop around the final excavation level. As a result, the increased stresses in the last 2 strut levels are higher for the final consolidation option than for the drained one as Tab. 7 indicates. Consequently, the maximum final consolidation wall movements cannot be as high due to the struts, which were installed in previous steps where undrained conditions were present.

- **Difference within the upper part of the wall**
  As seen in the construction phase sequence, the corresponding strut level is always installed after the previous excavation step is finished. Consequently, these struts are not subjected to any load from wall movement before the next step is performed. Hence, the separate strut installation implies that the wall can already develop higher deformations during each excavation step when drained conditions are present when compared to undrained conditions.

The drained and final consolidation graphs show exactly that the main difference is developed within the upper half of the wall. This is absolutely reasonable, because the last strut level is installed at -12 m below the surface.

At the upper part of the wall, the coupled 1 and 2 options show almost equal wall deformations as under drained conditions, since the intermediate consolidation steps (over 2 weeks) are performed before each strut level installation.

Tab. 7: Relative differences of axial forces in the centre struts (related to the undrained condition)

	Axial force N [kN] 1st strut level	relative difference [%]	Axial force N [kN] 2nd strut level	relative difference [%]	Axial force N [kN] 3rd strut level	relative difference [%]	Axial force N [kN] 4th strut level	relative difference [%]
undrained	309		771		958		813	
coupled 1	490	37	1042	26	1156	17	848	4
coupled 2	486	36	974	21	1170	18	816	0
consolidation	311	1	832	7	1287	26	1802	55
drained	358	14	1014	24	1229	22	1338	39

Coupled 1 vs. coupled 2

The coupled 2 option tends to develop lower values as it can be seen in Fig. 22 and Fig. 23. The difference results from the consolidation sequence each option considers and consequently affects the dissipation of negative excess pore pressures below the current excavation level. Since the intermediate consolidations for the coupled 1 option are performed after each excavation step, no support is given by the soil volume excavated when compared to the coupled 2 option, which allows for consolidation while the excavation is in progress. Due to the initially considered excavation level, differing by the current excavation step height when consolidation starts, the remaining negative pore pressures are lower for coupled 1 and higher for coupled 2 conditions as can be observed when comparing Fig. 20, right plot and Fig. 21.

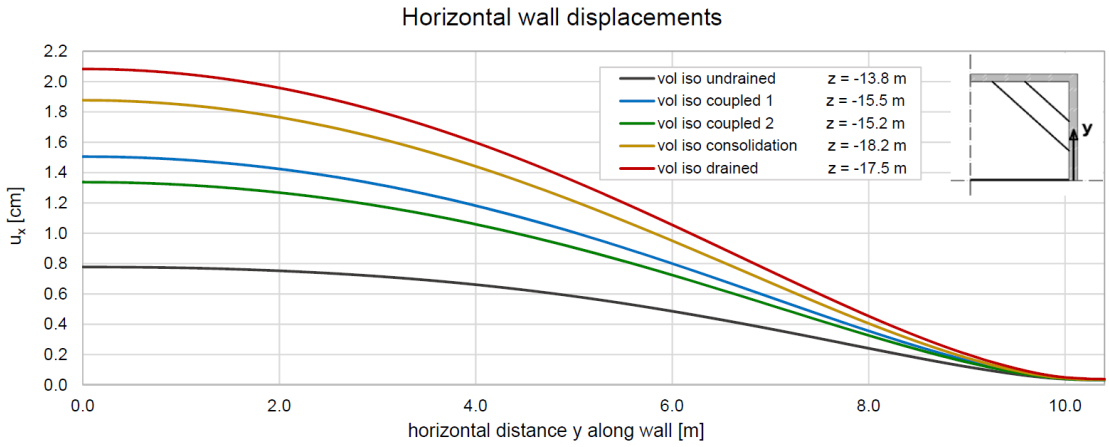

Fig. 24: Horizontal wall displacements along the wall (the horizontal cross section depth z corresponds to the depth where the corresponding maximum wall deformation from Fig. 22 occurs)

Wall deformations at the corner

As expected, the influence of the comparatively stiff corner increases towards the corner, which is shown in Fig. 24. At the wall corner, the different drainage conditions practically have no influence, leading to negligible differences in wall deformations. The horizontal

cross section considered for each drainage condition in Fig. 24, corresponds to the depth where the corresponding wall deformation from Fig. 22 reaches its maximum.

Bending moments M1 - centre

In accordance with wall deflections, undrained bending moments are strongly differing to the other options, whereas the difference among these options is much lower. Especially maximum values around the final excavation level are quite similar (Fig. 23).

The peak values at struts' levels are considered to be unrealistic. Since the modelled connection between node to node anchor and plate element correspond to a single point, the actual area of the strut is neglected. Therefore, these values are not considered in the following comparisons. Nevertheless, the tendency of higher peak values for the final consolidation option at the 3rd and 4th strut levels can be still observed.

Maximum values at the centre of the wall

Tab. 8 presents the maximum values of wall deformations and bending moments M1 of the different drainage conditions considered. The "relative difference" is related to the undrained condition and the percentage of "developed deformation" to the maximum difference obtained between the drained and the undrained option. Latter gives an idea of the influence the consolidation degree has on the different options.

Tab. 8: Relative differences according to maximum values from Fig. 22 and Fig. 23

	max horizontal wall displacements [cm]	relative difference [%]	developed deformation [%]	max bending moment M1 [kNm/m]	relative difference [%]
undrained	0.8			393	
coupled 1	1.5	47	54	708	44
coupled 2	1.3	38	38	663	41
consolidation	1.9	58	85	793	50
drained	2.1	62	100	778	49

As known, excess pore pressure dissipation per time decreases with increasing consolidation degree. This explains the tendency derived for the "developed deformations" in Tab. 8. The coupled calculations reach already 40 - 50 % of the maximum difference in deformations between drained and undrained conditions (1.3 cm), whereas the consolidation time considered for the coupled options corresponds only to 10 weeks and the time needed for a complete excess pore pressure dissipation (final consolidation option) is around 60 weeks.

Bending moments M1 – corner

Concerning the difference in drainage conditions, the same as discussed above applies to the bending moments M1 at the corner, displayed in Fig. 25. The maximum values are around 50 % lower than the ones obtained at the centre (Tab. 8). However, they have a reversed sign. The change of sign near the corner results from the stiff corner connection the isotropic continuum wall model implicates.

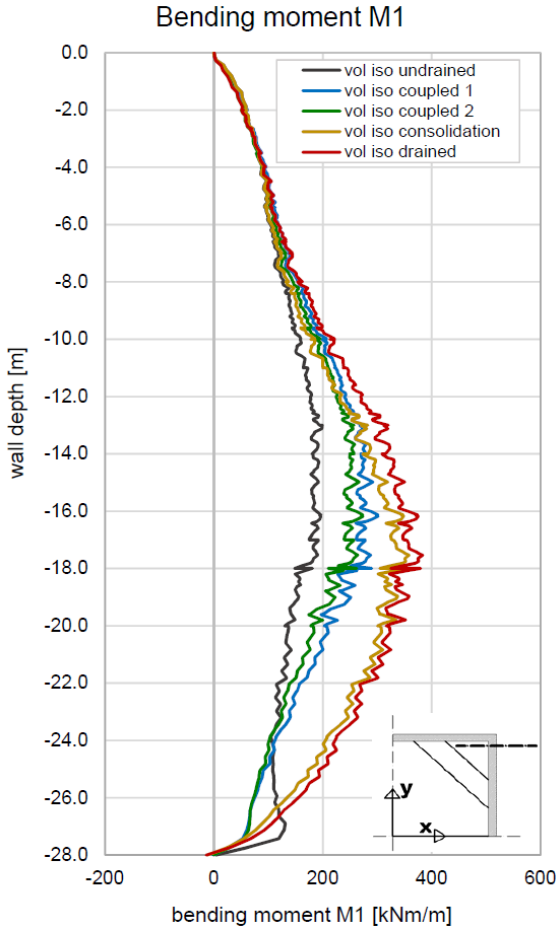

Fig. 25: Bending moments M1

5.2.2 Surface Settlements

The linear settlement distribution where the foundations are situated is caused by the linear elastic material model, which was chosen to model the foundations of adjacent buildings as can be seen in Fig. 26.

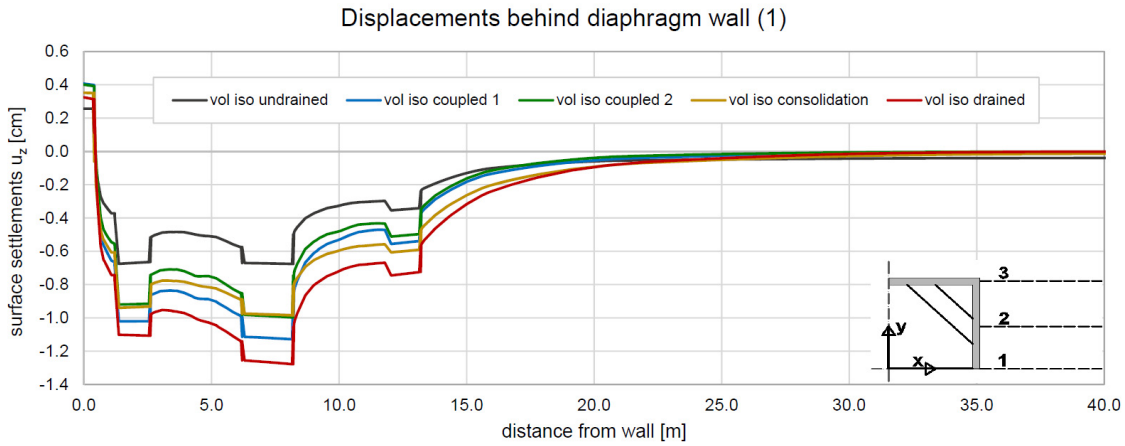

Fig. 26: Surface settlements

With increasing distance of surface loads from the wall, the depth of influenced diaphragm wall regions increases, whereas the impact decreases due to the stress distribution from additional loads in the soil. Therefore, the same tendency as is seen in wall deformations can be perceived when comparing surface settlements of different drainage conditions. The settlements behind the wall correspond with the wall deflections at the upper region, shown in Fig. 26 and Fig. 27, where the coupled calculations develop almost equal or higher settlements than the final consolidation. As the distance from the wall increases, the settlements from the final consolidation option become larger than the coupled ones, corresponding to the same characteristic as observed for wall deformations around the final excavation level.

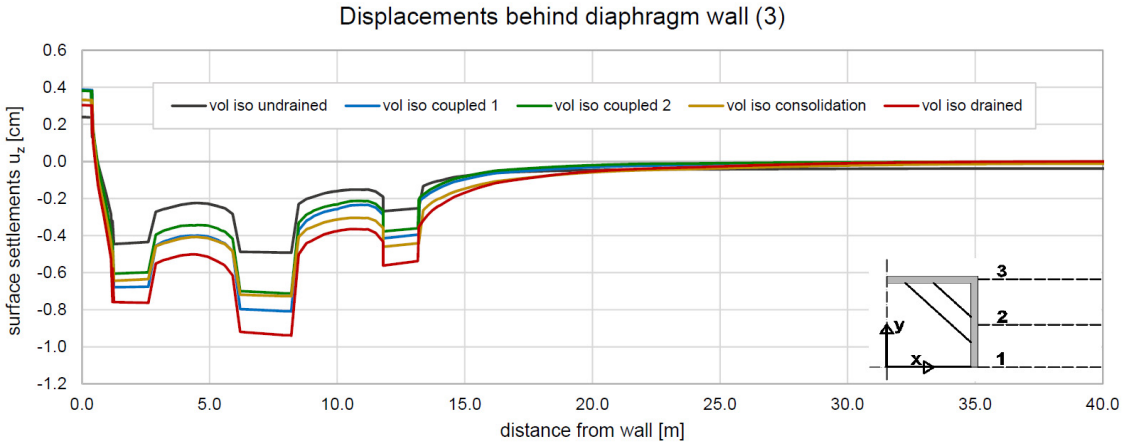

Fig. 27: Surface settlements

Qualitatively spoken, Fig. 26 and Fig. 27 give the same output, whereas the quantitative difference can be explained by the fact that the corner acts stiffer than the centre part of

the wall. This behaviour is obviously illustrated by the surface settlements along the line cross sections 4 and 5 (Fig. 28 and Fig. 29).

Tab. 9: Relative differences according to maximum values from Fig. 26 and Fig. 27

	max surface settlements (centre) [cm]	relative difference [%]	max surface settlements (corner) [cm]	relative difference [%]	relative difference (centre-corner) [%]
undrained	0.7		0.5		29
coupled 1	1.1	36	0.8	38	27
coupled 2	1.0	30	0.7	29	30
consolidation	1.0	30	0.7	29	30
drained	1.3	46	0.9	44	31

The absolute maximum values at a distance of approximately 7.5 m from the wall, given in Tab. 9, are of low relevance for general considerations, since they are strongly dependent on the applied surface loads and the foundation dimensions. However, the influence of the different drainage conditions is still obtained by the relative differences, related to the undrained condition.

Interestingly, the relative difference of the different drainage conditions between centre and corner settlements stays consistent at around 30 % (last column in Tab. 9). This confirms, that the mechanism induced by the stiff corners is not influenced by the different drainage conditions and consequently affects each condition equally. Apart from that, the relative difference depends on the present surface loads and foundation dimensions (see also 5.5 Building vs. Green Field). Therefore, these value has to be treated with caution.

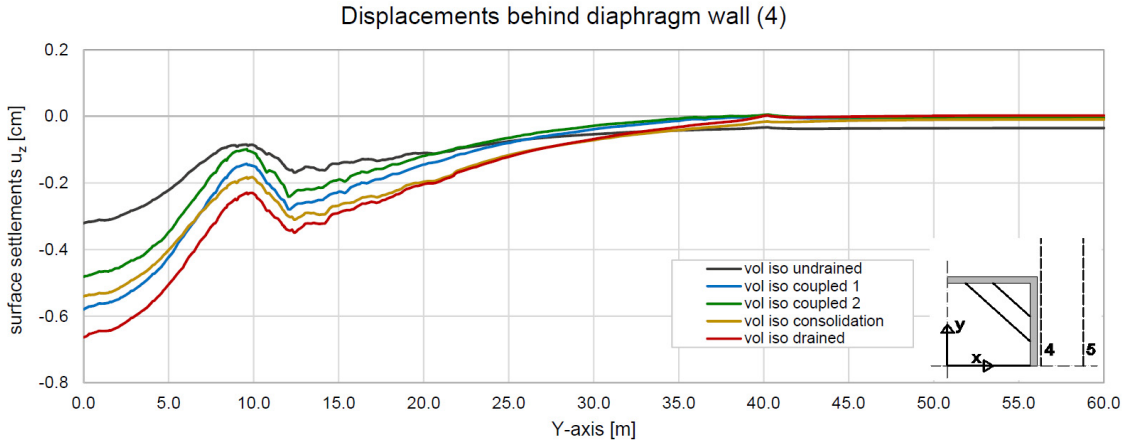

Fig. 28: Surface settlements

Since line cross section 4 is positioned 40 cm next to the outer edge of the actual wall and the plate foundation, the surface settlements are influenced by the wall and the linear elastic modelled plate foundation (Fig. 28). Up to y = 10 m the influence of the wall on

the settlements remains constant. With further distance from the wall, the influence of the wall decreases, leading to an increase in settlements (starting around y = 10 m). The almost linear settlement distribution from y = 12 – 22 m arises, since the influence of the linear elastic modelled plate foundation is still present. In comparison, the graphs along section 5, at a distance of 5 m from the wall (Fig. 29) are not affected any more.

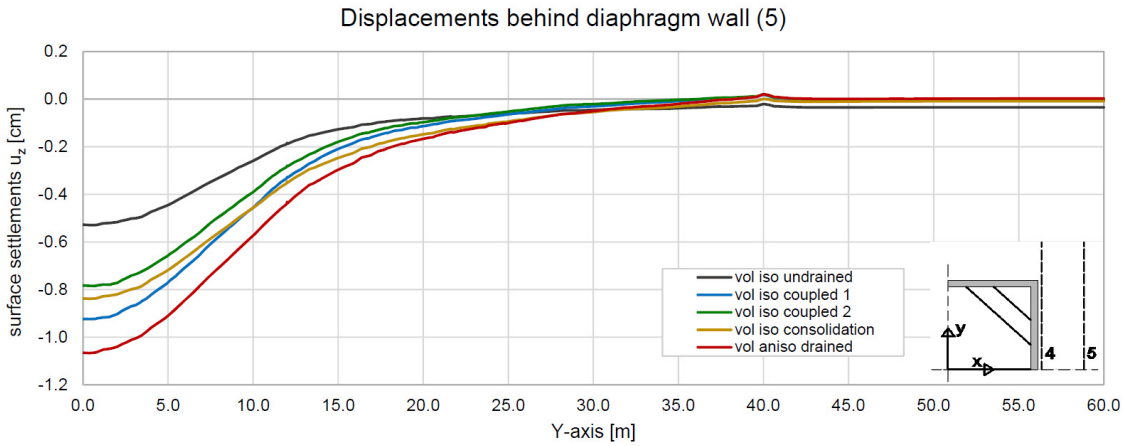

Fig. 29: Surface settlements

5.3 Continuum vs. Plate Modelling

For reasons of clarity, only the coupled 1 option is generally used to represent the differences obtained between different analyses performed. Further illustrations from other drainage conditions can be found in the appendix. As already briefly mentioned in 4.8: Performed Calculations, the coupled 2 option represents more closely drainage conditions that are expected in situ. However, the coupled 1 option has the advantage of being able to review consolidation analysis independently from other influences, since consolidation performance is completed separately after each excavation step and as has been shown in the previous chapter, differences to option coupled 2 are not significant.

In principal, plate modelling implicates higher wall deformations, bending moments and surface settlements. The circumstance that the plate has only a virtual thickness is the governing factor leading to the differences observed between continuum and plate models. In terms of modelling, the horizontal axes of the plate and continuum wall must be identical, in order to obtain comparable results. Therefore, the excavation volume and the distance to adjacent buildings are slightly increased when compared to the continuum wall model.

As the calculation results point out, the difference between continuum and plate modelling is also affected by anisotropic material properties. Therefore, relative differences between anisotropic continuum and plate wall models are presented as well. A more detailed discussion between isotropy and anisotropy is made in chapter 5.4.

5.3.1 Diaphragm Wall

For isotropic coupled 1 conditions, plate models develop slightly higher wall deflections and bending moments M1 as the comparisons in Fig. 30 and Fig. 31 illustrate. From this point of view, the difference seems negligible, whereas it becomes more relevant with increasing consolidation degree, as Tab. 10 indicates.

Moreover, the difference is also dependent on the considered material model (isotropy, anisotropy). When comparing Tab. 10 and Tab. 11, it can be seen that the relative differences from isotropic and anisotropic wall models differ at around 10 % in wall deformations for all drainage conditions. Bending moments M1 are slightly higher influenced by anisotropy.

In principal, the resulting differences are mainly caused by the mobilized shear forces acting between the wall and the adjacent soil due to the excavation. Concerning the continuum model, these shear forces, multiplied by the horizontal distance between axis and wall surface, produce a reverse moment. Consequently, the moment induced by the resulting earth pressure behind the wall is reduced, leading to lower wall deformations when compared to the plate model. Since plate elements have no actual thickness, the reverse acting moment cannot be generated. This conclusion is also made in Zdravkovic et al. (2005), where the same characteristic behaviour between plate and continuum modelling was obtained.

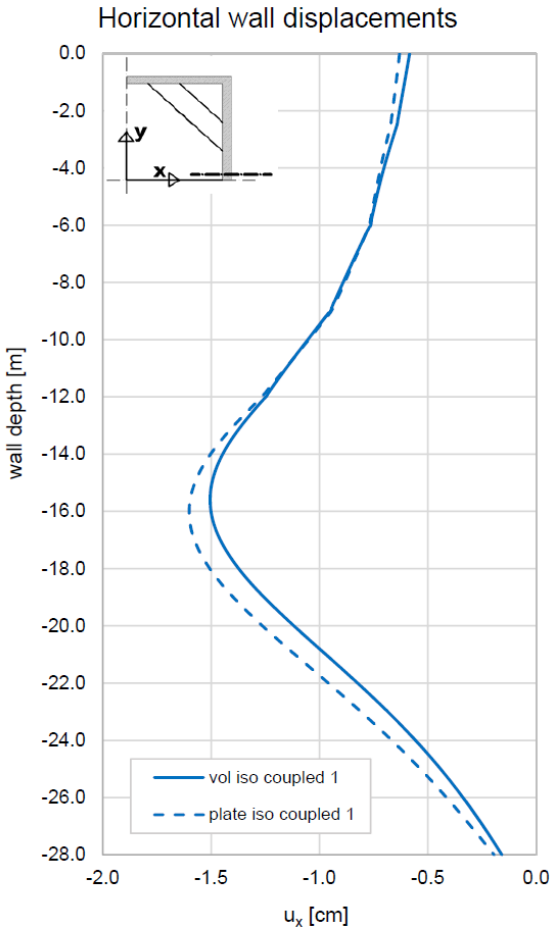

Fig. 30: Horizontal wall displacements

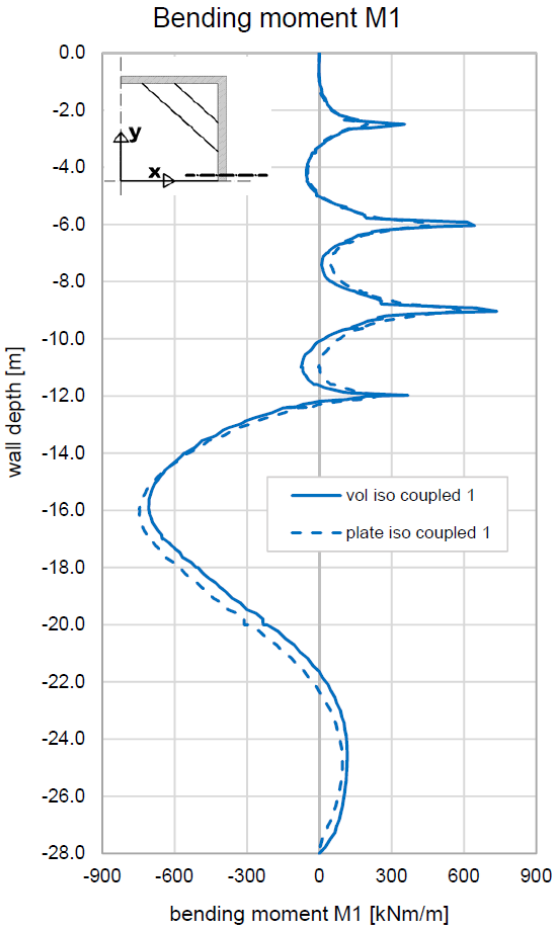

Fig. 31: Bending moments M1

Another influence occurs from the horizontal shear forces right below the diaphragm wall, mobilized by the wall movement. These resisting shear forces are only considered for continuum walls and partly contribute to the difference in bottom wall movements. The difference is negligible for the coupled 1 option, however it increases with further consolidation (see also Fig. 61, appendix).

Tab. 10: Relative differences of maximum wall deformations and bending moments M1 between isotropic continuum and plate models at the centre of the wall

	max horizontal wall displacements [cm]		relative difference [%]	max bending moment M1 [kNm/m]		relative difference [%]
	continuum	plate		continuum	plate	
undrained	0.8	0.8	0	393	408	4
coupled 1	1.5	1.6	6	708	746	5
coupled 2	1.3	1.5	13	663	703	6
consolidation	1.9	2.1	10	792	825	4
drained	2.1	2.4	13	778	824	6

Tab. 11: Relative differences of maximum wall deformations and bending moments M1 between anisotropic continuum and plate models at the centre of the wall

	max horizontal wall displacements [cm]		relative difference [%]	max bending moment M1 [kNm/m]		relative difference [%]
	continuum	plate		continuum	plate	
undrained	0.8	0.9	11	372	419	11
coupled 1	1.9	2.2	14	765	937	18
coupled 2	1.6	1.8	11	680	819	17
consolidation	2.6	3.2	19	954	1171	19
drained	3.0	4.0	25	942	1185	21

The bending moments M2 in Fig. 32 are obtained at a wall depth of 15.5 m, this approximately corresponds to the depth of maximum wall deformations. The main difference between plate and continuum modelling is obtained at the corner, also caused by the geometric difference. While the moment of the continuum wall starts to decrease along the actual wall thickness, the moment obtained from the plate still increases until the centre point of the corner (y = 10.4 m) is reached. The same characteristics seen in the connections between node to node anchors and plate elements are obtained for plate to plate connections. Since they do not account for an actual connection area at the corner, unrealistic peak values occur.

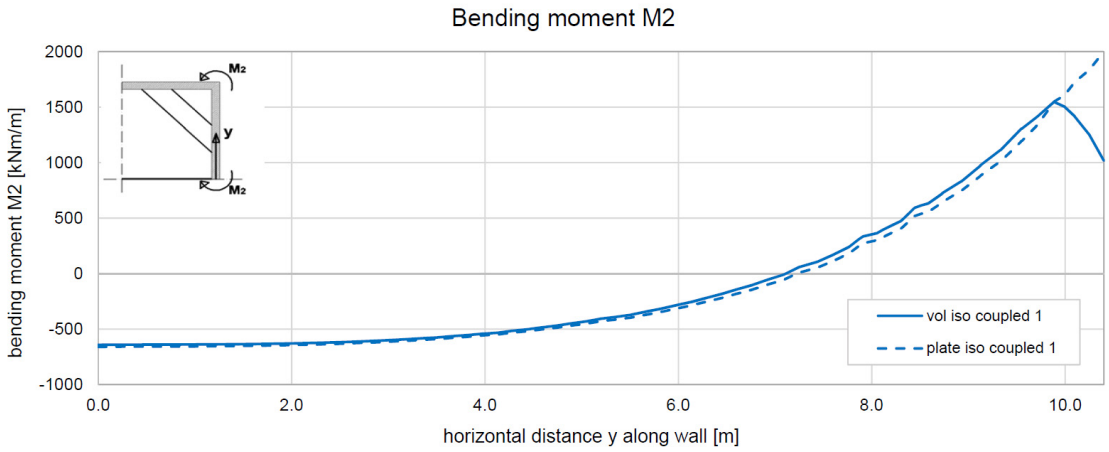

Fig. 32: Bending moments M2 at z = -15.5 m

The relative difference for isotropic material models at the centre of M2, given in Tab. 12, is also quite low. This is the same order as obtained for bending moments M1.

Tab. 12: Relative difference according to maximum values from Fig. 32 at the centre of the wall

	max bending moment M2 [kNm/m]	relative difference [%]
continuum	-641	3
plate	-660	

5.3.2 Surface Settlements

The resulting settlements right next to the wall (within 1 m from the wall) are strongly influenced by the horizontal offset between the wall surfaces of 40 cm (Fig. 33). As long as the surface settlements are influenced by the wall, this great difference remains. Therefore, plate modelling leads to much higher settlements within the immediate surroundings of the wall (Fig. 35).

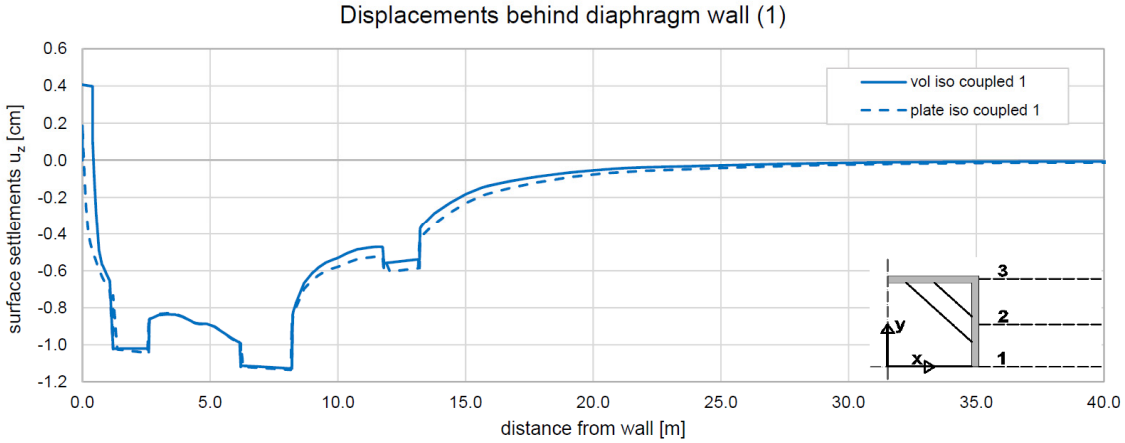

Fig. 33: Surface settlements

With increasing distance from the wall, the difference is determined by the difference obtained between wall deformations, since settlements and wall movements are related to each other. Therefore, the difference in surface settlements is also quite small for isotropic conditions and practically irrelevant (Fig. 33 and Fig. 34) for the coupled 1 option. Compared to the wall deformations, the surface settlements from the plate model are less affected by anisotropy, leading to lower variations than 10 % (Tab. 27, appendix). This characteristic can be explained by the small variations between both options at the upper half of the wall.

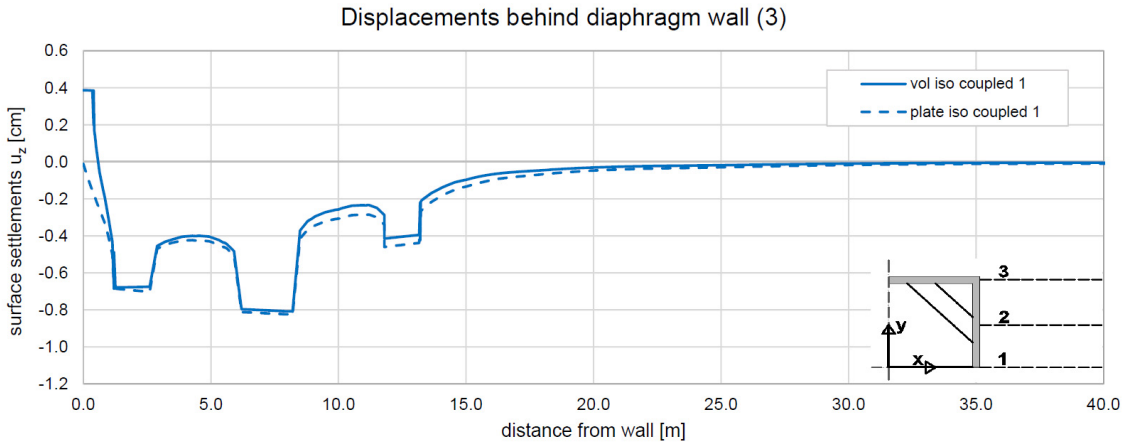

Fig. 34: Surface settlements

The difference obtained from Fig. 35 within the first 12 m along line cross section 4 only appears due to the outer wall surfaces offset of 40 cm in horizontal direction.

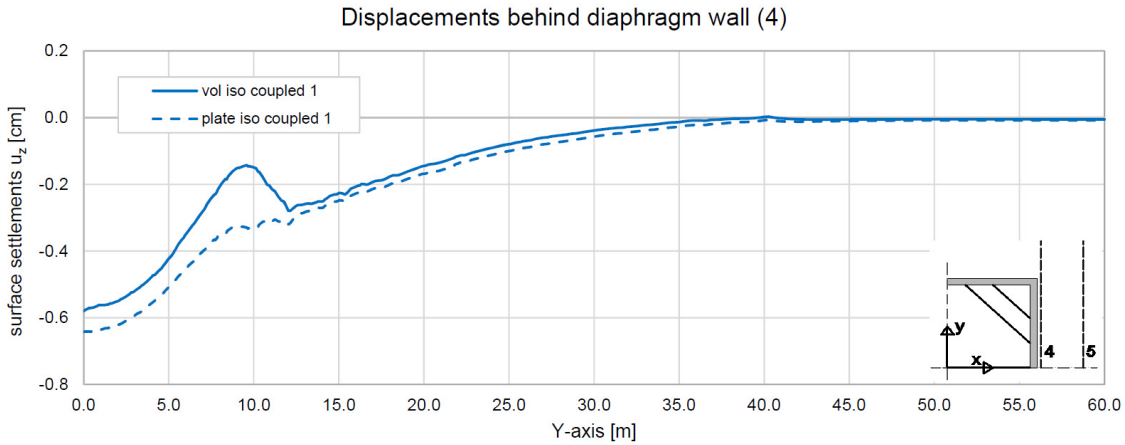

Fig. 35: Surface settlements

5.4 Isotropic vs. Anisotropic Modelling

As already discussed, a realistic modelling approach of the wall is of interest and importance. Due to the construction joints, anisotropic behaviour is expected rather than isotropic. The resulting structural forces at the corner – especially bending moments – are a bit misleading, even for anisotropic conditions. This can be explained by the assumptions made for anisotropic materials, which consider the horizontal bending stiffness to be 25 % of the vertical one. Since the bending stiffness in the horizontal direction determines the ability to develop restraining torques at the corner, the qualitative behaviour of the corner is strongly influenced by it.

5.4.1 Rigid Corner Connection

Diaphragm wall

When anisotropy is applied instead of isotropy, horizontal wall deformations increase (Fig. 36). The wall deformations are affected the most.

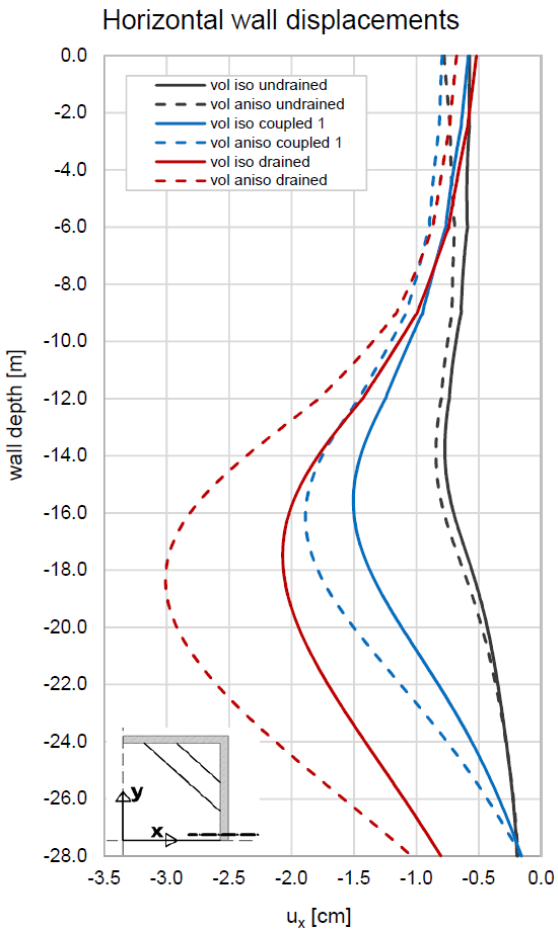

Fig. 36: Horizontal wall displacements

The relative differences increase towards the drained option and vary between 0 – 40 %. Therefore, the obtained values from comparisons between isotropy and anisotropy, apply strictly to the considered drainage condition. Whereas the maximum wall deformations of undrained conditions are basically not affected at all, the coupled 1 options differ at about half a centimetre and the drained ones already at about one centimetre.

Due to the qualitatively similar wall deformation curvatures in the middle of the wall, the corresponding bending moments M1 (Fig. 37) do not show as high relative differences as obtained for wall deformations (approximately 20 % lower, undrained option excluded).

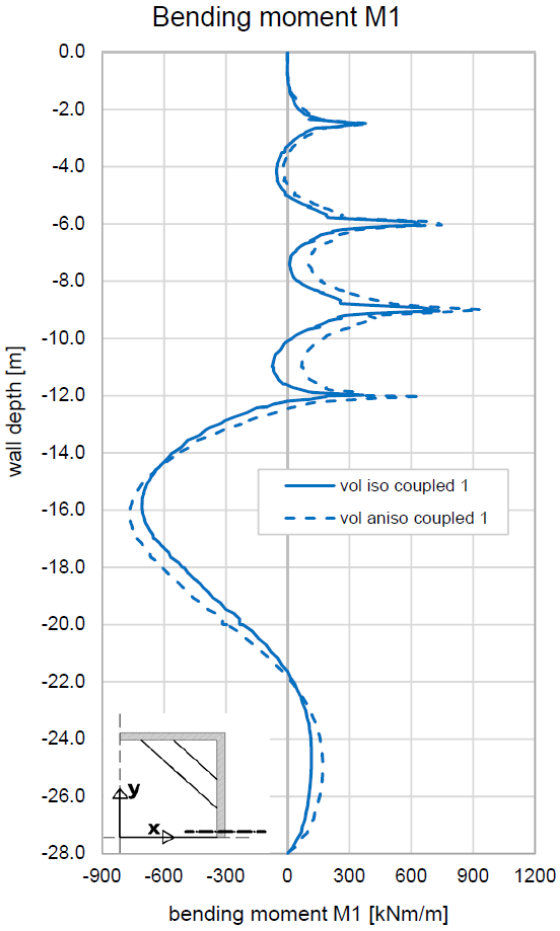

Fig. 37: Bending moments M1 (center)

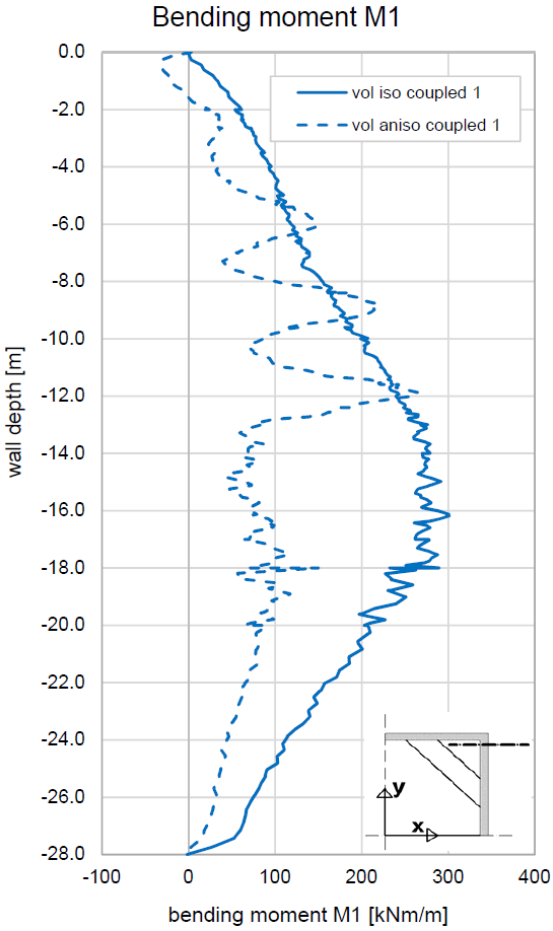

Fig. 38: Bending moments M1 (corner)

Since isotropic continuum wall modelling implicates a very stiff corner connection, high restraining torques can develop around the corner. Concerning bending moments M1 at the corner (Fig. 38), Zdravkovic et al. (2005) indicate that such bending moments require differently reinforced corner sections when compared to centre sections, which is usually not done in practice. Anyway, the joints decisively limit the bending stiffness in horizontal direction, which lower the stiff behaviour of the corner. Consequently, such high restraining torques in vertical direction are very unlikely. Compared to the isotropic model, the bending moments M1 at the corner (Fig. 38) around the final excavation level are much lower (approximately 60 – 70 %) for anisotropic conditions. This confirms that the anisotropic models consider for a more realistic wall behaviour, also around the corner parts of the wall.

The effect of the waling´s, integrated in the anisotropic wall model, can also be observed clearly in Fig. 38. Only the parts of the wall where the waling´s are situated can develop moments which are as high or even slightly higher as isotropic ones. Since stiffer mediums attract forces, the tendency towards higher peak values is reasonable.

However, the peak values only appear due to the simplified modelling approach in order to consider the waling´s. Therefore, these maximum values are not relevant for comparisons.

Tab. 13: Relative differences of maximum wall deformations and bending moments M1 between isotropic and anisotropic continuum models at the centre of the wall

	max horizontal wall displacements [cm]		relative difference [%]	max bending moment M1 [kNm/m]		relative difference [%]
	isotropic	anisotropic		isotropic	anisotropic	
undrained	0.8	0.8	0	393	372	5
coupled 1	1.5	1.9	27	708	765	8
coupled 2	1.3	1.6	23	663	680	3
consolidation	1.9	2.6	37	793	954	20
drained	2.1	3.0	43	778	942	21

The corresponding relative differences between isotropic and anisotropic plate modelling are presented in Tab. 14. The differences developed by the plate model are increased when compared to the continuum model at around 10 – 20 % as can be observed when comparing Tab. 13 and Tab. 14. This tendency corresponds with results shown in chapter 5.3 and indicate that the mechanisms, governing the differences between continuum and plate modelling, become more relevant for anisotropy.

Tab. 14: Relative differences of maximum wall deformations and bending moments M1 between isotropic and anisotropic plate models at the centre of the wall

	max horizontal wall displacements [cm]		relative difference [%]	max bending moment M1 [kNm/m]		relative difference [%]
	isotropic	anisotropic		isotropic	anisotropic	
undrained	0.8	0.9	13	408	419	3
coupled 1	1.6	2.2	38	746	937	26
coupled 2	1.5	1.8	20	703	819	17
consolidation	2.1	3.2	52	825	1171	42
drained	2.4	4.0	67	824	1185	44

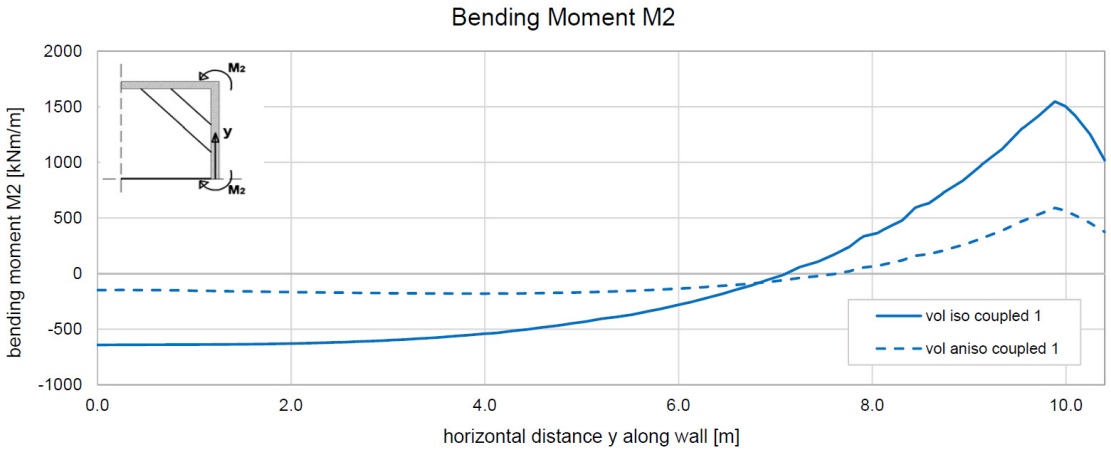

Fig. 39: Bending moments M2 at z = -15.5 m

The plotted bending moments M2 in Fig. 39 and the corresponding maximum values in Tab. 15 are obtained at a wall depth of -15.5 m. The lowered bending stiffness in the horizontal direction limits the development of bending moments M2 along the wall. The relative differences obtained at the centre and the corner wall sections are similar to the ones for the bending moments M1 at the corner (60 – 70 %). Due to the remaining horizontal bending stiffness, the bending moment changes sign towards the corner. Compared to the bending moments M1, the magnitude of the bending moments M2 at the corner is quite high.

Tab. 15: Relative differences according to maximum values from Fig. 39

	max bending moment M2 [kNm/m]		relative difference [%]	
	centre	corner	centre	corner
isotropic	-641	1548	72	62
anisotropic	-180	590		

The reduction of the axial stiffness in horizontal direction of about 75 % leads to a difference in horizontal axial forces N2 of approximately 50 % as the graphs in Fig. 40 show. The decrease of the horizontal axial force N2 for anisotropic conditions results in an increase of horizontal wall deformations along the wall, induced by the lowered horizontal axial stiffness in order to consider for joint closure. The maximum difference between horizontal wall deformations along the wall is <1 mm. Therefore the lowered axial stiffness has no influence on the investigated behaviour of diaphragm walls. This does not necessarily apply to different excavations and anisotropic material assumptions, which is why the assumed ratio between horizontal and vertical Young´s moduli cannot be lowered randomly.

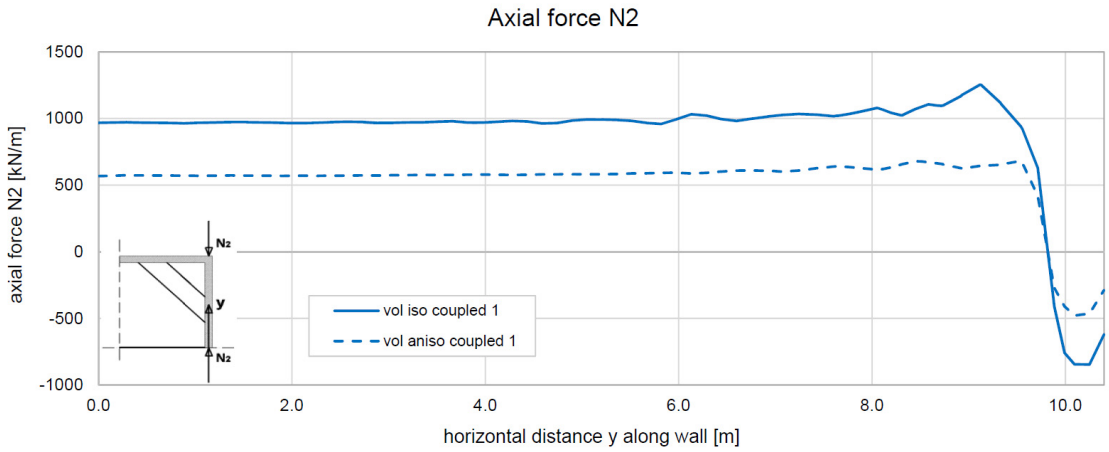

Fig. 40: Axial force N2 at z = -15.5 m

The axial force developments around the corner in Fig. 40 give a wrong impression. Due to the joints, such tensile stresses cannot occur in reality. They only arise from the linear elastic material model of the wall, which allows for tensile stresses to develop.

Surface settlements

As expected, the anisotropic model develops higher surface settlements, corresponding to larger wall deformations as can be observed from Fig. 41 and Fig. 42. Due to the influence of the stiff corner, the settlements decrease towards the corner, whereas the relative difference between centre and corner remains constant and shows the same order as obtained for isotropic conditions (Tab. 16).

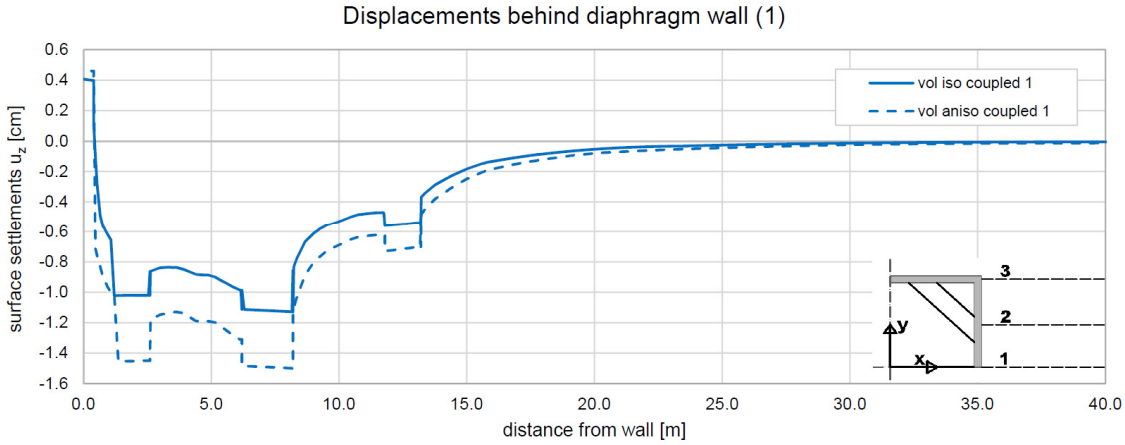

Fig. 41: Surface settlements

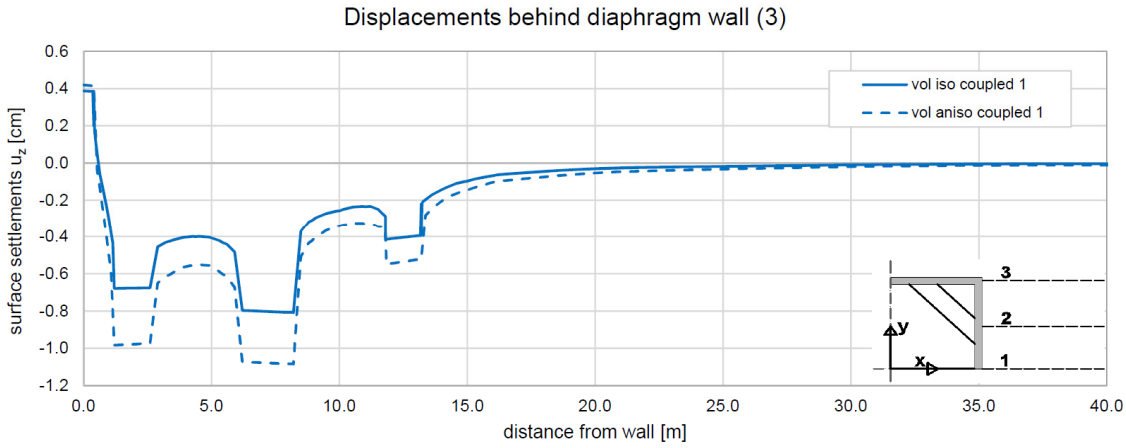

Fig. 42: Surface settlements

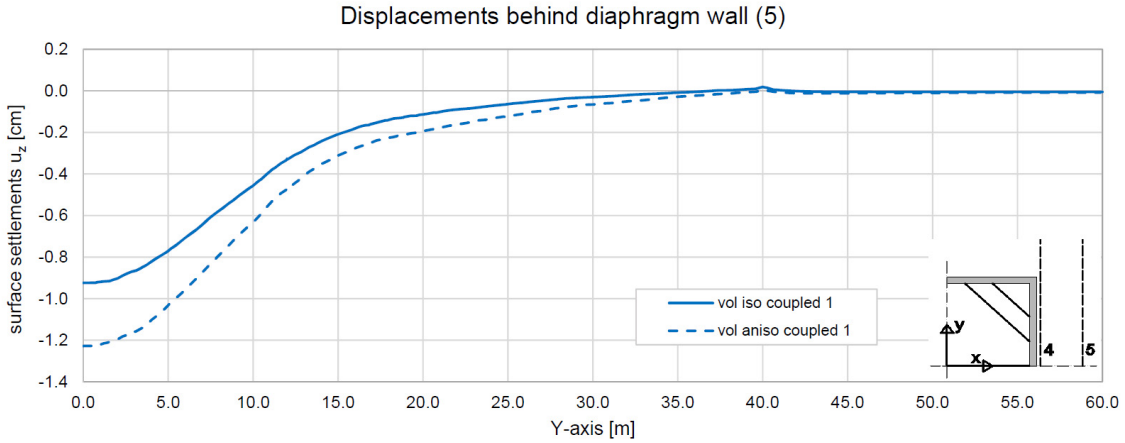

Fig. 43: Surface settlements

Besides the difference between isotropic and anisotropic behaviour obtained from Fig. 43 and Fig. 44, another influence can be observed when comparing the diagrams. Apart from the linear settlement distribution the plate foundation implies (x = 0 – 10 m; Fig. 44), the magnitude of settlements behind the short side (line section 10), at a distance of 5 m from the wall, are much lower when compared with the long side (line section 5). This indicates the influence different wall lengths, surface loads and support measures (no middle strut considered at the short side of the wall) have. However, the main difference results from the different surface loads applied behind each wall side.

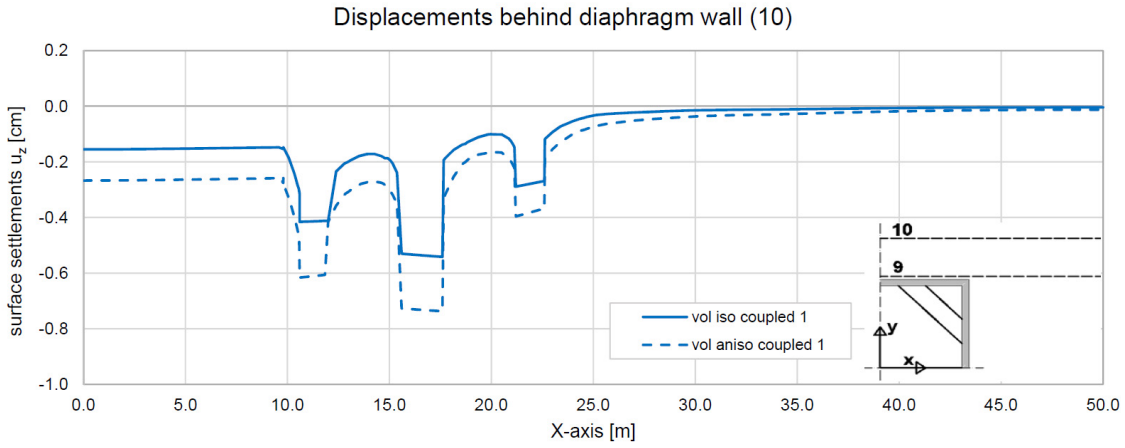

Fig. 44: Surface settlements

The relative differences in surface settlements between isotropic and anisotropic behaviour are less dependent on the present drainage conditions than wall deformations and bending moments M1 as indicated in Tab. 16. Since maximum surface settlements arise at a distance of approximately 7 m to the wall, they correspond better with wall deformations at the upper regions of the wall. The comparatively low variation between the drainage conditions becomes quite clear from Fig. 36. Head distortions are similar for each drainage condition due to the decreasing influence of negative excess pore pressures around the upper parts of the wall.

Tab. 16: Relative differences of maximum surface settlements between isotropic and anisotropic continuum models

	max surface settlements (centre) [cm]		relative difference [%]	max surface settlements (corner) [cm]		relative difference [%]	relative difference (centre-corner) [%]	
	isotropic	anisotropic		isotropic	anisotropic		isotropic	anisotropic
undrained	0.7	0.9	29	0.5	0.6	20	29	33
coupled 1	1.1	1.5	36	0.8	1.1	38	27	27
coupled 2	1.0	1.3	30	0.7	0.9	29	30	31
consolidation	1.0	1.4	40	0.7	1.0	43	30	29
drained	1.3	1.8	38	0.9	1.4	56	31	22

5.4.2 Hinged Corner Connection

Within the scope of modelling approaches available, plate connections can also be modelled as hinged connections. In Zdravkovic et al. (2005) isotropic hinged plate models give similar results as the anisotropic rigid plate models. In terms of modelling, such a simplification is of interest, which is why hinged connections are investigated as well. The hinge model also gives an idea of the effect both corner connections have on the wall behaviour at the centre of the wall.

By modelling a hinged connection, the development of restraining torques is completely prevented. Therefore, it is assumed that the hinge model simulates the actual behaviour of the corner too soft.

Diaphragm wall

Due to the hinged connection, the corner is acting much softer than compared to the rigid connection. As a result, the difference in wall deformations, bending moments as well as surface settlements for equal material properties is quite high. The comparatively soft response of the corner also explains why the hinge plate models are less affected by anisotropy than the rigid plate models, as can be seen in Fig. 45 and Fig. 47.

The difference for isotropic hinge and rigid plate models is as high as the difference between anisotropic and isotropic plate models. Therefore, isotropic hinge and anisotropic rigid plate models develop the same wall deformations and bending moments M1 at the centre of the wall. This corresponds with the outcome presented in Zdravkovic et al. (2005).

Since the isotropic rigid plate model has no relevance, the relative differences in Tab. 17 are always related to the anisotropic rigid plate model. As already observed from Fig. 45, the maximum wall deformations between the anisotropic rigid and isotropic hinge plate models are practically the same. When considering anisotropy for the hinge model as well, the difference increases and varies between 10 – 30 %, depending on the drainage condition. Again, undrained conditions are almost not affected by the differing modelling approaches.

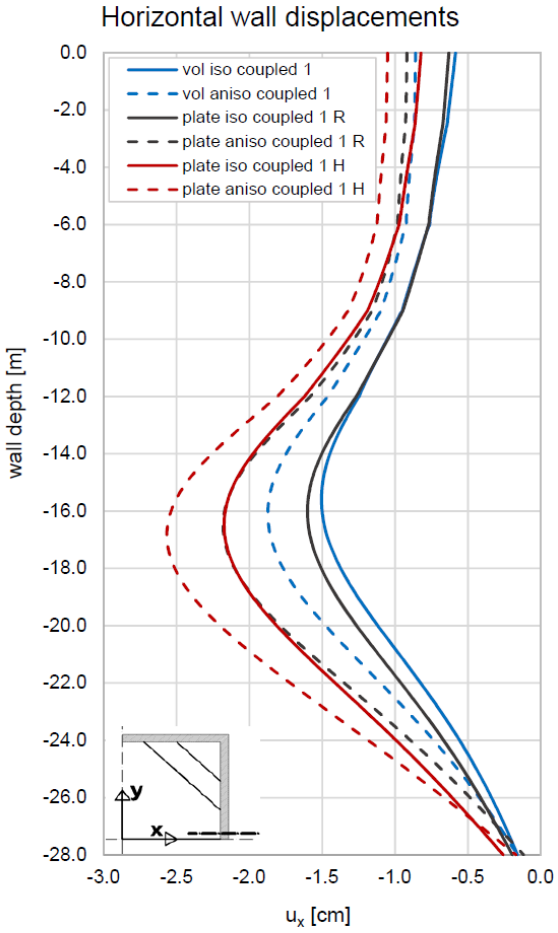

Fig. 45: Horizontal wall displacements

Tab. 17: Relative differences of maximum wall deformations between rigid and hinged modelled corner connections at the centre of the wall

	max horizontal wall displacements [cm]				relative difference [%]		
	continuum	plate			continuum - aniso plate rigid	plate (aniso rigid - iso hinge)	plate (aniso rigid - aniso hinge)
	aniso	aniso/rigid	iso/hinge	aniso/hinge			
undrained	0.8	0.9	0.9	1.0	11	0	11
coupled 1	1.9	2.2	2.2	2.6	14	0	18
coupled 2	1.6	1.8	1.8	2.1	11	0	17
consolidation	2.6	3.2	3.1	3.9	19	3	22
drained	3.0	4.0	3.9	5.2	25	3	30

The differences in the load transfer onto the centre struts between the anisotropic continuum and plate model as well as the anisotropic rigid and isotropic hinge plate model are quite small (Tab. 18). This results from the similar wall deformations and bending moments M1 obtained at the centre of the wall between these options. However, the difference in axial forces increases for the corner struts, especially between rigid and hinged models as can be seen in Tab. 19 (the axial strut forces given in Tab. 19 correspond to the shorter corner struts). Due to the hinged connection, the hinge plate

model develops higher wall deformations at the corner when compared to the rigid plate or continuum model as shown in Fig. 46.

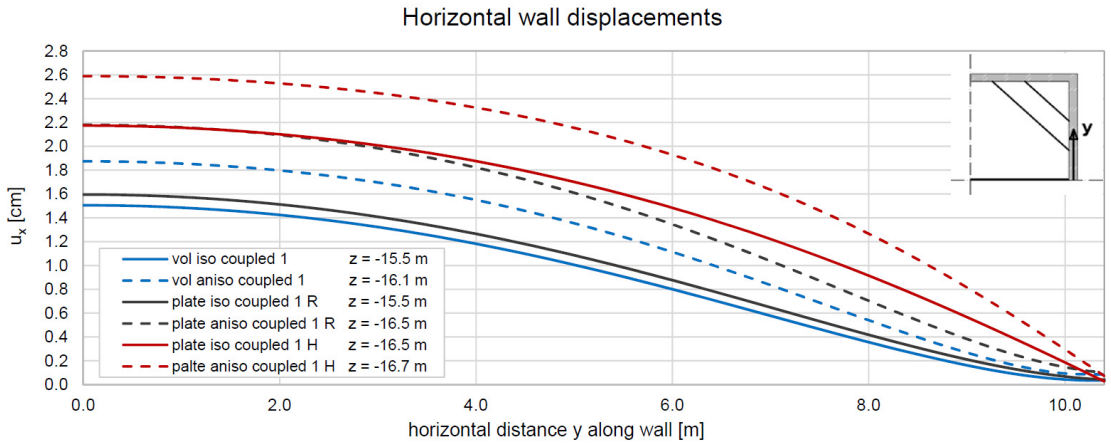

Fig. 46: Horizontal wall displacements along the wall (the horizontal cross section depth z corresponds to the depth where the corresponding maximum wall deformation from Fig. 45 occurs)

Tab. 18: Relative differences of axial forces in the centre struts between rigid and hinged modelled corner connections for coupled 1 conditions

	Axial force N [kN]				relative difference [%]		
	continuum	plate			continuum-plate rigid	plate (aniso rigid - iso hinge)	plate (aniso rigid - aniso hinge)
Centre strut	aniso	aniso/rigid	iso/hinge	aniso/hinge			
1 st strut level	466	461	482	464	1	5	1
2nd strut level	1097	1003	1022	1037	9	2	3
3rd strut level	1294	1203	1271	1325	8	6	10
4th strut level	1072	1125	1116	1282	5	1	14

Tab. 19: Relative differences of axial forces in the corner struts (shorter ones) between rigid and hinged modelled corner connections for coupled 1 conditions

	Axial force N [kN]				relative difference [%]		
	continuum	plate			continuum-plate rigid	plate (aniso rigid - iso hinge)	plate (aniso rigid - aniso hinge)
Corner strut	aniso	aniso/rigid	iso/hinge	aniso/hinge			
1 st strut level	388	463	735	737	16	59	59
2nd strut level	1147	1346	1943	2021	15	44	50
3rd strut level	1498	1991	2831	3083	25	42	55
4th strut level	1647	2272	2803	3495	28	23	54

In principal, the same behaviour as for wall deformations at the centre is also obtained for bending moments M1 (Fig. 47). The relative difference between isotropic hinge and anisotropic rigid plate model is negligible and the difference for anisotropic conditions is half as high (5 – 15 %) (Tab. 20) as in wall deformations.

As expected, bending moments M1 at the corner are significantly affected by the hinged connection. As a result, the bending moments have a reversed sign when compared to

the other options. As seen in Fig. 48, the difference between the isotropic and anisotropic hinge model is quite small due to the great influence the hinged connection implies.

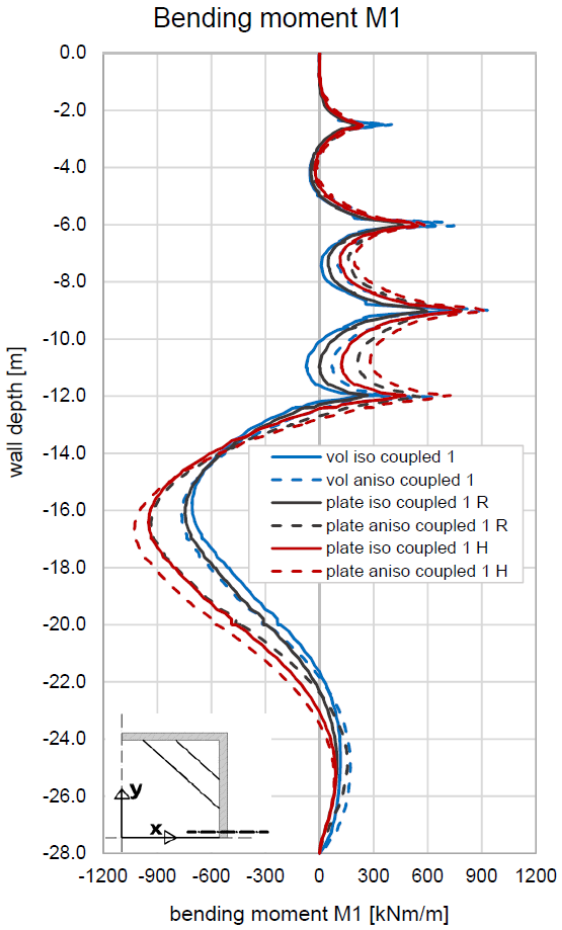

Fig. 47: Bending moments M1 (center)

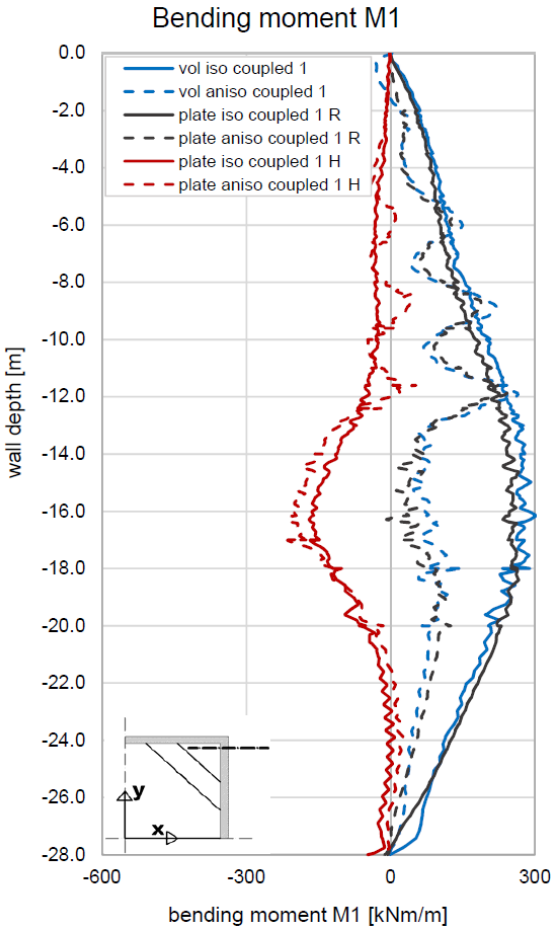

Fig. 48: Bending moments M1 (corner)

Tab. 20: Relative differences of maximum bending moments M1 between rigid and hinged modelled corner connections at the centre of the wall

	max bending moment M1 [kNm/m]				relative difference [%]		
	continuum	plate			continuum - aniso plate rigid	plate (aniso rigid - iso hinge)	plate (aniso rigid - aniso hinge)
	aniso	aniso/rigid	iso/hinge	aniso/hinge			
undrained	372	419	460	453	11	10	8
coupled 1	765	937	950	1029	18	1	10
coupled 2	680	819	831	868	17	1	6
consolidation	954	1171	1095	1315	19	6	12
drained	942	1185	1154	1388	21	3	17

Concerning the horizontal bending moments M2 in Fig. 49 at the centre of the wall, the hinge models develop similar values as the corresponding rigid models with same material properties. Towards the corner, they start to develop in the opposite direction compared the rigid models. Maximum bending moments are obtained between centre and corner.

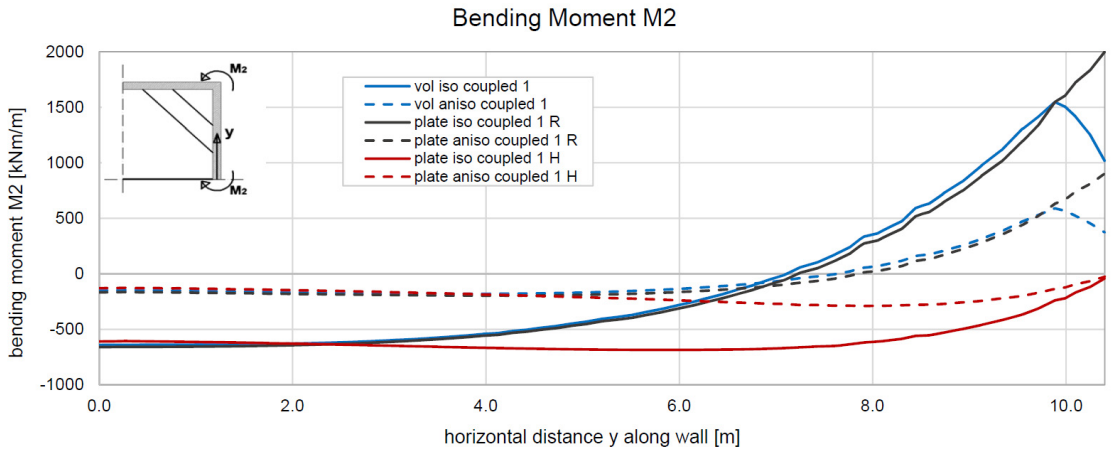

Fig. 49: Bending moments M2 at z = -15.5 m

One disadvantage is that hinged connections can only be modelled between plate elements. Consequently, the difference between plate and continuum wall models is not known. However, it is assumed that the actual differences tend to be similar to the relative differences obtained between anisotropic continuum and plate modelling (Tab. 11) than to the relative differences resulting from isotropic conditions (Tab. 10).

Surface settlements

Due to the interaction between wall deformations and surface settlements near the wall, the same as for horizontal wall deformations can be concluded for surface settlements (Fig. 50 and Fig. 51).

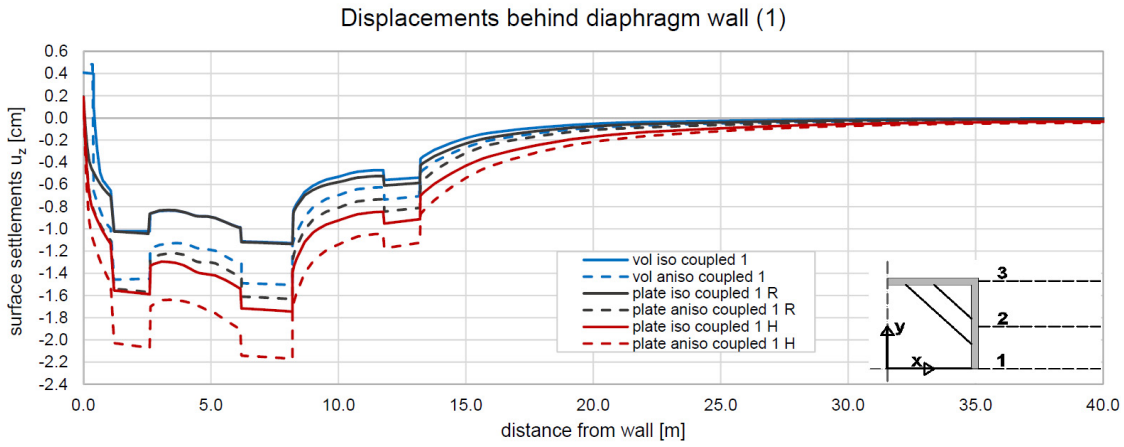

Fig. 50: Surface settlements

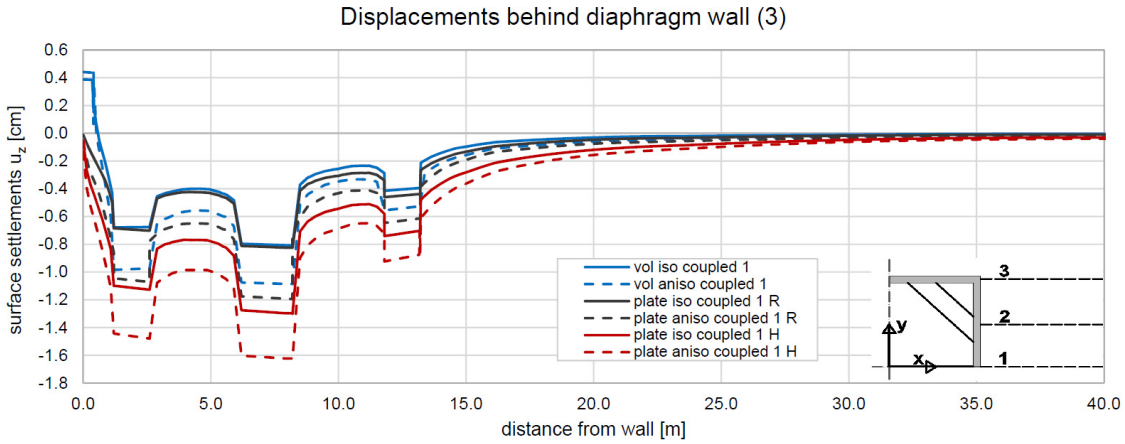

Fig. 51: Surface settlements

5.5 Building vs. Green Field

In order to get a sense of the influence of adjacent buildings on results, the comparison between “building” and “free field” is made. As the name already explains, the free field option considers a free surface where no loads are applied. The main difference between the two options occurs due to the additional stresses induced by adjacent buildings and their foundations. Since displacements, resulting from surface loads are reset to zero, only remaining stresses are considered. The surface loads assumed behind the short side of the wall are quite small in comparison to the ones behind the long side. By coincidence, the load applied behind the short side is similar to the weight of the replaced soil volume. This leads to negligible additional stresses induced by this load, which is why the difference between the two options at the short side results only from the linear elastic modelled plate foundation.

5.5.1 Diaphragm Wall

Long side

The wall deformations of the two variations differ mainly at the upper half of the wall, especially at the first few meters (see Fig. 52). Since the first strip foundation is positioned quite close to the diaphragm wall (Fig. 1), the highest additional stresses occur within the first few meters behind the wall. As a result, the building option develops comparatively high head distortions of the wall. With increasing depth, additional stresses decrease and consequently the difference in wall deformations as well. Hence, maximum bending moments at the final excavation stage are quite similar (Fig. 53).

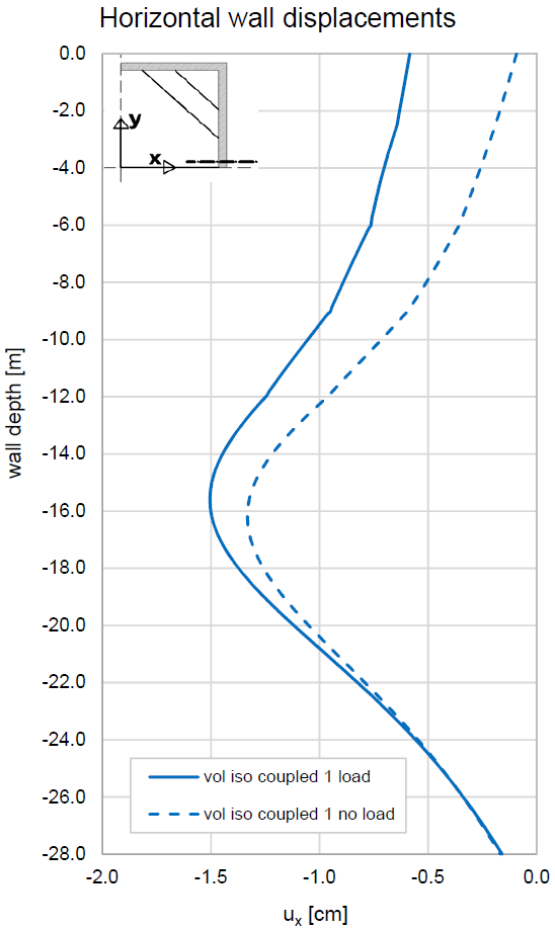

Fig. 52: Horizontal wall displacements

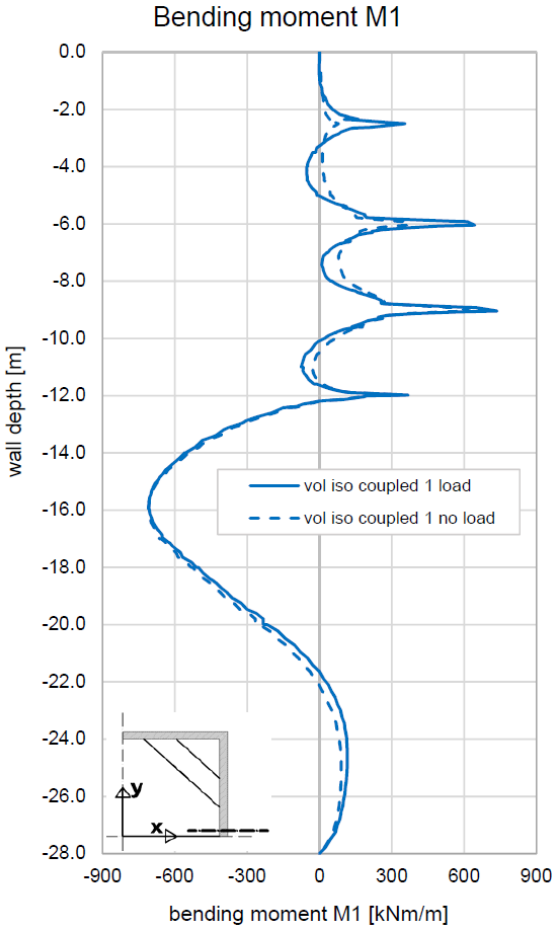

Fig. 53: Bending moments M1

As the deformation graphs and the relative differences (Tab. 21) show, head distortions are more critical, when additional loads are applied right next to the excavation.

Tab. 21: Relative differences according to maximum values from Fig. 52 and Fig. 53 between building and free field option

	max horizontal wall displacements [cm]		relative difference [%]		max bending moment M1 [kNm/m]	relative difference [%]
	head	max	head	max		
building	0.6	1.5	83	11	708	0
free field	0.1	1.3			710	

Short side

As already mentioned, the resulting additional stresses behind the short side of the wall are almost none. Hence, the differences between the two options, as pictured in Fig. 54 and Fig. 55, are negligible.

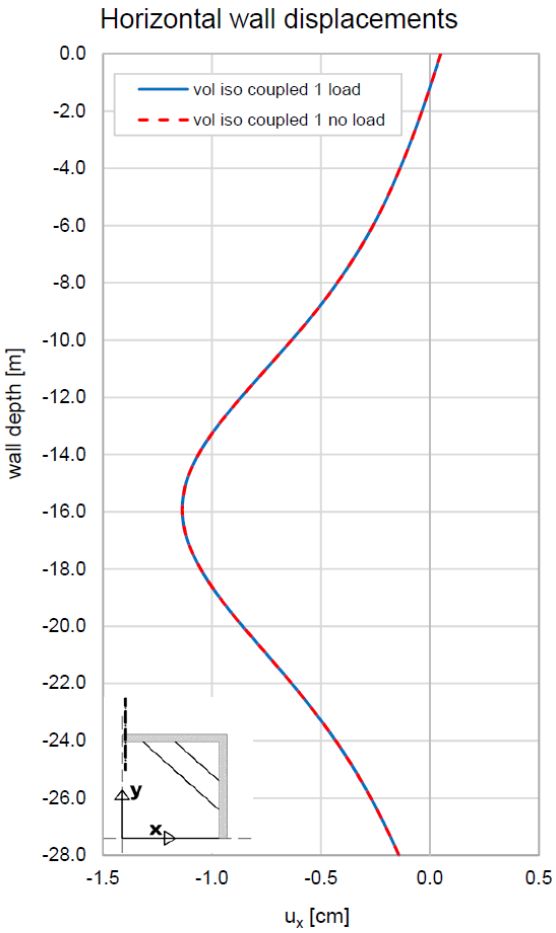

Fig. 54: Horizontal wall displacements

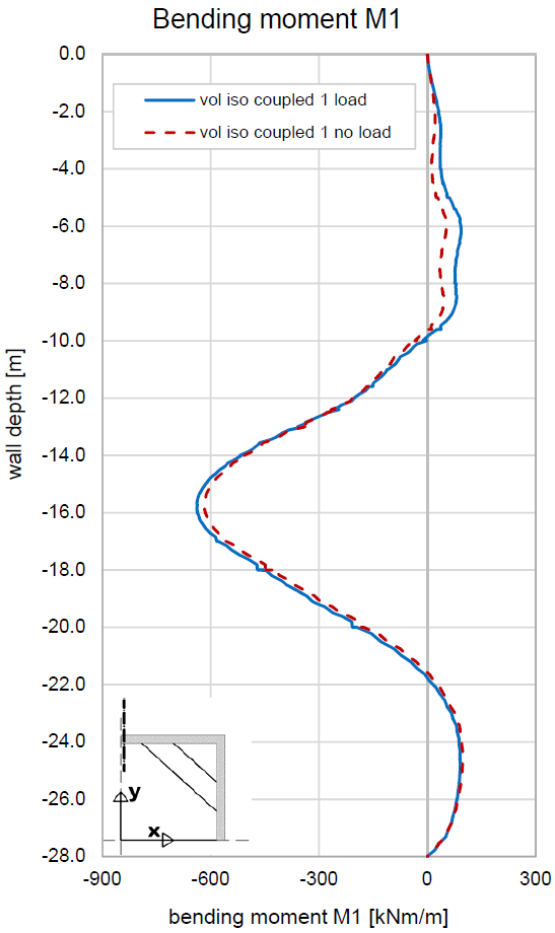

Fig. 55: Bending moments M1

5.5.2 Surface Settlements

The difference obtained in surface settlements is governed by the linear elastic modelled foundations as well as the additional load, representing adjacent buildings. The difference on the long side is mainly governed by the high loads the strip foundations transfer into the soil. Behind the short side, surface settlements are only influenced by the distributing effect of the linear elastic foundations, as the plate foundation does not induce any relevant additional stresses.

Maximum settlements behind the centre part of the wall occur a bit closer when no load is applied (horizontal distance ~ 5 m), compared to the building option where maximum settlements are developed below the middle strip foundation.

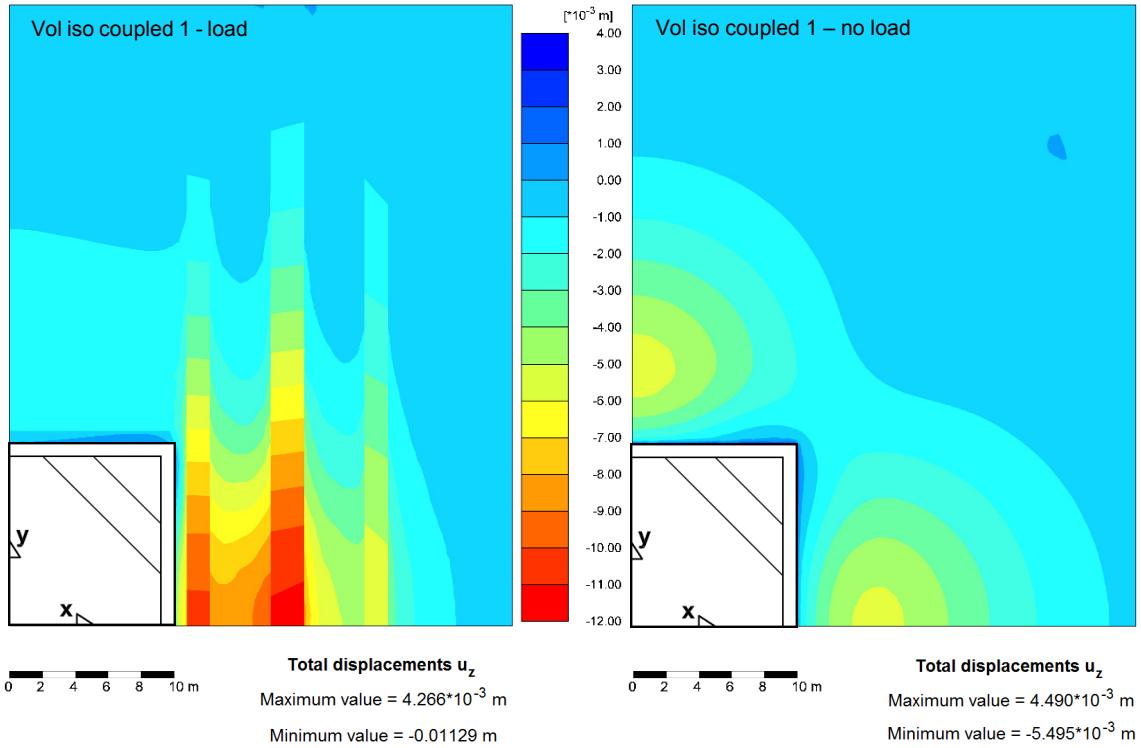

Fig. 56: Comparison of surface settlements between the two surface load conditions

For a better illustration of the affected area behind the excavation, surface settlement shadings are displayed in Fig. 56. As can be seen in the right plot, the developed settlements behind both sides are quite similar. This is reasonable, as the excavation is almost quadratic and the strut support measures differ only at the middle strut, which is considered for the long side. The effect of a stiffer system behaviour towards the corner, leading to lower surface settlements, can be observed as well.

Long side

The wall deformations that developed due to the surface loads are mainly dependent on the magnitude of the remaining additional stresses in the soil. Since the surface settlements are similarly influenced as wall deformations higher values are obtained for the building option as can be observed in Fig. 57 and Fig. 58.

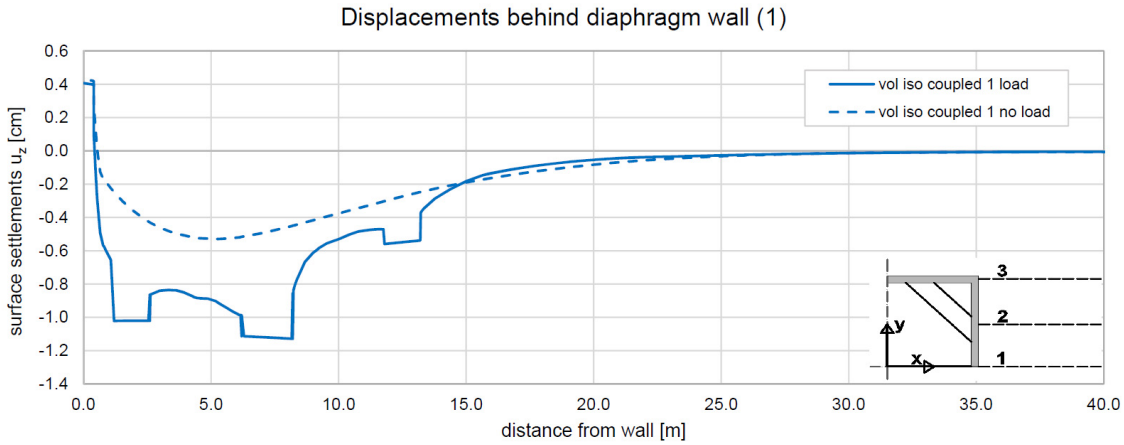

Fig. 57: Surface settlements

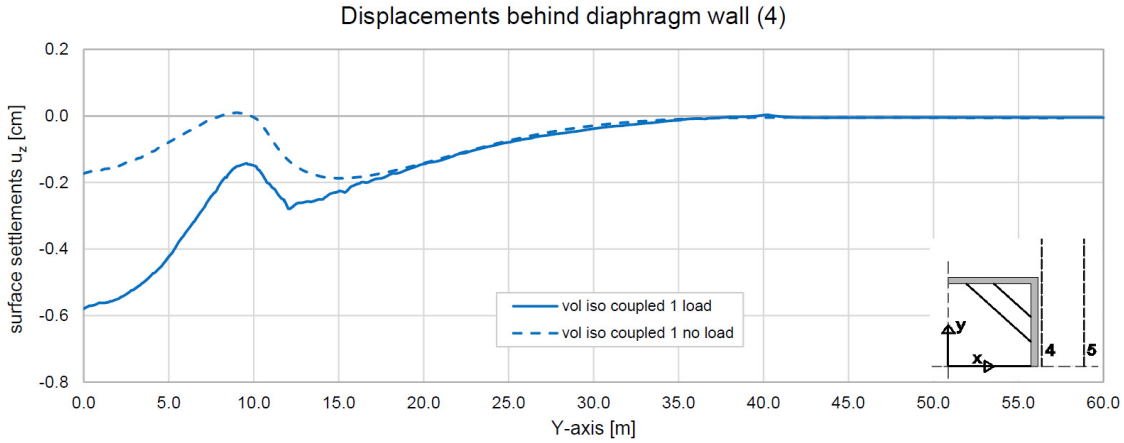

Fig. 58: Surface settlements

The load conditions also influence the decrease in surface settlements towards the corner, since the difference is influenced by the present surface loads and foundations. Although the building option develops higher settlements than the free field option the relative difference between centre and corner settlements increases up to 60 % (Tab. 22) when no surface loads are applied. This can be explained by the more concentrated settlement trough behind the centre part of the wall for the free field option compared to the building option. The latter is strongly influenced by the linear elastic modelled foundations. Since the settlements are linearly distributed over the entire foundation, regions beyond the influenced range of the excavation are affected as well. Fig. 56 illustrates this influence quite clearly.

Tab. 22: Relative differences according to maximum values from Fig. 57 between building and free field option

	max surface settlements (centre) [cm]	relative difference [%]	max surface settlements (corner) [cm]	relative difference [%]	relative difference (centre-corner) [%]
building	1.1	55	0.8	75	27
free field	0.5		0.2		60

Short side

The comparison between the two options shows that the maximum settlements for the loading case are lower than the ones generated by the no load option (Fig. 59 and Fig. 60). Again, this difference is caused by the influence of the stiff foundation elements.

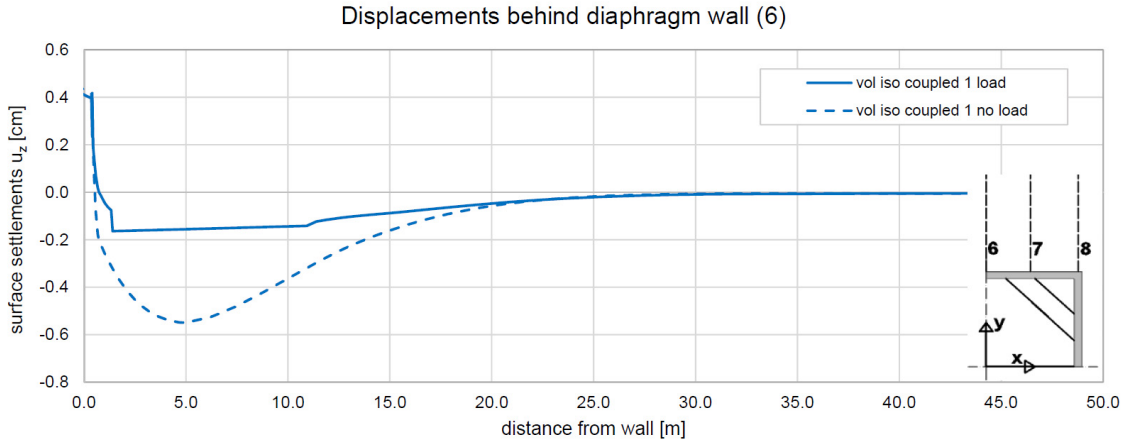

Fig. 59: Surface settlements

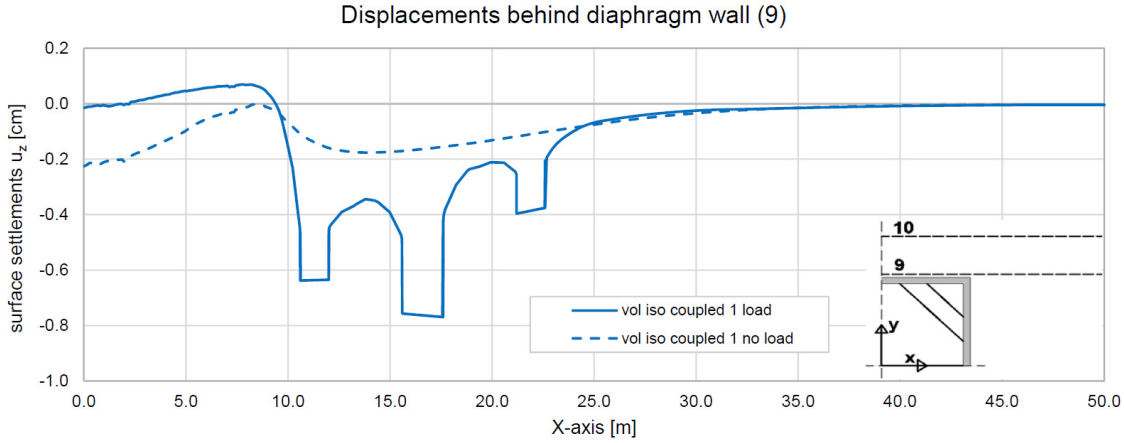

Fig. 60: Surface settlements

6 Conclusion

The following conclusions are drawn from the knowledge obtained during the analysis of all completed calculations. Furthermore, aspects of particular importance are emphasized.

In general, the discussed differences between the different options are related to the isotropic continuum wall model, otherwise it is mentioned explicitly.

6.1 Drainage Conditions

The first set of analysis is concerned with varying drainage conditions and associated excess pore water pressure dissipation. As the consolidation degree increases, the magnitude of wall deformations, bending moments and surface settlements increase. Compared to the undrained option, short consolidation times (coupled options) already lead to significant differences, due to the nonlinear relation concerning excess pore water pressure dissipation over time.

Wall deformations

The obtained differences, especially at the upper region of the wall result from the varying sequences considered for consolidation performances. As a result, the structural support inside the excavation is loaded differently. Highest stresses within the 4th strut level are developed by the final consolidation option. Concerning the stresses present within the strut level at -12 m, drained conditions develop around 30 % and undrained conditions already 60 % lower stresses compared to final consolidation conditions. The different loading of support measures also influences maximum wall displacements. The final consolidation option develops around 10 % lower maximum wall displacements than the drained one.

The coupled options develop around 40 – 50 % of the wall deformation range limited by undrained and drained conditions. The relative difference in maximum wall deformations between the coupled and the undrained options also varies between 40 – 50 %. Coupled deformation curves at the upper half of the wall are almost the same as the drained one.

Bending moments M1

Since bending moments are derived from the corresponding wall deformation, differences of maximum values around the excavation level are also mainly

dependent on drainage conditions. Except for undrained conditions, the maximum bending moments are quite similar. Undrained calculations develop around 40 – 50 % lower bending moments than the other conditions.

Surface settlements

Concerning the difference in drainage conditions, surface settlements correspond with the qualitative difference obtained in wall deformations, since they interact with each other.

Quantitatively spoken, surface settlements are strongly dependent on the foundations present in the adjacent area of the excavation (applied load as well as influence of rigidity of foundation elements).

The relative differences between centre and corner surface settlements behind the wall are around 30 % for all drainage conditions considered.

As the investigations on different modelling approaches (isotropy/anisotropy, plate/continuum modelling) prove, undrained analysis are generally less affected than other drainage conditions. The obtained differences are almost negligible but increase rapidly with short consolidation times and consequently the difference for other drainage conditions increases. Therefore, the difference between undrained and other drainage conditions does not remain the same for different modelling approaches. The maximum wall deformation for undrained conditions is around 60 % smaller than the drained option develops for isotropic continuum wall models and increases for plate and anisotropic modelling approaches (Tab. 23). Due to the wall “weakened” by anisotropy, the drainage condition becomes more relevant than for other modelling approaches.

Complete undrained conditions are very unlikely to occur in reality and consequently inappropriate to consider for excavation applications, since relevant maximum values are significantly lower when compared to realistic drainage conditions.

6.2 Continuum vs. Plate Modelling

The tendency towards increased wall deformations and surface settlements in plate elements results from the geometric difference, since they do not account for an actual wall thickness. Hence, the plate modelling approach corresponds to a conservative approach. In principle, the difference between plate and continuum modelling is caused by two individual aspects – the reverse acting moment and the horizontal offset between the wall surfaces:

The moment induced by the mobilized shear stresses at the interface of wall and soil can only develop for continuum wall models. Consequently, higher wall deformations and surface settlements are obtained for plate walls.

Due to the geometric difference, a horizontal offset of 40 cm between the wall surfaces arises in both directions. As a result, the settlements next to the wall differ exactly by this offset as long as the settlements are influenced by the wall.

The difference between both options depends on the drainage condition as well as the considered material behaviour of the wall (isotropic, anisotropic). Isotropic walls show quite small differences and reach their maximum at around 10 % for drained conditions. Whereas the difference seems negligible for isotropic material, it becomes relevant for anisotropic material. Compared to isotropic properties, the difference is about 10 % higher for anisotropic ones. Therefore, the influence of the mechanisms determining the difference between continuum and plate modelling increases for anisotropic conditions.

6.3 Isotropy vs. Anisotropy

Wall deformations

The difference is influenced by the drainage conditions and increases as the consolidation degree increases. Undrained conditions are almost not affected by anisotropy, compared to drained calculations, which develop around 40 % higher wall deformations for anisotropic continuum models.

Bending moments

Due to similar wall deflections, bending moments M1 at the centre are less affected by anisotropy than wall deformations (maximum relative difference ~ 20%). In comparison, bending moments M1 at the corner are much higher influenced as the relative difference about 60 – 70 % shows.

Concerning bending moments M2, anisotropy causes a difference at about 70 % at the centre and 60 % at the corner. Whereas the magnitude of horizontal bending moments at the corner is still quite high. From this point of view, the assumption of a lower bending stiffness in the horizontal direction would seem reasonable.

Axial stiffness in horizontal direction

The lowered axial stiffness in horizontal direction of about 25 % does not affect the overall behaviour, as the resulting difference (< 1 mm) between isotropic and anisotropic wall deformations along the wall (y-direction) confirms.

Isotropic hinge plate model

The influence of a hinged connection at the centre of the wall is very high on isotropic wall models. Bending moments are also highly affected by the hinge model. Maximum wall deformations and bending moments M1 are as high as for anisotropic rigid conditions.

Developed bending moments M1 and M2 do not change sign towards the corner due to the hinged connection. Therefore, the difference between hinge and rigid models is also of qualitative nature.

Horizontal bending moments M2 between the centre and the corner are a bit misleading, since maximum values develop a few meters before the corner is reached. At the centre they show equal values as obtained from the isotropic rigid plate model.

Concerning results at the centre of the wall, the isotropic hinge plate model develops equal wall deformations and bending moments as the anisotropic rigid plate model. However, this may be a coincidence for this particular example and cannot be generalized.

The results obtained in this study are well in agreement what has been presented by Zdravkovic et al. (2005). Hence anisotropic wall modelling is generally recommended.

Besides the dependency on the current drainage condition, the excavation geometry is also of influence (Zdravkovic et al. (2005)). This is due to the 3D effects. As the diaphragm wall corners behave more stiffly than the middle parts, lower wall deformations are seen within the influenced areas of the corners. The smaller the horizontal dimensions of the excavation, the higher the influence of the corners. This significantly determines the development of wall deformations. Due to the quadratic dimension of the present excavation pit, it is very likely that the influence of the corners causes smaller deformations in anisotropic 3D modelling as compared to a 2D plane strain model as has been shown by Moormann, C. & Klein, L. (2014) and Zdravkovic et al. (2005).

Perspective of further possible modelling approaches

Due to the limit of linear elastic modelling for plate elements, no failure criterion is considered. For a better simulation of the wall behaviour, it is reasonable to prevent tensile stress development normal to the joint direction and to consider a MC failure criterion within the joints. This approach can be easily applied in the JRM, whereas one drawback arises concerning the output of structural forces for continuum elements. Nevertheless, the influence on wall deformations and surface settlements can still be investigated.

6.4 Building vs. Green Field

The variation of adjacent surface loads concerns mainly surface settlements and head distortions of the wall. Maximum wall deformations and bending moments are not significantly affected but surface settlements are influenced to some extent.

7 References

Brinkgreve, R.B.J.; Kumarswamy, S.; Swolfs, W.M. (2015)
Plaxis 3D Anniversary Edition. Manuals, Part 1 – 4, Delft, Netherlands.

Dong, Y.P.; Burd, H.J.; Houlsby, G.T. (2016)
Finite-element analysis of a deep excavation case history. Géotechnique 66, No. 1, 1-15.

Lüftenegger, R. (2006)
Numerische Berechnung einer tiefen Baugrube in Salzburg. Diplomarbeit, Institut für Bodenmechanik und Grundbau, Technische Universität Graz.

Moormann, C.; Klein, L. (2014)
Bemessung tiefer Baugruben mit rechteckigem Grundriss unter Berücksichtigung des räumlichen Erddrucks. Bautechnik 91, Heft 9, 633-655, Ernst & Sohn, Berlin.

Schweiger, H.F. (2015)
Computational Geotechnics. Lecture WS 2015/16, Graz University of Technology.

Schweiger, H.F.; Scharinger, F.; Lüftenegger, R. (2009)
3D finite element analysis of a deep excavation and comparison with in situ measurements. Geotechnical Aspects of Underground Construction in Soft Ground –Ng, Huang & Liu (eds) 193-199, Taylor & Francis Group, London.

Zdravkovic, L.; Potts, D.M.; St. John, H.D. (2005)
Modelling of a 3D excavation in finite element analysis. Géotechnique 55, No. 7, 497-513.

8 Appendix

8.1 Drainage Conditions

8.1.1 Comparison of Maximum Results

Tab. 23: Relative differences of maximum wall deformations between drainage conditions (related to the undrained contidion)

maximum wall displacements u_x [cm]							
		continuum	relative difference [%]	plate rigid	relative difference [%]	plate hinge	relative difference [%]
undrained	isotropic	0.8		0.8		0.9	
	anisotropic	0.8		0.9		1.0	
coupled 1	isotropic	1.5	47	1.6	50	2.2	59
	anisotropic	1.9	58	2.2	59	2.6	62
coupled 2	isotropic	1.3	38	1.5	47	1.8	50
	anisotropic	1.6	50	1.8	50	2.1	52
consolidation	isotropic	1.9	58	2.1	62	3.1	71
	anisotropic	2.6	69	3.2	72	3.9	74
drained	isotropic	2.1	62	2.4	67	3.9	77
	anisotropic	3.0	73	4.0	78	5.2	81

Tab. 24: Relative differences of maximum bending moments M1 between drainage conditions (related to the undrained contidion)

maximum bending moment M1 [kNm/m]							
		continuum	relative difference [%]	plate rigid	relative difference [%]	plate hinge	relative difference [%]
undrained	isotropic	397		408		460	
	anisotropic	372		419		453	
coupled 1	isotropic	708	44	746	45	950	52
	anisotropic	765	51	937	55	1029	56
coupled 2	isotropic	663	40	774	47	831	45
	anisotropic	680	45	819	49	868	48
consolidation	isotropic	792	50	825	52	1095	64
	anisotropic	954	61	1171	64	1315	66
drained	isotropic	778	49	824	50	1154	60
	anisotropic	942	61	1185	65	1388	67

8.2 Continuum vs. Plate Modelling

8.2.1 Isotropic Model

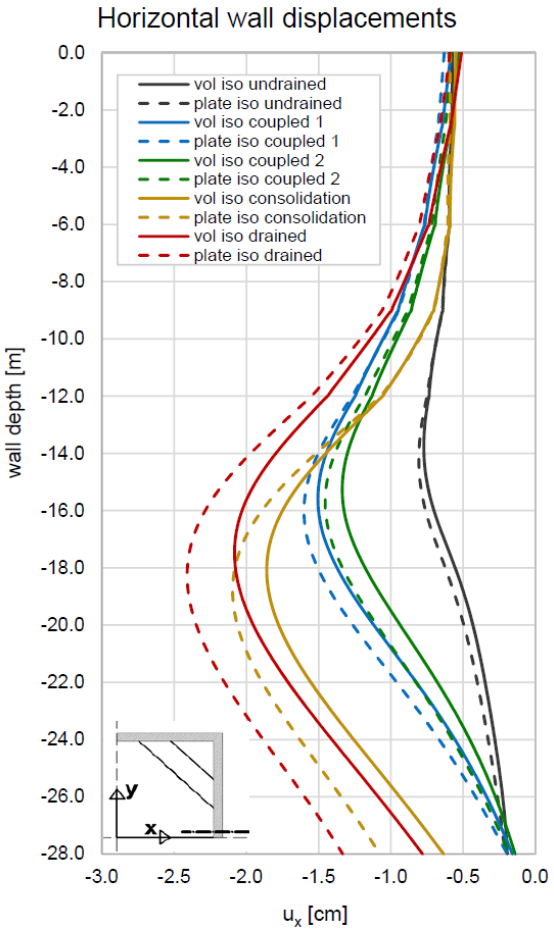

Fig. 61: Horizontal wall displacements (isotropic)

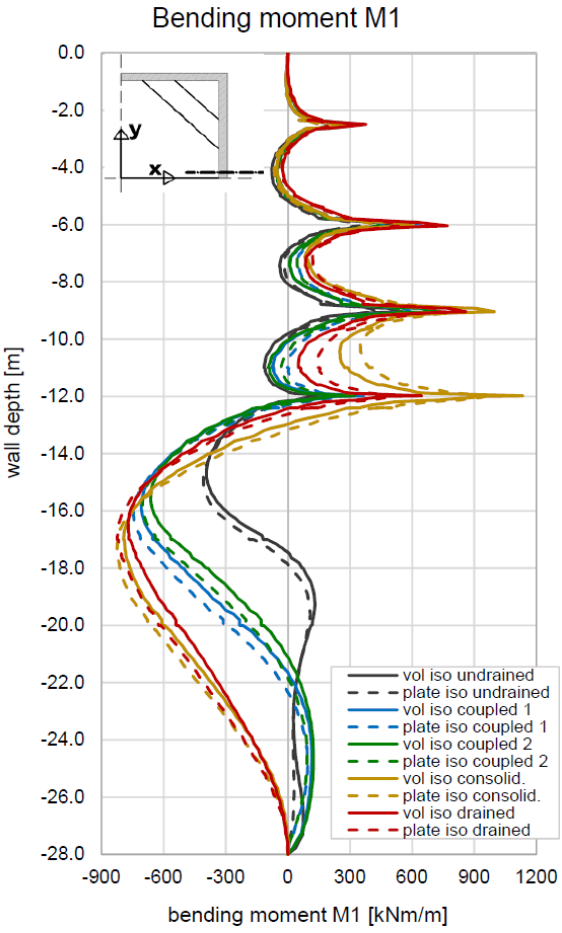

Fig. 62: Bending moments M1 (isotropic)

8.2.2 Anisotropic Model

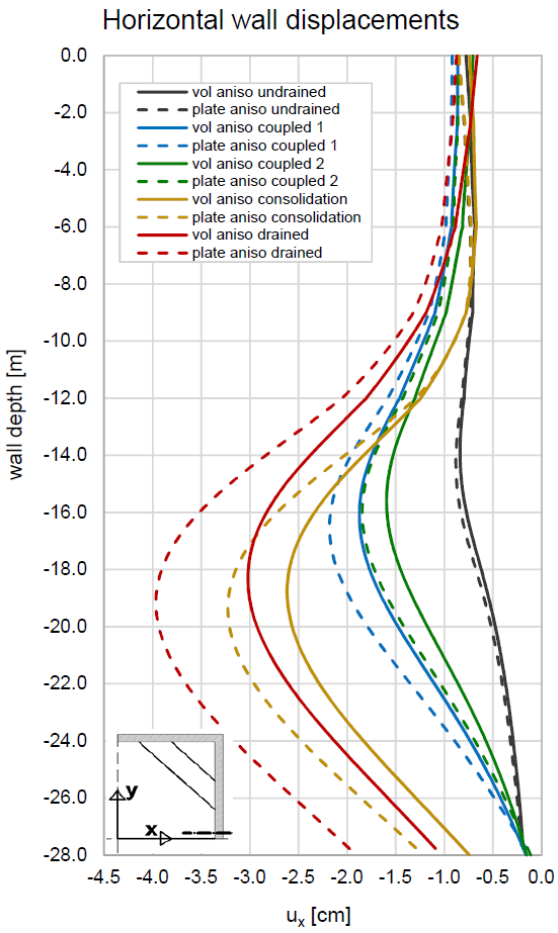

Fig. 63: Horizontal wall displacements (anisotropic)

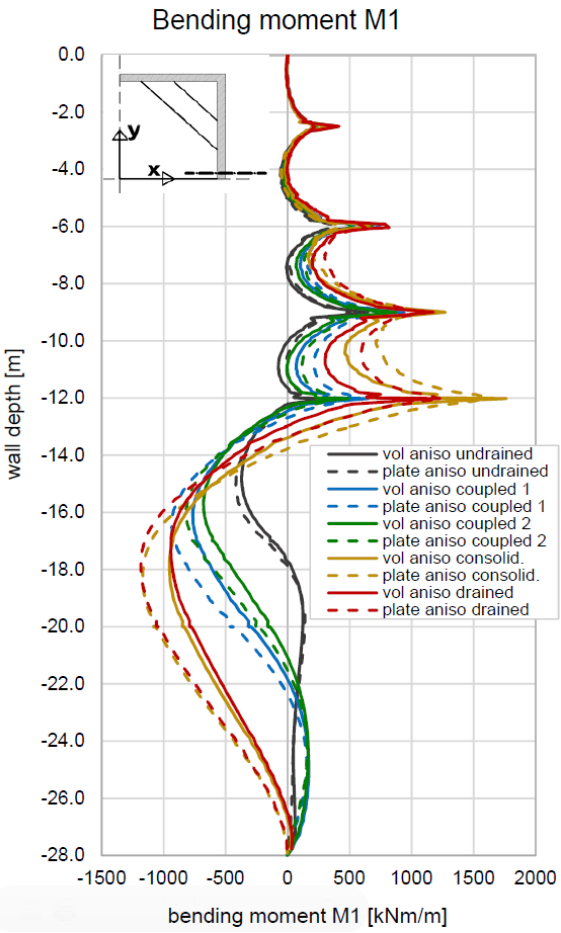

Fig. 64: Bending moments M1 (anisotropic)

8.2.3 Comparison of Maximum Results

Diaphragm wall

Tab. 25: Relative differences of maximum wall deformations between plate and continuum models

maximum wall displacements u_x [cm]					
		isotropic	relative difference [%]	anisotropic	relative difference [%]
undrained	continuum	0.8	0	0.8	11
	plate	0.8		0.9	
coupled 1	continuum	1.5	6	1.9	15
	plate	1.6		2.2	
coupled 2	continuum	1.3	8	1.6	11
	plate	1.5		1.8	
consolidation	continuum	1.9	10	2.6	19
	plate	2.1		3.2	
drained	continuum	2.1	13	3.0	25
	plate	2.4		4.0	

Tab. 26: Relative differences of maximum bending moments M1 between plate and continuum models

maximum bending moment M1 [kNm/m]					
		isotropic	relative difference [%]	anisotropic	relative difference [%]
undrained	continuum	397	3	372	11
	plate	408		419	
coupled 1	continuum	708	5	765	18
	plate	746		937	
coupled 2	continuum	663	14	680	17
	plate	774		819	
consolidation	continuum	792	4	954	19
	plate	825		1171	
drained	continuum	778	6	942	21
	plate	824		1185	

Surface settlements

Tab. 27: Relative differences of maximum surface settlements between plate and continuum models

maximum surface settlements u_z [cm]									
		isotropic		relative difference [%] (u_z 1)	relative difference [%] (u_z 3)	anisotropic		relative difference [%] (u_z 1)	relative difference [%] (u_z 3)
		u_z 1	u_z 3			u_z 1	u_z 3		
undrained	continuum	0.7	0.5	0	0	0.9	0.6	0	14
	plate	0.7	0.5			0.9	0.7		
coupled 1	continuum	1.1	0.8	0	0	1.5	1.1	6	8
	plate	1.1	0.8			1.6	1.2		
coupled 2	continuum	1.0	0.7	0	0	1.3	0.9	7	10
	plate	1.0	0.7			1.4	1.0		
consolidation	continuum	1.0	0.7	9	22	1.4	1.0	13	23
	plate	1.1	0.9			1.6	1.3		
drained	continuum	1.3	0.9	19	25	1.8	1.4	28	26
	plate	1.6	1.2			2.5	1.9		

8.3 Isotropy vs. Anisotropy

8.3.1 Continuum Model

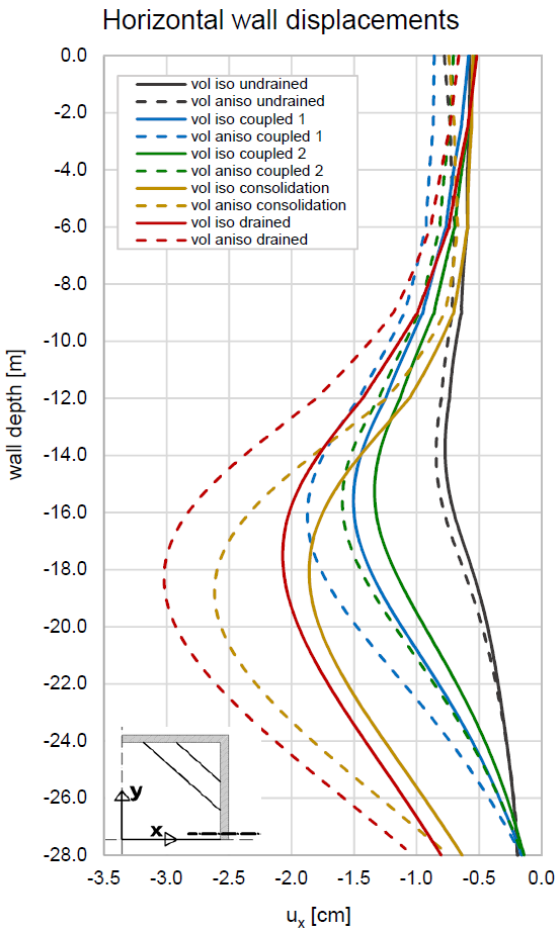

Fig. 65: Horizontal wall displacements (continuum)

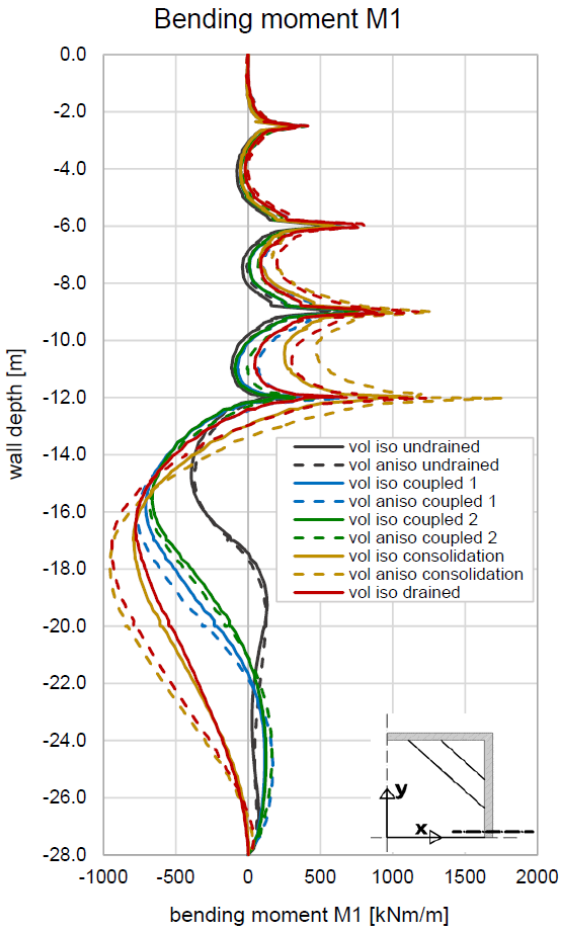

Fig. 66: Bending moments M1 (continuum)

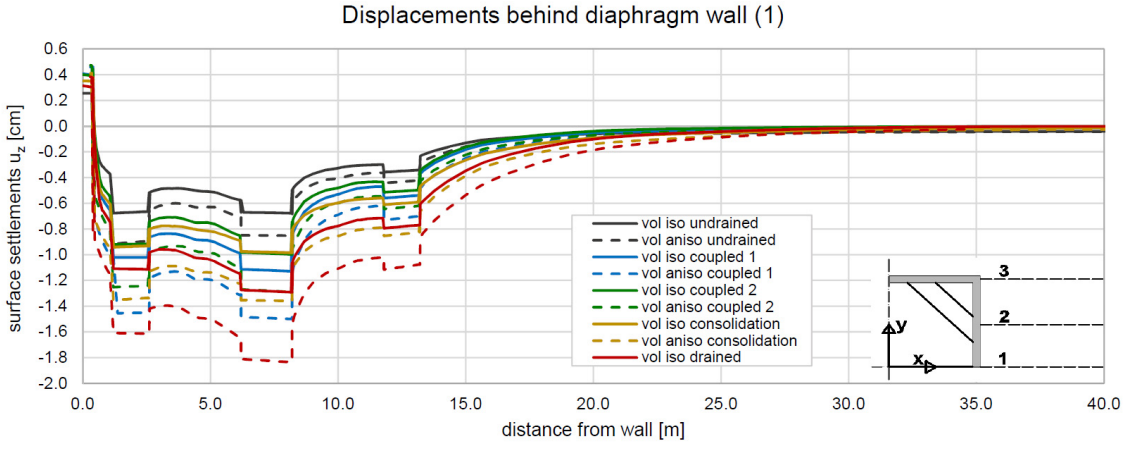

Fig. 67: Surface settlements (continuum)

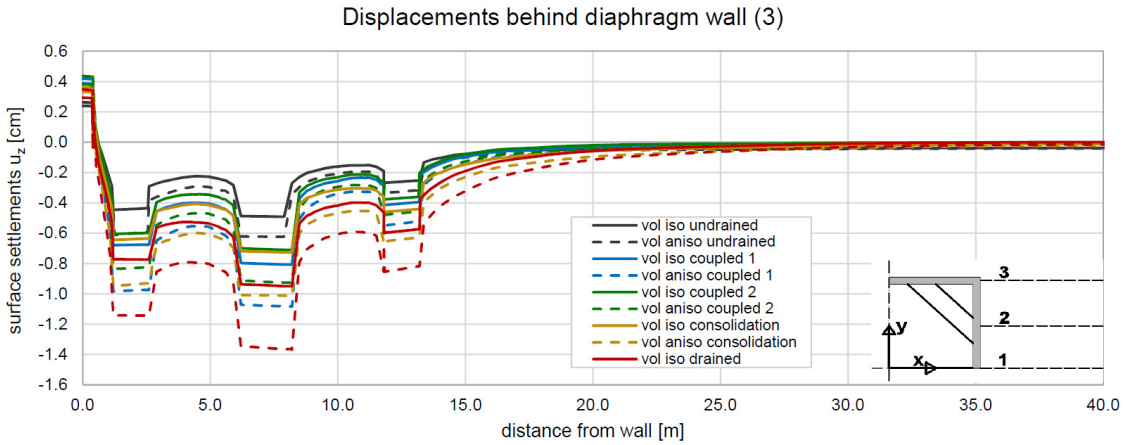

Fig. 68: Surface settlements (continuum)

8.3.2 Rigid Plate Model

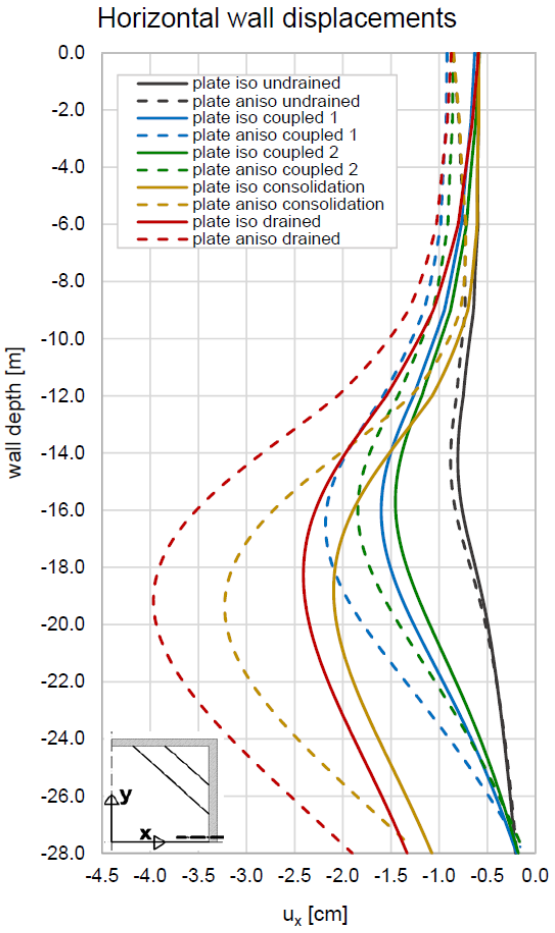

Fig. 69: Horizontal wall displacements (plate - rigid)

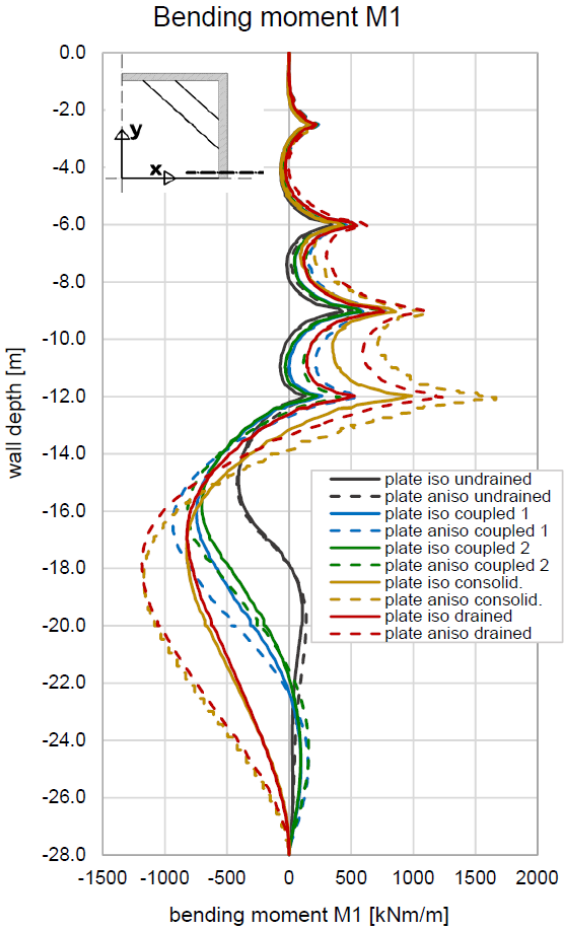

Fig. 70: Bending moments M1 (plate - rigid)

8.3.3 Hinge Plate Model

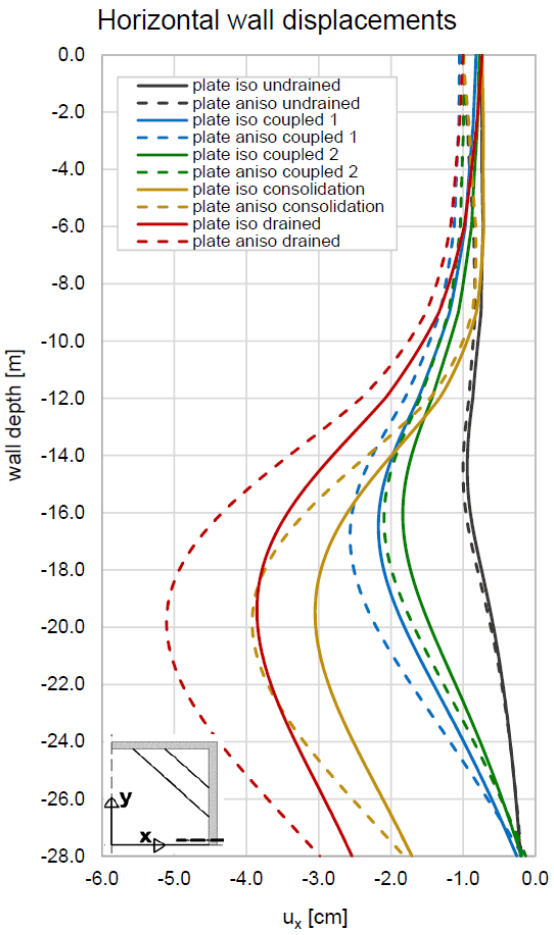

Fig. 71: Horizontal wall displacements (plate - hinge)

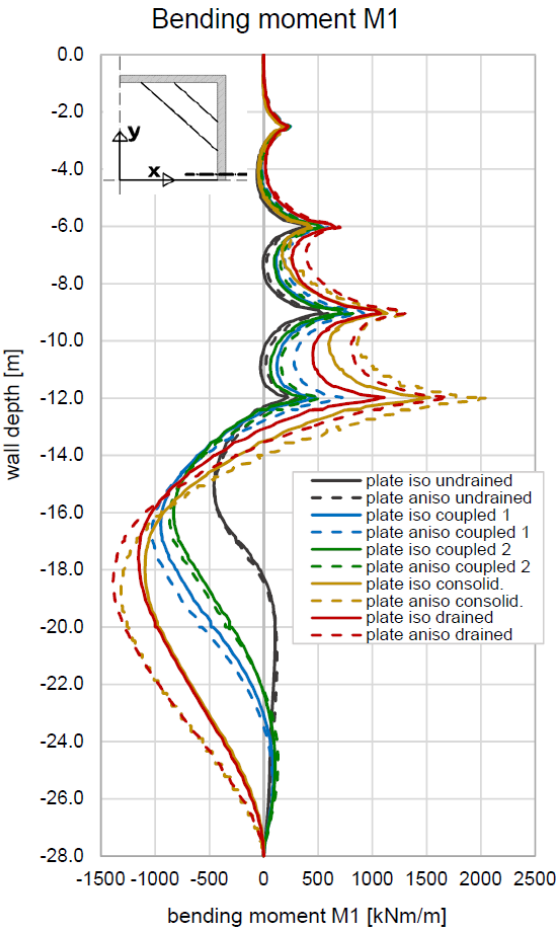

Fig. 72: Bending moments M1 (plate - hinge)

8.3.4 Plate Rigid Anisotropic vs. Hinge Isotopic

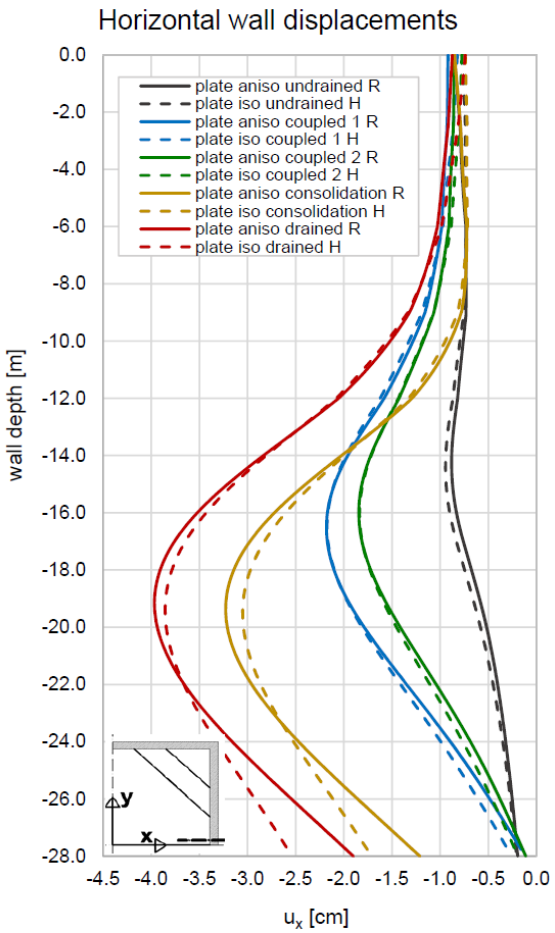

Fig. 73: Horizontal wall displacements (plate)

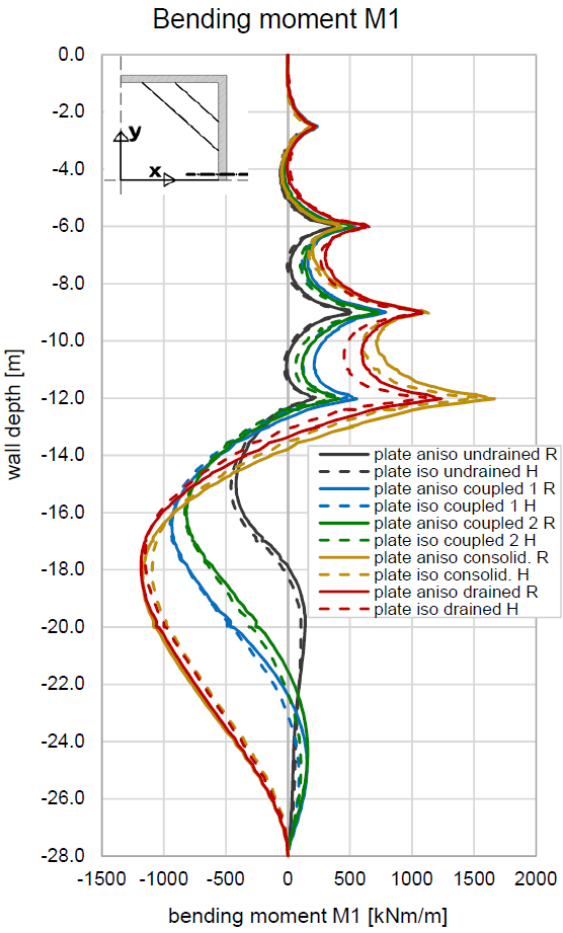

Fig. 74: Bending moments M1 (plate)

8.3.5 Comparison of Maximum Results

Diaphragm wall

The relative differences given in the last column of Tab. 28 and Tab. 29 correspond to the comparison made in 8.3.4: Plate Rigid Anisotropic vs. Hinge Isotopic

Tab. 28: Relative differences of maximum wall deformations between isotropic and anisotropic models

maximum wall displacements u_x [cm]								
		continuum	relative difference [%]	plate rigid	relative difference [%]	plate hinge	relative difference [%]	relative difference [%]
undrained	isotropic	0.8	0	0.8	13	0.9	11	0
	anisotropic	0.8		0.9		1.0		
coupled 1	isotropic	1.5	27	1.6	38	2.2	18	0
	anisotropic	1.9		2.2		2.6		
coupled 2	isotropic	1.3	23	1.5	20	1.8	17	0
	anisotropic	1.6		1.8		2.1		
consolidation	isotropic	1.9	37	2.1	52	3.1	26	3
	anisotropic	2.6		3.2		3.9		
drained	isotropic	2.1	43	2.4	67	3.9	33	3
	anisotropic	3.0		4.0		5.2		

Tab. 29: Relative differences of maximum bending moments M1 between isotropic and anisotropic models

maximum bending moment M1 [kNm/m]								
		continuum	relative difference [%]	plate rigid	relative difference [%]	plate hinge	relative difference [%]	relative difference [%]
undrained	isotropic	397	6	408	3	460	2	10
	anisotropic	372		419		453		
coupled 1	isotropic	708	8	746	26	950	8	1
	anisotropic	765		937		1029		
coupled 2	isotropic	663	3	774	6	831	4	1
	anisotropic	680		819		868		
consolidation	isotropic	792	20	825	42	1095	20	6
	anisotropic	954		1171		1315		
drained	isotropic	778	21	824	44	1154	20	3
	anisotropic	942		1185		1388		

Surface settlements

Tab. 30: Relative differences of maximum surface settlements between isotropic and anisotropic models

maximum surface settlements u_z [cm]									
		continuum		relative difference [%] (u_z 1)	relative difference [%] (u_z 3)	relative difference [%] (u_z 1 - 3)			
		u_z 1	u_z 3						
undrained	isotropic	0.7	0.5	29	20	29			
	anisotropic	0.9	0.6			33			
coupled 1	isotropic	1.1	0.8	36	38	27			
	anisotropic	1.5	1.1			27			
coupled 2	isotropic	1.0	0.7	30	29	30			
	anisotropic	1.3	0.9			31			
consolidation	isotropic	1.0	0.7	40	43	30			
	anisotropic	1.4	1.0			29			
drained	isotropic	1.3	0.9	38	56	31			
	anisotropic	1.8	1.4			22			

		plate rigid		relative difference [%] (u_z 1)	relative difference [%] (u_z 3)	relative difference [%] (u_z 1 - 3)			
		u_z 1	u_z 3						
undrained	isotropic	0.7	0.5	29	40	29			
	anisotropic	0.9	0.7			22			
coupled 1	isotropic	1.1	0.8	45	50	27			
	anisotropic	1.6	1.2			25			
coupled 2	isotropic	1.0	0.7	40	43	30			
	anisotropic	1.4	1.0			29			
consolidation	isotropic	1.1	0.9	45	44	18			
	anisotropic	1.6	1.3			19			
drained	isotropic	1.6	1.2	56	58	25			
	anisotropic	2.5	1.9			24			

		plate hinge		relative difference [%] (u_z 1)	relative difference [%] (u_z 3)	relative difference [%] (u_z 1 - 3)	relative difference [%] (u_z 1)	relative difference [%] (u_z 3)
		u_z 1	u_z 3					
undrained	isotropic	0.9	0.7	33	29	22	0	0
	anisotropic	1.2	0.9			25		
coupled 1	isotropic	1.7	1.3	29	23	24	6	8
	anisotropic	2.2	1.6			27		
coupled 2	isotropic	1.5	1.1	20	27	27	7	10
	anisotropic	1.8	1.4			22		
consolidation	isotropic	1.8	1.4	33	29	22	13	8
	anisotropic	2.4	1.8			25		
drained	isotropic	2.8	2.2	29	27	21	12	16
	anisotropic	3.6	2.8			22		

The relative differences given in the last two columns of Tab. 30 correspond to the comparison made in 8.3.4: Plate Rigid Anisotropic vs. Hinge Isotopic.